# Controls of basement fabric on cover faulting in strike-slip regimes: analogue physical models of faults using plaster

Maria Helena Seim

Thesis for the degree

Master of Science


Department of Earth Science

University of Bergen

01.06.2015

# Abstract

The full complexity of deformation associated with natural faults is difficult to understand, given the lack of three-dimensional exposure in outcrop and the limitations of seismic resolution in the sub-surface. Analogue physical experiments are therefore widely used to gain insight into the nature and evolution of deformation associated with fault growth. In this study we use plaster of Paris to gain insight into fault evolution in strike-slip regimes; specifically, we investigate the effect of different basement structural templates on the evolution of faults in the cover (plaster). The small-scale structures developed in plaster experiments can quite accurately mimic natural fault systems. The grain size and rheology of plaster of Paris makes the development and preservation of detailed structural geometries possible.

Basement templates with differently angled restraining and releasing bends were made, for studying structures formed by transpressive and transtensive deformation, respectively. A cover sequence of plaster mixture was poured into a sealed box; manual movement (pulling by hand) controlled the amount of strain and deformation in the ensuing experiments.

Based on the finished models, results show how the positive flower structure geometry is affected by the restraining bend angle. Specifically, the pop-up structures comprise more fault blocks in models with lower-angled restraining bends, and the fault blocks form at a later stage in the deformational process in experiments with higher-angled bends. The geometry of the fault blocks changes according to the bend angle. The results also give insight into pull-apart basin development; they indicate that the aspect ratio of the pull-apart basins increases when increasing the angle of the releasing bends.

Analogue plaster modelling can, as seen herein, provide valuable insight into fault evolution and associated minor deformation.

# Acknowledgements

The completion of this thesis marks the end of five great and challenging years at the University of Bergen, and I would like to acknowledge several people for great support along the way.

First of all, I would like to express my gratitude to my main supervisor, Atle Rotevatn (UiB, Department of Earth Science) for great guidance and encouragement during the last two years. I would also like to thank my co-supervisor Haakon Fossen (UiB, Department of Earth Science) for the great help during this process, particularly when it comes to the experimental work. I would also like to thank my co-supervisor Eivind Bastesen (UiB, CiPR) whom has been of great assistance with the experimental work. Signe Ottesen (Statoil ASA) and Tore Odinsen (Statoil ASA), my co-supervisors have taught me how to run strike-slip experiments and I am very grateful for your help.

I would like to thank Statoil ASA for sponsoring this master project.

I am very grateful for my friends and lab-partners Margrethe Sæterdal Bøyum and Marie Djupevåg Eri for the great time we have had when working on these experiments. Thank you both for all of your assistance with the experiments, and for being great support throughout this process! I would also like to acknowledge my other lab-partners Christine Andersen, Renate Tveit and Ingvild Blækkan for the great assistance and fun that we have had when working on the experiments.

Hamed Fazli Khani has partaken in many of the experiment days and offered great input which I am very grateful for. I am also thankful for Jozef Kusior's assistance with the carpentry work.

I would also like to thank all of the students that assisted with the cameras and the lamps during the experiments. As many hands are needed for doing this work successfully, you have been of great help!

I would like to thank my friends and family for the encouragement and motivation throughout this process. A special thanks goes to my aunt and uncle Torunn and Tim for taking the time to proof-read parts of my master thesis.

Maria Helena Seim

# Table of Contents

# 1 Introduction

## 1.1 Background and rationale

Analogue modeling studies on the extensional regime have shown that the basement configuration strongly influences the structures that form in the overlying cover (e.g. McClay, 1990; Gabrielsen & Clausen, 2001). There has not been as much research done on the role of basement configuration on strike-slip features. For this thesis analogue modeling is performed with the intention to learn more about how basement configuration affects the structures formed in the overlying plaster cover.

As fault complexes in nature show the structures at their final state of deformation, the structural development cannot be fully understood from studying natural fault complexes only (Lindanger et al., 2004). Outcrops in the field generally provide limited exposure of a structural system and they are two-dimensional. They therefore do not give a full picture of a structural system, but they allow for detailed studies of the exposed features. Seismic data provides a better picture of the structural systems in three dimensions, but due to the resolution of the data small, sub-seismic structures cannot be studied (Steen et al., 1998; Pringle et al., 2004). Small-scale structures also influence the fluid flow in the sub-surface, which makes them important features for the petroleum industry (Knipe et al., 1998). Given the above limitations, a full understanding of the complexity of strike-slip geometry and growth is hard to obtain based on outcrop and subsurface studies.

Experiments using plaster generate detailed, realistic models representing natural fault complexes (Gabrielsen & Clausen, 2001). The complexity of the structural system can be studied in 3D, and the development can be studied during the experiments, as well as from the pictures documenting the evolution. The models embody large-scale structures as well as the associated sub-seismic features formed under the experimental conditions. By doing analogue modeling the temporal formation and evolution of faults and concomitant structures can be studied. The experiments can provide additional valuable data or confirm the already existing information over an area (Clifton et al., 2000).

## 1.2 Aims and objectives

The main aim for this study is to gain new insight to the geometry, nucleation and growth of strike-slip faults and concomitant features through experimental modeling. Specifically the aim is to get a

better understanding of the relationship between structural basement configuration and the structures in the sedimentary cover, particularly pertaining to releasing and restraining bends.

This is achieved through the following objectives:

- Perform analogue plaster modeling using basement templates with differently angled restraining and releasing bends.
- Analyze and compare structures in pictures taken during the experiments.
- Make videos by compiling the pictures from each experiment and use these for studying the evolution of structures.
- Compare the experiments with similar experimental conditions to see if similarities can be drawn between the models.
- Compare some structures with similar structures in nature.

## 1.3 Strike-slip faults

**Introduction**

One can define strike-slip faults as faults with displacement parallel to their strike, where one fault block moves laterally relative to the other block (Fossen, 2010). They are common in various geological settings in both oceanic- and continental tectonic plates, and are found as both small-scale structures as well as structures stretching over tens to hundreds of kilometers (Cunningham & Mann, 2007; Fossen, 2010). The earthquake that occurred in San Francisco in 1906, caused by the San Andreas Fault, gave strike-slip faults scientific importance and attention worldwide. These structures were recognized for their geological importance before this event, particularly after the earthquake in New Zealand in 1888 that resulted in strike-slip displacement (Sylvester, 1988). In the 1960-70s the theory of plate tectonics gradually became accepted amongst geoscientists, and they got a new understanding of the tectonic and mechanical nature of these faults. Earthquakes are more often associated with these types of faults compared to normal and reverse intraplate faults (Sylvester, 1988).

**Classification**

Strike-slip faults are divided into different groups based on i) their vertical and lateral extent and ii) where they are located (Sylvester, 1988). They are interplate or intraplate features and their motion is either dextral, which means right-lateral, or sinistral, which means left-lateral (Cunningham & Mann, 2007; Fossen, 2010), (Fig. 1.1). The main classes of strike-slip faults are called transform and

transcurrent faults, and these are further divided into subgroups based on their characteristics (Sylvester, 1988).

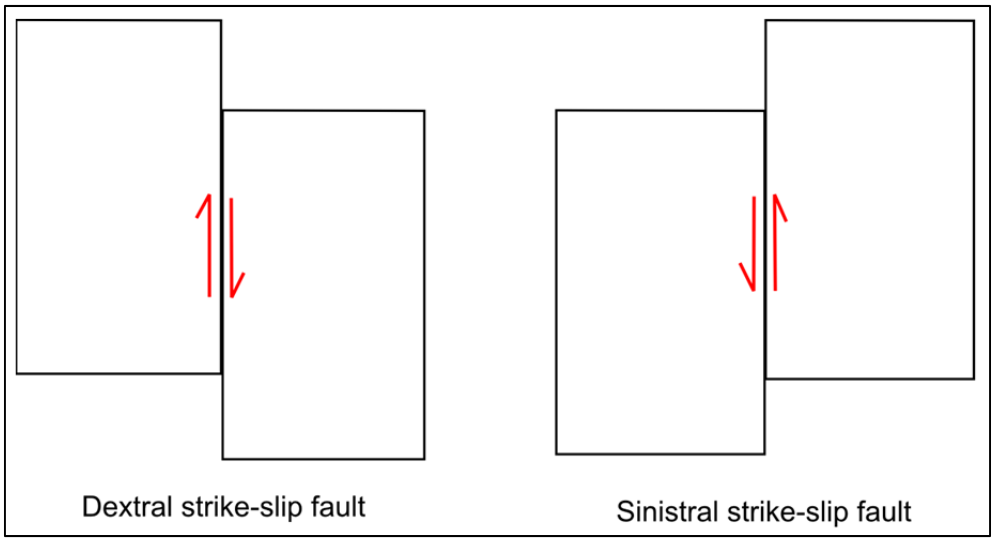


**Figure 1.1:** Dextral and sinistral strike-slip faults.

Transcurrent faults are intraplate structures. They do not cut through the entire lithosphere, but are restrained to basement rock and the upper, sedimentary rock. Transcurrent faults, referred to as wrench faults by some geologists, are close to vertical features with a great lateral extent (Sylvester, 1988; Wilcox et al., 1973). Their free tips move as the displacement grows, and the fault's length increases (Fossen, 2010).

Transform faults are interplate structures that form plate boundaries or divide plates (Fossen, 2010). They cut through the lithosphere and are therefore more deep-cutting than the transcurrent features (Sylvester, 1988). They are characterized by being long faults or fault zones, and the San Andreas Fault is a 1200 km long example of such a structure (Fossen, 2010).

There are four main types of transcurrent faults, according to Sylvester (1988). *Transfer faults* have tips that terminate against fractures or other faults, and they transfer displacement between two features. Because of their restricted tips, they have a limited growth possibility, but their scale-range is still wide. *Tear faults* are responsible for the differential offset in an allochton or between this block and a close-lying structure. *Indent-linked strike-slip faults* are responsible for a part of the total displacement (Sylvester, 1988). They are located in areas of uplift and shortening (Woodcock & Daly, 1986). *Intracontinental transform faults* are also confined to the crust, and are therefore under this category (Sylvester, 1988).

According to Sylvester (1988), there are three main types of transform faults. *Ridge transform faults* cut the oceanic lithosphere perpendicular to mid-ocean ridges, and they are only active between the ocean-ridge parts. The fault's length is proportional to the spreading rate of the mid-ocean ridge (Fossen, 2010). *Boundary transforms* divide oceanic as well as continental plates. They are active for a long time, and their linear extent is large (Woodcock & Daly, 1986). *Trench-linked strike-slip faults* are only responsible for a part of the total displacement of a boundary, and are therefore not considered real transform features. Since they do cut through the lithosphere, they are categorized as transform faults. Trench-linked faults are located parallel to a trench, and can develop into long structures over a long period of time (Woodcock & Daly, 1986).

**Simple and Pure Shear**

Major strike-slip faults form in areas dominated by simple shear. The length of these faults can be over a thousand kilometers, and they can have hundreds of kilometers of displacement. For strike-slip faults in general the maximum principal stress, $\sigma_1$, is oriented with an angle to the fault plane, making the fault blocks move along each other (Fossen, 2010). The fault zone may be tens of kilometers wide, and it comprises characteristic features developed during the horizontal movement (Sylvester, 1988). Riedel-shear fractures (R-shears) develop with a NE-SW orientation relative to an E-W oriented dextral strike-slip fault (Fig. 1.2). The angle between these structures and the main fault plane is found by calculating ($\phi/2$), where $\phi$ is defined as the angle of internal friction (Sylvester, 1988). R'-shears form with the angle ($90° - \phi/2$), and these are antithetic structures, meaning that they are oriented oppositely from the main fault plane, and together with the R-shears these features form a conjugate set of fractures or faults (Wilcox et al., 1973; Sylvester, 1988) (Fig.1.2).

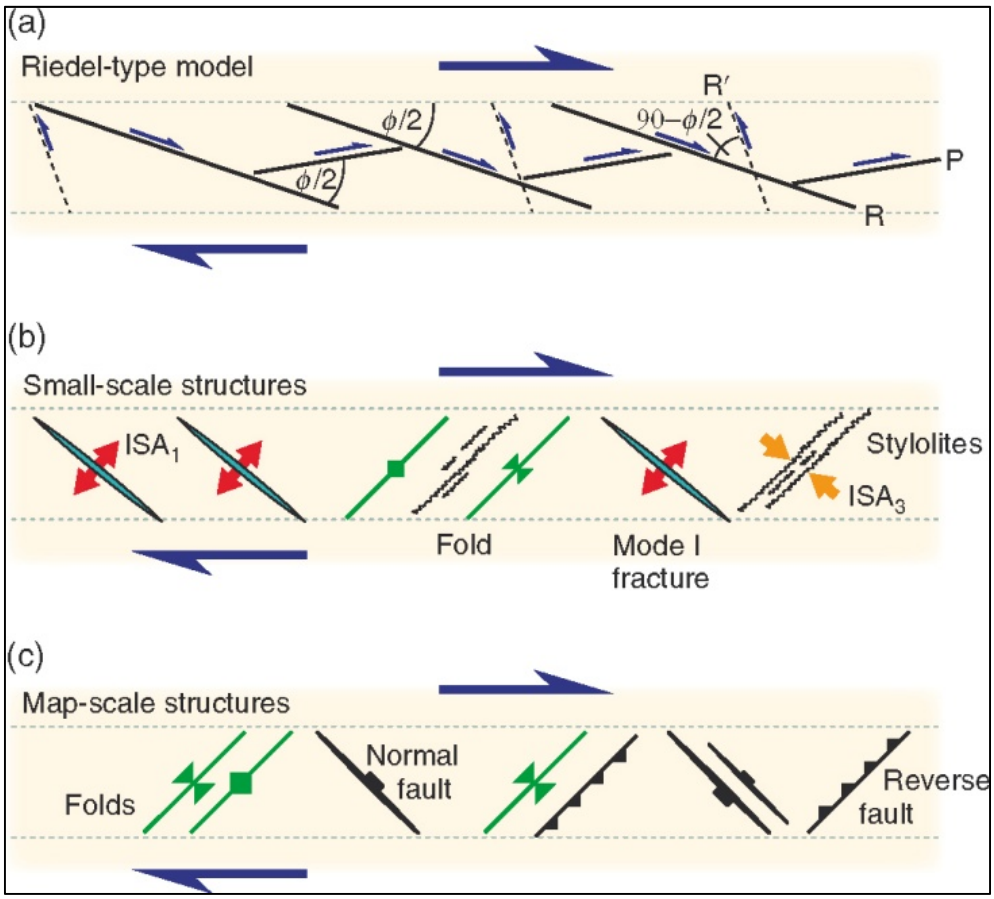


**Figure 1.2:** Secondary structures formed during simple shear (Fossen, 2010).

P-shear fractures tend to form after the development of the R-shears, and they are aligned between the surfaces of the R- and R'-shears (Fossen, 2010). T-fractures, or extension fractures, are also found along many strike-slip faults (Fig. 1.2). These form at approximately 45° to the orientation of the main fault, thus almost normal to the maximum instantaneous stretching axis (Sylvester, 1988; Fossen, 2010). Other secondary features that may form along a simple shear fault are folds, stylolites and normal and reverse faults (Fossen, 2010). The fold axis will in this case be oriented at less than 45° to the main fault plane, but it may rotate further depending on the amount of fault displacement (Wilcox et al., 1973).

Where pure shear is the dominating kinematic component strike-slip faults can develop in the form of conjugate sets (Fig. 1.3). These will be shorter faults compared to the ones developed under simple shear, due to lack of space. They have an angle of ϕ and -ϕ to the direction of shortening (Sylvester, 1988). Figure 1.3 shows that $\sigma_1$, the maximum principal stress, divides the acute angle between the two faults (Fossen, 2010). Normal faults and extensional fractures can be found perpendicular to the elongation axis in these zones, and compressional features, such as folds and

thrust faults, can be found normal to the shortening axis. These types of strike-slip faults are often associated with fold-thrust belts, where they cut across the fold orientations (Sylvester, 1988).

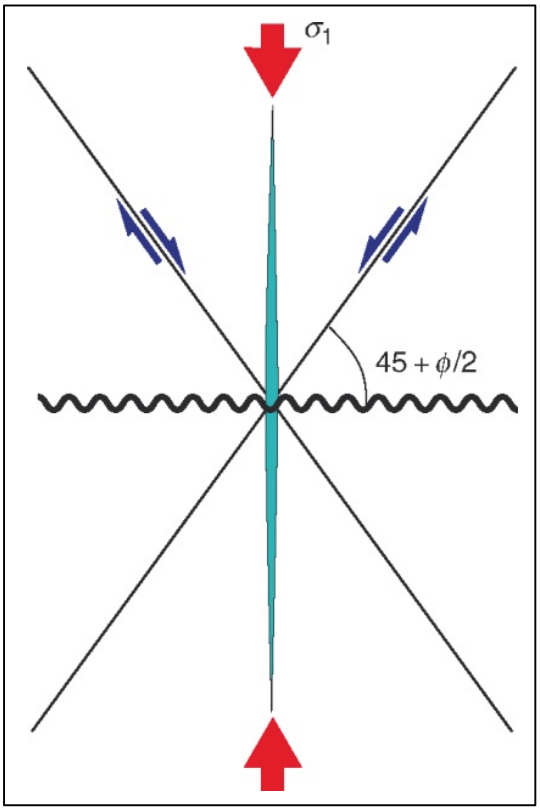


**Figure 1.3:** Conjugate set of faults (Fossen, 2010).

**Restraining and Releasing Bends**

Strike-slip faults tend to have a fairly straight plane in the vertical direction, but laterally the fault planes can comprise bends. Based on the relative motion of the fault and the direction of the bend, contractional or extensional features form in that area (Fossen, 2010). Transpressional deformation occurs at restraining bends, and transtension is associated with releasing bends (Fig. 1.4). “Fault bend” or “stepover” are terms used for sites where two strike-slip faults link together at an offset to form a curved and continuous structure. More rhomb-shaped stepovers do not define one continuous fault, rather two separate faults with displacement transfer in between (Cunningham & Mann, 2007).

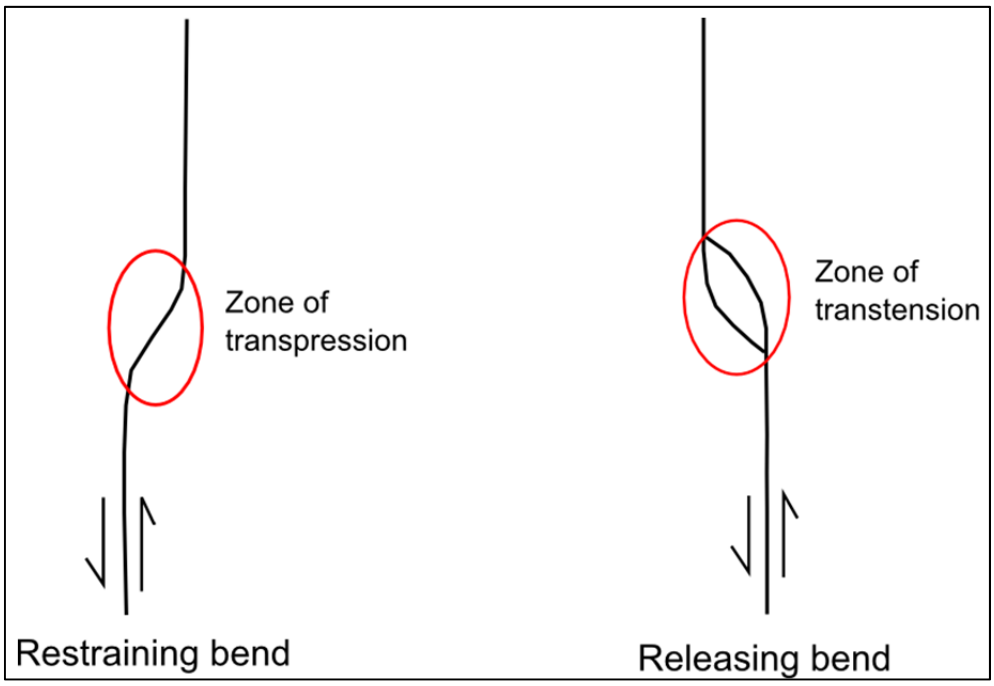


**Figure 1.4:** Restraining and releasing bend.

Restraining bends lead to shortening, and therefore uplift and vertical thickening of the crustal block. A higher amount of strain will affect the uplifted areas (Sanderson & Marchini, 1984). Elevated areas resulting from transpression might become a source of sediment for the lower topography nearby with time (Crowell et al., 1989). Structures associated with this type of deformation are folds and reverse faults. These features will be high-angled compared to the parts of the shear zone unaffected by transpression (Sanderson & Marchini, 1984). At sites characterized by double restraining bends, the uplifted crust can be called a positive flower structure (Cunningham & Mann, 2007), (Fig. 1.5).

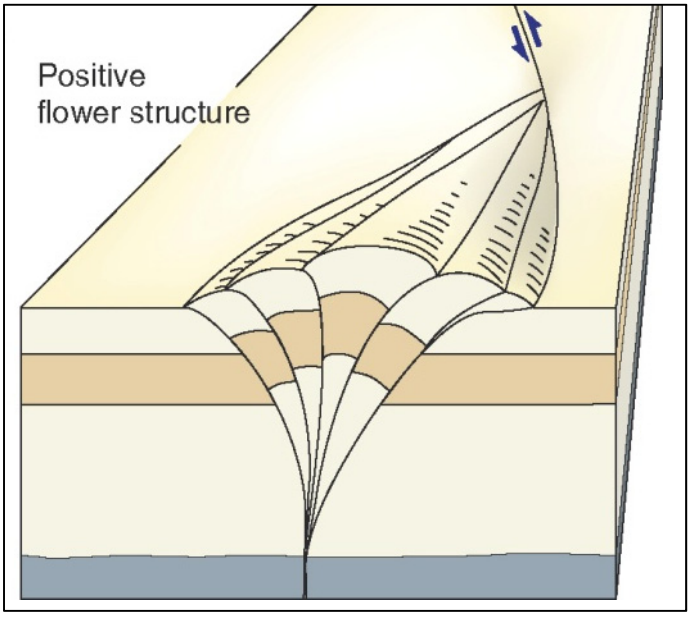


**Figure 1.5:** Positive flower structure (Fossen (2010)).

Crust that has been affected by transtension at releasing bends is stretched and thus thinner at this site than elsewhere in the region. Pull-apart basins form as a result of the thinned and subsiding crust, and these depressions can be receivers of sediment from uplifted topography nearby (Crowell et al., 1989). Features one can expect to find at sites of transtension are normal faults, veins, dykes and folds. The folds will be at a low-angle to the unaffected parts of the shear zone, and the other mentioned structures will be high-angled (Sanderson & Marchini, 1984). Where double releasing bends dominate, the subsided crust can be called a negative flower structure (Cunningham & Mann, 2007), (Fig. 1.6).

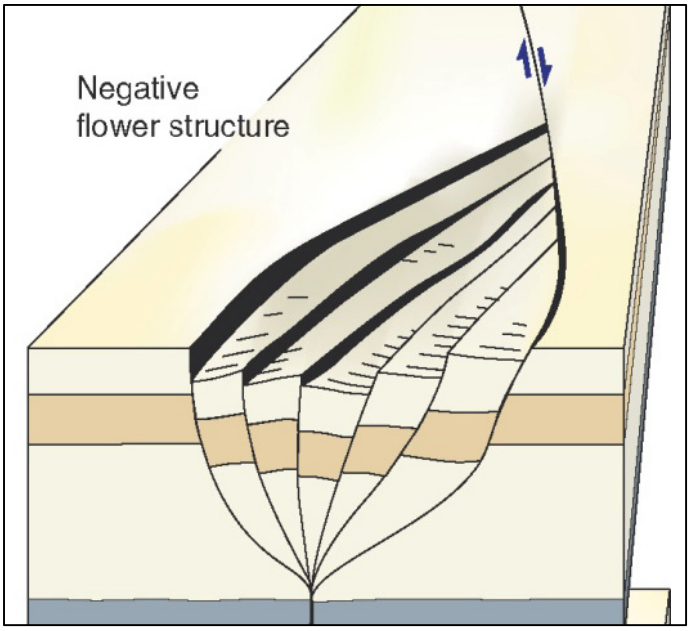


**Figure 1.6:** Negative flower structure (Fossen (2010)).

# 2 Methodology

## 2.1 Introduction

This chapter describes the methods used to perform analogue modeling of strike-slip deformation, using plaster of Paris as the modeling material (2.2 and 2.3). The concept of scalability for analogue models is described in this chapter along with a section covering some of the historical background for experimental studies (2.4 and 2.5). Some of the qualities for the plaster type used in this study are described in section 2.6 and the last sub-chapter describes the material's advantages and limitations in association with analogue experiments (2.7).

## 2.2 Methodology (set-up)

A frame for the plaster is built for each experiment, consisting of a fixed part (part A in dark brown, Fig. 2.1) that is mounted onto a table, and a movable part (part B in light brown, Fig. 2.1). These parts are comprised of wooden planks that are high enough (4.5 cm) to keep the plaster from overflowing the edges. Plywood (thickness of 0.9 cm) and a jigsaw are used to build basement templates for the strike-slip experiments. The plywood plate is mounted onto the movable part of the frame, as shown in Figures 2.1 and 2.2. A plastic barrier/ liner is added on top of the fixed part of the frame, but under the movable part, to prevent leakage (Fig. 2.2). The frame is sealed with a soft barite mixture (barite and water mixed together, with a consistency of soft butter) along the inside edges of the movable frame, as well as where the two parts of the frame are joined (the grey parts in Figure 2.1 and the white mixture in Figure 2.2).

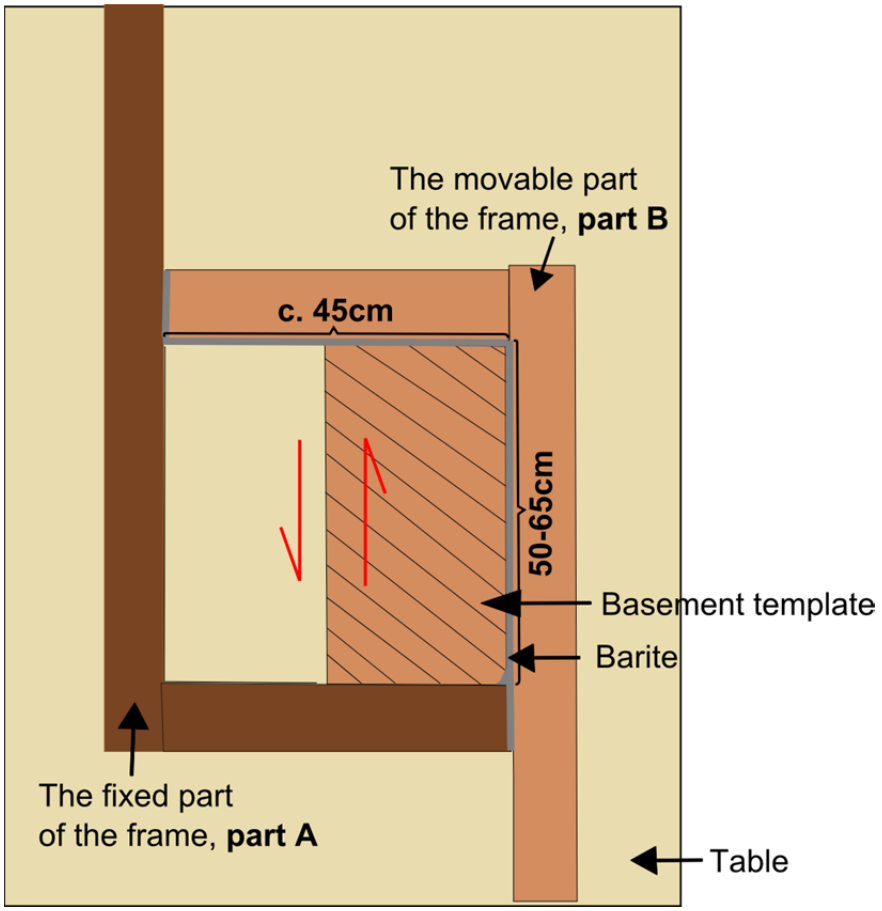


**Figure 2.1:** Top-down view of the setup for the experiments.

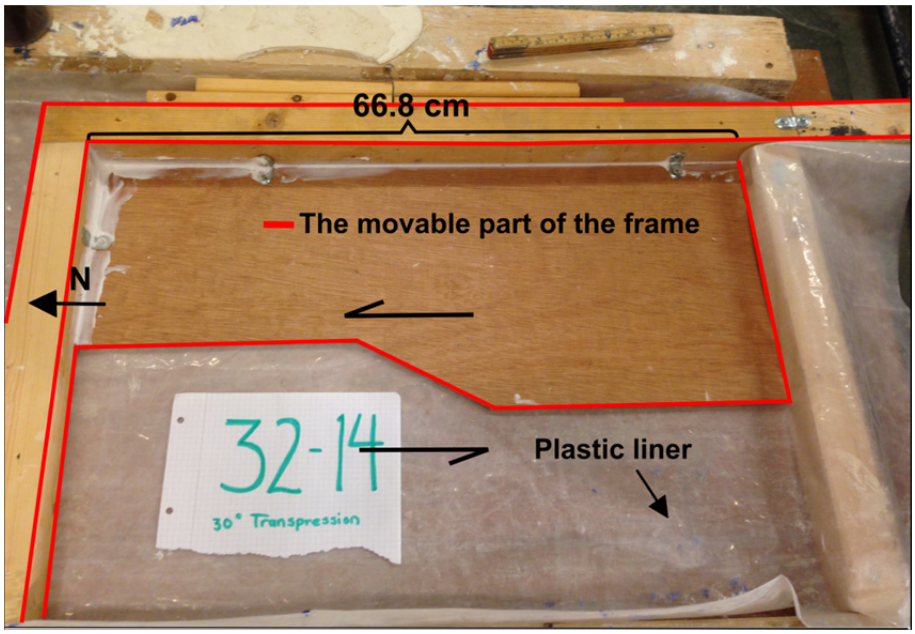


**Figure 2.2:** A top-down view of the setup for model 32-14. The parts that are outlined in red are mounted together and constitute the movable part of the frame.

The plaster is mixed with cold water, and this mixture is stirred until it has the consistency of thick pancake batter. From experience the plaster mixture should consist of approximately 1 ½ parts plaster per 1 part water (measured in liters). According to Saint Gobain Formula the mixture should contain 1.55 parts plaster per 1 part water measured in weight (http://www.saintgobainformula.com/Products/Plaster/Molda-3-Normal). The plaster is poured into the frame which at this point is fixed and not moving while the experiment is being prepared. Marker stripes are applied on the top surface of the wet plaster, normal to the displacement direction. This is done with a paint brush and acrylic paint (Fig. 2.3). The consistency of the plaster is checked repeatedly by dipping the head of a nail into the mixture. When the nail is pulled out of the plaster and a mound forms, the plaster has consolidated sufficiently to deform by brittle deformation yet still being able to yield under manually driven force. Part B is (manually) moved upwards along the long side of part A (Fig. 2.4). This motion represents movement along the basement fault template, and the plaster on top of the plywood plate moves with the frame, while the plaster outside of the plate does not move.

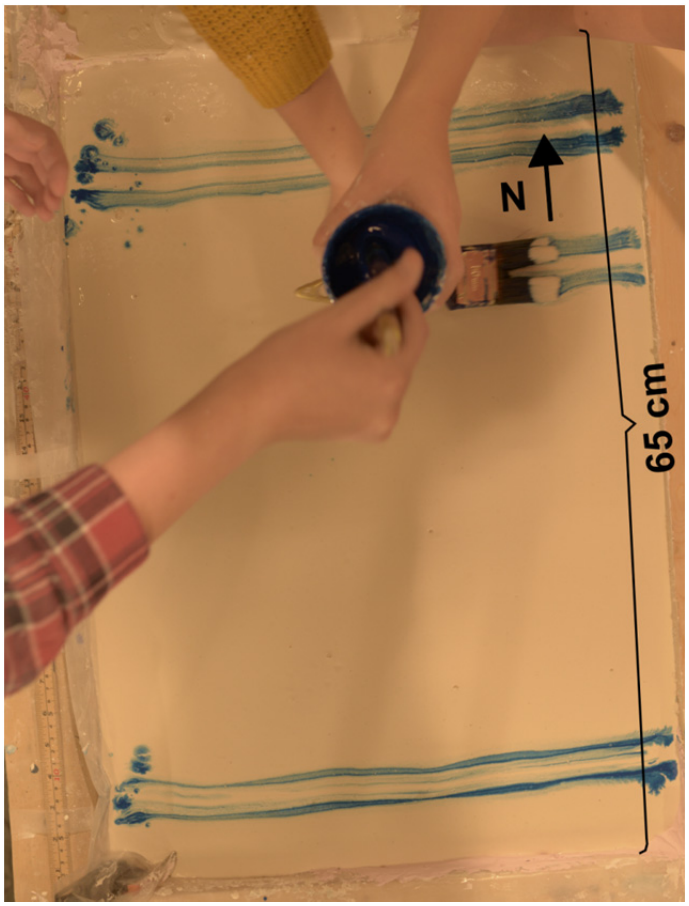


**Figure 2.3:** Marker stripes applied to the plaster (Exp. 34-14).

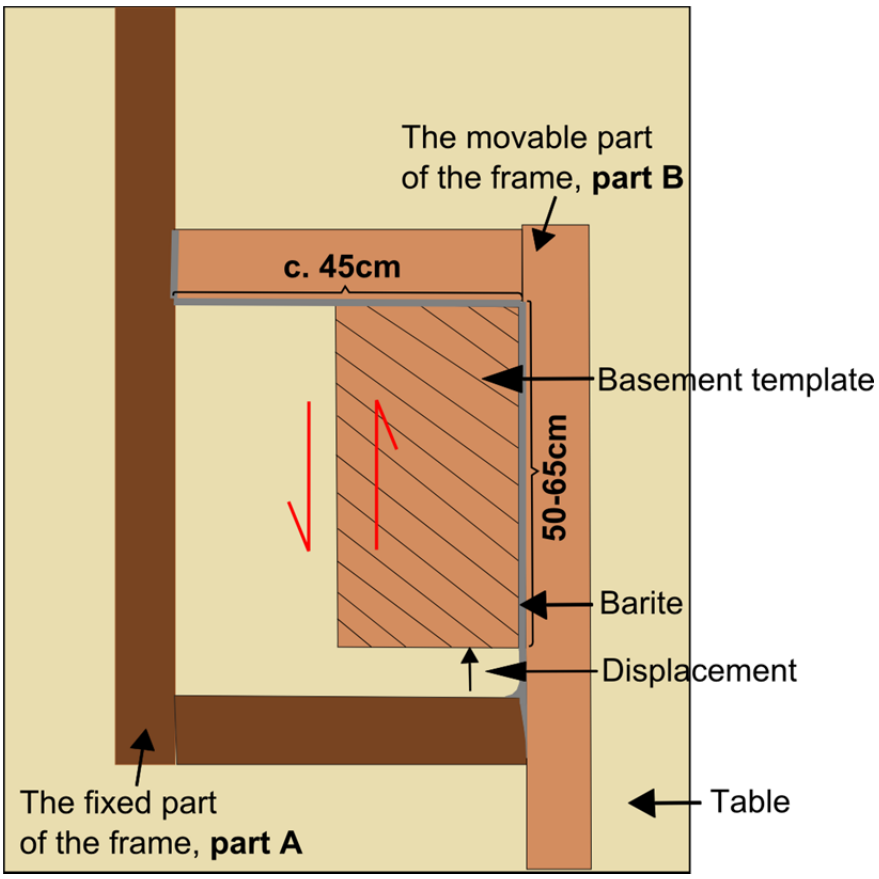


**Figure 2.4:** Top-down view of the set-up after displacement (without the plaster).

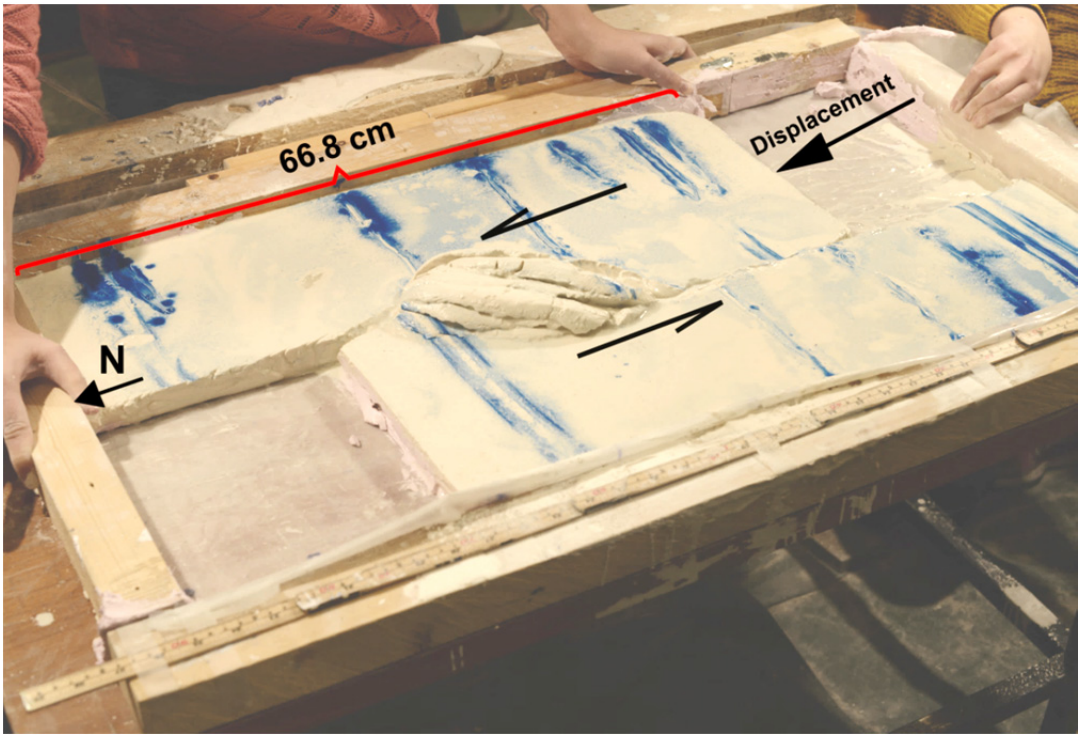


**Figure 2.5:** An oblique view of a model after displacement (experiment 32-14).

Pictures are taken approximately every quarter of a second, from directly above the experiment (pictures are taken from three angles, but the most important images are the ones shot top-down allowing a map-view inspection of the experiments). This makes it possible to observe the spatio-temporal evolution of structures during each experiment. The painted stripes are used as points of reference to measure the amount of displacement/ deformation throughout and after each experiment. Exact measurements of model dimensions are also done before and after deformation. After the model is subjected to deformation, it is left to completely solidify for about an hour, during which it releases heat.

## 2.3 Data processing

Three Nikon D800 cameras with AF-S Nikkor 50 mm f/1.4 G lenses were used for documenting the experiments. The pictures were used for analysing the deformational process for each experiment, and these had a resolution of 7360 x 4912 pixels. The software Inkscape was used for making figures that illustrated the models at different stages throughout the deformation. The interpretational figures were made by tracing structures in layers added on top of the pictures. The finished plaster models were also studied. Videos were made of each experiment in Microsoft PowerPoint and they comprised the pictures taken continuously during the deformational events (Appendix A). The duration of the videos was approximately the same as for the experiments they displayed and they were good tools for studying the development of the models.

## 2.4 Scalability

When developing a model representing a natural structural zone there are several aspects that need to be taken into consideration; one of these aspects is scalability. Koenigsberger and Morath (1913) were the first geoscientists that applied the concept of scalability to structures, but the scalability work by Hubbert (1937) is more well-known and has been the basis for later work in this matter. The models need to have similar geometric, kinematic, as well as dynamic properties to their natural examples in order to be an ideal representation (Hubbert, 1937; Ramberg, 1981; Schlische & Withjack, 2009).

*Geometric similarity* is achieved when the model is a geometric copy of a different scale of the natural prototype. The length between any pair of corresponding points in the model and its natural prototype thus has to have a constant ratio (Ramberg, 1981).The model and its natural counterpart are *kinematically similar* when the model remains geometrically analogous to the natural prototype

at corresponding times throughout the evolution. *Dynamic similarity* is achieved when the ratio between the mechanical forces acting on equivalent particles in the model and the original is constant, given that the model and the original are kinematically and geometrically similar (Langhaar, 1951; Ramberg, 1981).

When aiming to make models similar to fault zones in nature one has to consider the scale difference, as well as the strength difference. A body of any material generally has a higher strength the smaller the body is. A lot of models made by scientists earlier were not good representations of their natural counterparts, due to the use of materials that were too strong at the modelling scale relative to the strength and size of the natural features (Hubbert, 1937). Cloos (1930) focused on the importance of the strength and scale relationships between the original and the model in his experimental work.

One of the models made for this thesis represents a real natural fault zone and the other models represent different types of strike-slip situations that can resemble many strike-slip zones in general. The models are not exact scale representations of natural fault complexes, but because the models are made of plaster they contain small-scale structures as well as large-scale structures and the structures in such models closely resemble structures formed in the crust (Fossen & Gabrielsen, 1996).

## 2.5 Experimental structural geology: Previous work

**Introduction**

Experimental modeling has been used as a method to acquire knowledge about structural geology for a long time. Sir James Hall, referred to as the father of experimental geology, pressed pieces of cloth or clay layers together to replicate folding from a specific area (Cadell, 1889). Since then, a lot of different materials have been used in experiments, the most conventionally applied ones being clay and sand. Other substances have occasionally been used in combination with these materials, such as honey and silicone putty (Dauteuil & Mart, 1998; Mart & Dauteuil, 2000; Vendeville et al., 1987). Plaster is a less common modeling substance compared to sand and clay, but it has been used in several studies the last few decades (Fossen & Gabrielsen, 1996; Gabrielsen & Clausen, 2001; Lindanger et al., 2004; Mansfield & Cartwright, 2001; Sales, 1987).

Analogue modeling has been carried out through time to imitate and get a better understanding of the deformation processes that have taken place in natural deformation zones. Attempts have been made to replicate the formation and evolution of different structures and structural zones through

the deformation of various materials. Examples of previous experimental work are given below, divided into categories of models made by clay, sand, sand in combination with other materials, as well as plaster. Because there has been less focus on the strike-slip regime in experiments in the past, examples of extensional and contractional modeling are also given.

**Clay**

Clay has been one of the most commonly used materials in geological experiments throughout time. It holds the ability to fracture and fold under a wide range of viscosities and its physical properties can be changed by adding water (Cloos, 1955). One can thus choose which viscosity is best suited for making its relative strength proportionate to the relative strength of the natural counterpart (Hubbert, 1937). Some disadvantages with clay are that very small structures do not form in this substance, and due to its grain size the models do not replicate the structures in nature perfectly scale-wise (Emmons, 1969; Fossen & Gabrielsen, 1996).

According to Hubbert (1937) the models developed by Hans Cloos up until 1930 were some of the first realistic analogue models developed in terms of the strength relationship between the model and the original. After calculating the required approximate strength of the modeling material, Cloos used clay with the consistency of thick cream (Hubbert, 1937). Hans Cloos' method was used in experiments done in the 1950s as well, and the models made presented a variety of structures, some of them being strike-slip faults with the development of en échelon fractures (Cloos, 1955). Wilcox et al. (1973) studied the process of wrench faulting (also known as transcurrent faulting) using clay overlying two tin sheets.

The process of inversion was studied in the 90s, when a movable wall attached to a base plate was pulled to extend a clay layer, and then pushed to invert the extensional structure. Several colored clay layers were added as the model was extended in order to see the effect of deformation on newly deposited layers (Eisenstadt & Withjack, 1995). In more recent years clay has been widely used for analogue modeling of extension. Clifton et al. (2000) studied the effect rift obliquity had on faults by displacing a metal plate below a clay layer. The middle part of the clay layer was on top of a latex sheet, and rifting started when the sheet stretched uniformly as the metal plate was moved (Clifton et al., 2000). Henza et al. (2011) examined how existing faults affected new faults formed in a second extensional phase. These experiments were set up similarly to previous experiments such as the modeling set-up made by Clifton et al. (2000), described above. Schlische et al. (2002) focused on the secondary features formed by oblique-slip normal faults, and they also made some strike-slip models. Wet clay layers of different colors represented the sedimentary cover, which for the strike-

slip models were placed on top of a fixed plate and a movable plate representing the two fault blocks (Schlische et al., 2002).

**Sand**

Sand has the ability to produce faults and fractures, but very small-scaled features do not develop in this material. Its large grain size presents a problem when comparing the model's characteristics to the attributes of the natural crustal rock (Fossen & Gabrielsen, 1996). Compared to models consisting of clay, sand models have wider fault zones, and the deformation is spread over a smaller amount of structures, mainly larger faults. Because faults propagate and link up fast in sand models compared to clay (and plaster) models, the fault planes become quite straight, and the models will less often contain relay ramps (Henza et al., 2010). Unlike clay and plaster, dry sand lacks the cohesive strength that is present in natural crustal rock. Models made with both sand and clay are harder to preserve than plaster models, but a gelatine solution can be infused into sand models to preserve them (Fossen & Gabrielsen, 1996; Naylor et al., 1986).

One modeling technique applied to sand was to place the substance in a divided frame, where one side/ fault block was moved along the other block, resulting in a strike-slip fault zone. Two different sand colors were used in order to show the displacement more clearly (Emmons, 1969). Naylor et al. (1986) examined the characteristics of faults formed in the cover above a basement transcurrent fault by moving one part of a table laterally against the other part of the table. McClay (1990) used sand when running extensional experiments due to its ability to produce the main structures formed in the upper part of the crust, important for hydrocarbon exploration. Braun et al. (1994) applied sand to examine the deformation associated with listric normal faulting. More recently, Schlische and Withjack (2009) studied the formation and evolution of fault domains in the extensional regime using sand in some of the experiments. This was carried out in a similar manner to the experiments done by Clifton et al. (2000), where the sand deformed with the underlying latex sheet (Schlische & Withjack, 2009). McClay and Bonora (2001) performed analogue modeling using sand to examine the formation of positive structures developed by transpression at restraining bends. Some of their experiments involved synkinematic sedimentation with the addition of differently colored sand layers during deformation (McClay & Bonora, 2001).

**Sand in combination with other materials**

Sand has also been used in combination with other materials. Brun et al. (1994) used sand and silicone to model detachment faults, wherein the sand represented the brittle upper crust and the silicone mimicked the ductile lower crust. Salt tectonics has been the focus of many experimental

studies in the 1990s and in more recent years, in which sand has represented part of the sedimentary cover material (e.g. Brun & Fort, 2011; Fort et al., 2004; Vendeville, 2005). Analogue modeling was performed to examine deformation in cover material, resulting from underlying reactivated basement- and salt extensional faults. Silicone polymer represented the salt in these experiments, and the cover material was modeled using dry quartz sand as well as spherical glass beads (Dooley et al., 2005). Dooley et al. (2007) studied the development of thrust belts with a salt base, utilizing silicone and silica sand as well as hollow ceramic microspheres representing the salt and the cover material, respectively. These scientists also modeled the process of lateral compression on salt stocks, using the same materials as for their thrust belt study (Dooley et al., 2009). Smit et al. (2008) examined the effect of the model's rheology and the stepover width on the development and geometry of pull-apart basins. They used sand as a representation of the brittle crustal material and a layer of silicone was used in some experiments as the ductile crust.

**Plaster**

Plaster has also been used for geological modeling purposes throughout the years. Cadell (1889) used plaster of Paris interlayered with sand in his experiments in the 1800s in order to produce structures formed in a more brittle regime, as the experiments done earlier represented a more plastic regime. In these experiments the plaster powder was spread between damp sand layers, where the sand acted as a source of moisture for the plaster. When it had absorbed enough water the model was deformed, and if given enough time for consolidation it behaved in a brittle manner (Cadell, 1889).

Sales (1987) started using plaster in modeling mainly because of its ability to preserve and develop smaller scale structures, which had not been possible in methods involving other materials. Unlike Cadell's experiments, these plaster experiments did not involve the use of sand; the plaster was in some cases underlain by barite representing the basement structure. The model set-up for the strike-slip experiments consisted of a wooden frame and two basement boards. The main fault would form where the two boards met, in the overlying plaster (Cadell, 1889; Sales, 1987).

Mansfield and Cartwright (2001) did a plaster modeling project focusing on the linkage of faults in the extensional regime. Crystacal plaster and barite was deformed in a similar manner to the experiments done by Sales (1987). In the last 2-3 decades, many plaster experiments have been run in the structural geology laboratory at the University of Bergen. The fundamentals of the method described by Sales (1987) have been followed for the plaster modeling at this University. In the early 90s Ottesen (1991) and Odinsen (1992) focused on strike-slip and extensional fault modelling,

respectively, for their master theses. Extensional experiments were also run by Fossen and Gabrielsen (1996), as well as by Gabrielsen and Clausen (2001) more recently. Lindanger et al. (2004) studied the structures developed in the hanging wall in extensional experiments, using a ramp-flat-ramp basement. For this master thesis some small adjustments have been made in the experimental set-up, further described in the methodology chapter.

## 2.6 Plaster of Paris

Plaster of Paris was used in these experiments and it is characterized by its fine and uniform grain-size (Fossen & Gabrielsen, 1996). The type of plaster used in this study is called Molda 3 Normal Plaster and its chemical composition is $CaSO_4 * ½ H_2O$. It has a gypsum purity of at least 91 %, and it is white in color. 97% of the plaster has a grain size less than 100 µm (http://www.saintgobainformula.com/Products/Plaster/Molda-3-Normal). Early on in the deformation of models the plaster has a finite amount of ductile strain due to its relatively high cohesive strength (Mansfield & Cartwright, 2001).

## 2.7 Advantages and limitations with plaster as the modeling material

**Advantages with plaster as the modeling material**

Plaster modeling is a quick process, and several models can be made in one day. When considering the grain size of the plaster type used, a model scaled up from the size of 50 cm to a natural area of 1 km gives a grain size of less than 10 cm (http://www.saintgobainformula.com/Products/Plaster/Molda-3-Normal). This characteristic makes the development and preservation of detailed, structural geometries possible, and the mm- to cm-scale structures developed in such models are known to quite accurately reproduce natural fault systems on the scale of hundreds of meters to kilometers (Fossen & Gabrielsen, 1996).

Following the experiment the plaster solidifies completely and the resulting model can be saved for further analysis. The structures developed in the plaster may shed light on small-scaled structural geometries that would fall below seismic resolution when present in natural fault systems (Fossen & Gabrielsen, 1996). This type of experiment is therefore helpful for a better understanding of the smaller-scale processes that occur in nature (Gabrielsen & Clausen, 2001).

**Limitations with plaster as the modeling material**

The plaster mixture can behave quite differently depending on several factors. The relative amount of water and plaster needs to be consistent in the experiments, as well as the temperature of the water. The mixture must be stirred properly to make the mixture as homogeneous as possible. If the mixture is not given enough time to thicken, water will percolate to the surface and ruin the marker stripes in addition to affecting the small-scaled structures developed with displacement. If it is too thick when poured into the frame, there will not be enough time to apply marker stripes, and the plaster will not spread out and form an even layer. This is why the mixture must have the consistency of thick pancake batter when poured into the frame. The deformational structures in the fault zones will be less complex when the plaster is deformed at a more brittle stage, whereas the ductile strain component is larger in experiments where weaker plaster is deformed (Lindanger et al., 2004). It is therefore important that the plaster mixture for the different experiments is made the same when comparing the models. In cases where the plaster is poured into the frame too early, plaster powder is sifted on top of the plaster prior to the application of marker stripes, in order to bind some of the the water percolating to the surface.

The thickness of the basement template might affect the experiments; due to this the basement templates made for this project all have a thickness of 9 millimeters. The friction between the plaster mixture and the table is another influencing factor.

# 3 Description of experiments

## 3.1 Introduction

The focus of this chapter is the description of the plaster experiments performed for this thesis. Some of the experiments are shown in less detail than others, as only certain aspects of these models are of importance. Sub-chapter 1.2 describes experiment 32-14, 34-14 and 36-14, which are models containing positive flower structures formed by transpressional bends at different angles to the main fault trend. The three next experiments (40-14, 39-14 and 37-14) are described in sub-chapter 1.3. These were made for comparing the deformation resulting from releasing bends of variable angle relative to the main fault trend in the basement templates. The last sub-chapter (1.4) documents experiments where basement templates resulted in both transpressive and transtensive structures. An overview of the experiments performed in this study is found in Table 3.1.

**Table 3.1**

| Experiment number | Date | Experimental conditions (Basement geometry) | Deformation |
|---|---|---|---|
| 1. 32-14 | 06.11.14 | 30° restraining bend | Transpression |
| 2. 34-14 | 06.11.14 | 45° restraining bend | Transpression |
| 3. 36-14 | 02.12.14 | 60° restraining bend | Transpression |
| 4. 40-14 | 03.12.14 | 30° releasing bend | Transtension |
| 5 . 39-14 | 02.12.14 | 45° releasing bend | Transtension |
| 6. 37-14 | 02.12.14 | 60° releasing bend | Transtension |
| 7. 19-14 | 19.02.14 | Two irregularities (paired restraining and releasing bends) | Transpression and transtension |
| 8. 08-13 | 13.11.13 | A large releasing bend and a small irregularity (paired restraining and releasing bend) | Transtension dominated. Transpression at the small irregularity |

**Table 3.1:** An overview of the experiments described in chapter 3 is given in this table.

The structures that formed in strike-slip experiments were located quite close to the main fault trace, and the deformation was active along the entire fault more or less simultaneously. Generally, a lot of brittle deformation occurred at the edges of each model. These were considered to be caused by so-called 'edge effects', which arose from the influence of the bounding box of the experiment. These are obviously not present in nature and were therefore disregarded. Figures throughout this chapter show the areas that were affected the most by the "edge effects" for each experiment.

All experiments were performed with sinistral fault movement. The experiments were given orientations to use as reference points in order to make the descriptions easier to follow; experiment

19-14 represented a natural fault zone and the orientations in this experiment were therefore the same as for the real fault zone. The marker stripes applied to the plaster were also used as reference points in the descriptions; these were given numbers from the southern edges of the experiments (shown in figures for each experiment). Percentages given in the descriptions represent the amount of displacement completed at specific stages in the deformation process, relative to the total amount of displacement (the total displacement being 100 %). Videos of the experiments are found on a in Appendix A. All the videos were made with north pointing up towards the northern edge of the video.

## 3.2 Transpressive experiments

Experiment 32-14, 34-14 and 36-14 resulted in models containing positive flower structures formed by transpressional bends of 30°, 45° and 60° angles, respectively. The faults that divided the flower structures into several fault blocks in these experiments were reverse and thrust faults. Reverse faults have a higher angle than 30° and thrust faults have an angle less than 30° (Fossen, 2010). The angles of these faults were hard to measure in the transpressive models and the term reverse fault was therefore used in the descriptions. These experiments were performed for gaining insight into the structural influence pertaining to restraining bends of different angles.

### 3.2.1 Experiment 32-14: 30° restraining bend

The basement template utilized in this experiment comprised a 30° restraining bend, leading to transpression (Fig. 1). The plaster mixture was slightly stiff when deformation was initiated, but the results were still of good quality. The pictures were not taken instantly from the time of movement initiation for this particular experiment, and the duration of movement and percentages representing the amount of movement completed are therefore slightly less precise compared to the values of the other experiments. The majority of the motion and all of the brittle deformation was documented. The plaster mixture was poured into the frame too early, and water percolated to the top, thus disrupting the marker stripes (Fig. 2). Seven marker stripes were applied to the plaster and the first one was located the furthest south (Fig. 2). General information about the setup and duration of experiment 32-14 is found in Table 3.2 and a video of the experiment is found in Appendix A (Video 1).

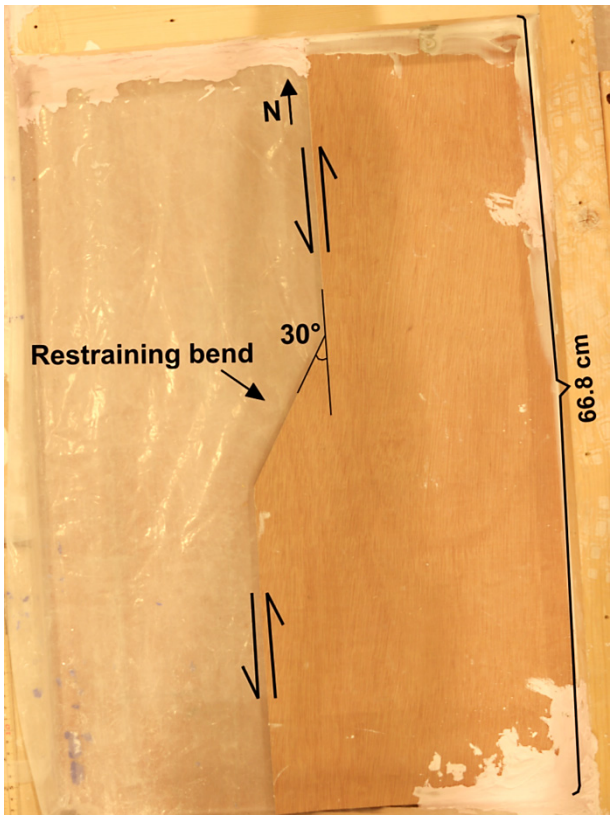


**Figure 3.1:** The basement template for experiment 32-14.

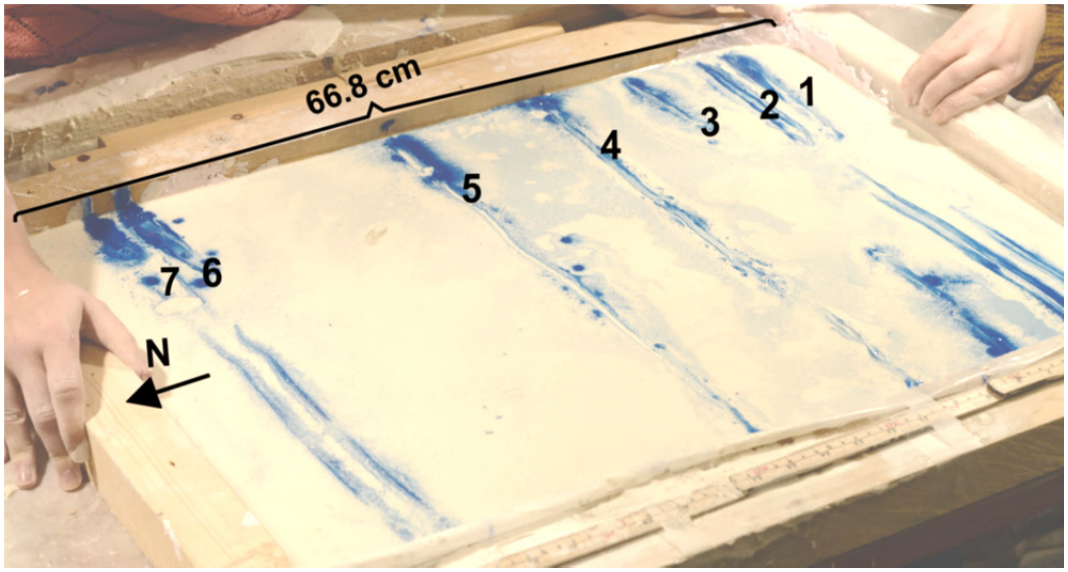


**Figure 3.2:** Marker stripes applied to the plaster (numbered from the southern edge).

**Table 3.2**

| | |
|---|---|
| Date of the experiment | 06.11.2014 |
| Plaster mixture | 9.5 liters of plaster and 6 liters of water |
| Plaster to water ratio | 1.58:1 |
| Duration | 11 seconds |
| Length of the short sides of the frame | 45 cm |
| Length of the long sides before and after displacement | Before displacement: 66.8 cm<br>After displacement: 87.7 cm |
| Total displacement | 20.9 cm |

**Table 3.2:** General information about the setup and duration of experiment 32-14 is given in this table.

The model started showing signs of brittle deformation after circa 7 % of the total movement of 20.9 cm (Fig. 3.3 A and B). Two fault traces became visible in the northern and the southern part of the model, and they consisted of several NNW-SSE oriented fractures/ fault segments arranged in a relatively straight line (N-S; Fig. 3.3 A and B). The fractures were characterized as riedel shear fractures and were synthetic relative to the main fault direction. Plaster had started accumulating and forming a pop-up structure in the area outlined in red in Figure 3.3 B. This figure also shows the location of the fault traces.

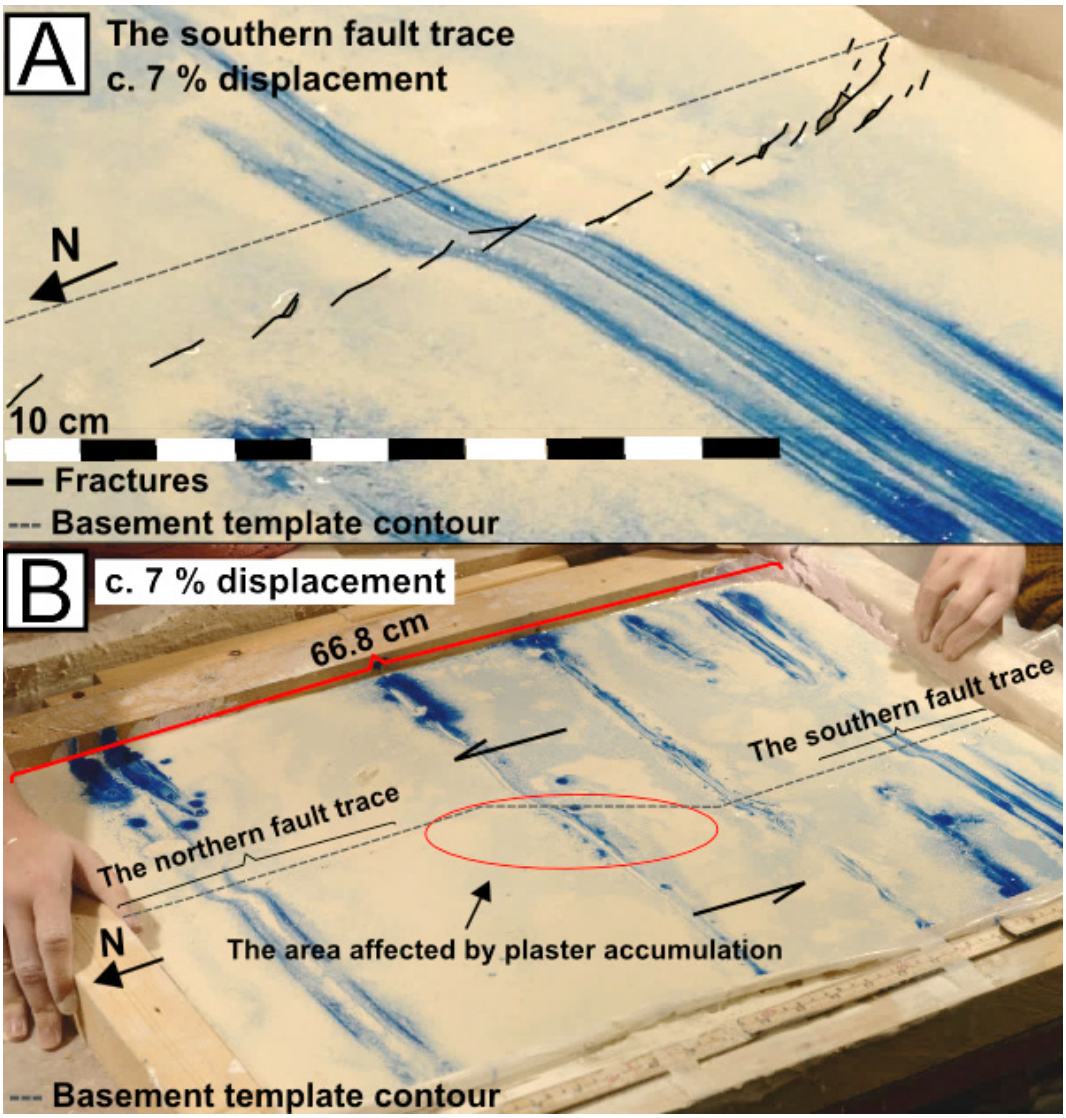


**Figure 3.3 A:** The southern fault trace (oblique view).
**B:** The model after 7 % of the displacement (oblique view).

The fault traces extended close to the pop-up structure shortly thereafter and they became more continuous with time as fault segments linked up. After c. 11 % of the displacement the positive structure was quite prominent and it could be defined as a positive flower structure (Fig. 3.4). The south-western part of the positive flower had moved slightly upwards relative to the flat plaster layer, thus representing a hanging wall in a reverse fault. The reverse faulting propagated northwards affecting the north-western side of the flower structure, and a hard link between the two fault traces had thus formed. Figures 3.5 A and B shows the flower structure c. 21 % into the movement.

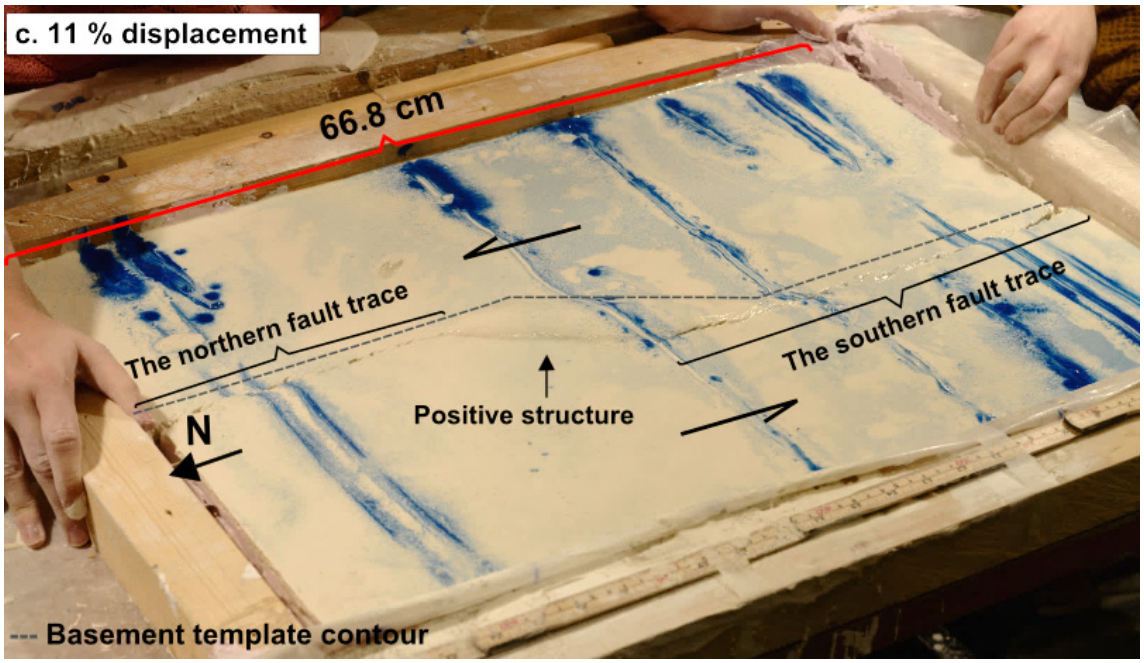


**Figure 3.4:** The model after c. 11 % of the displacement (oblique view).

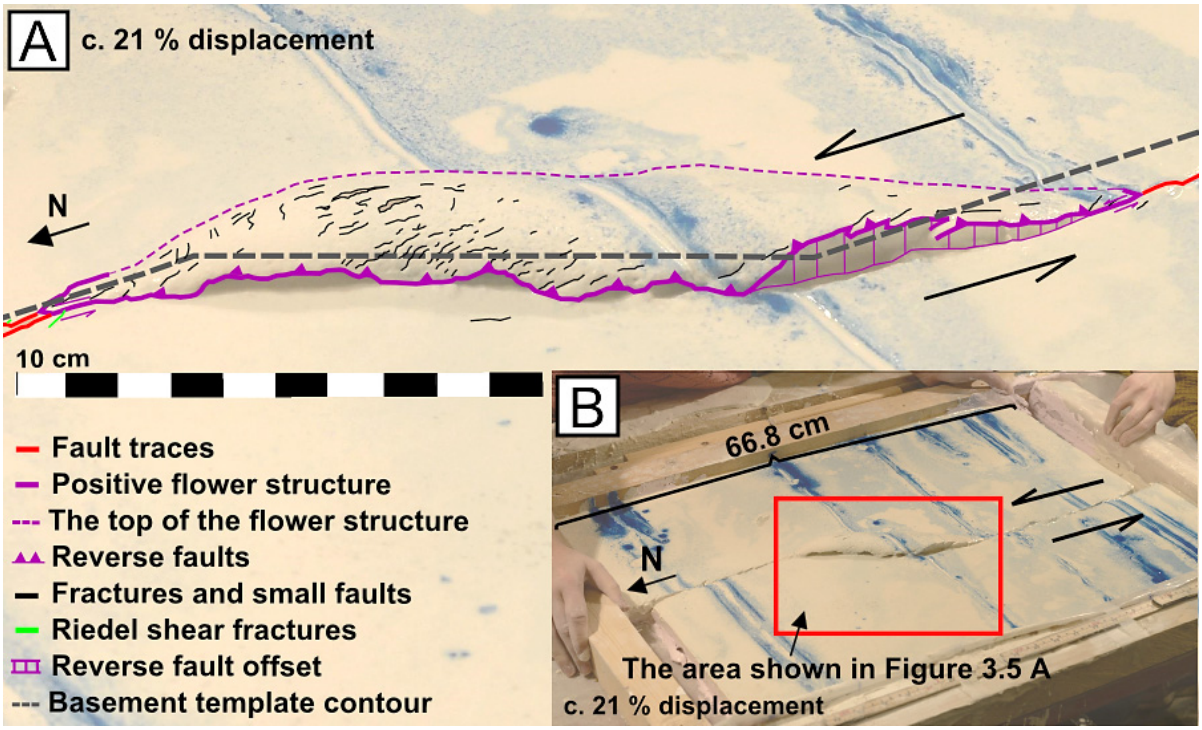


**Figure 3.5 A:** The positive structure c. 21 % into the displacement (oblique view).
**B:** The area lined in red represents the area shown in Figure 3.5 A (oblique view).

Between 23 % and 100% of the displacement another six fault blocks developed, bringing the total amount of fault blocks constituting the positive flower to seven (Figs. 3.7, 3.8 and 3.9). The formation of these blocks was evident by the plaster accumulation northwest of the flower structure, as shown in Figures 3.6 A and B which illustrates the flower after the formation of the second block. The fault blocks were separated by reverse faults and they evolved in sequence. The fault blocks thus propagated towards the foreland, placing the youngest blocks beneath the older ones and closest to the foreland (to the north) (Morley, 1988).

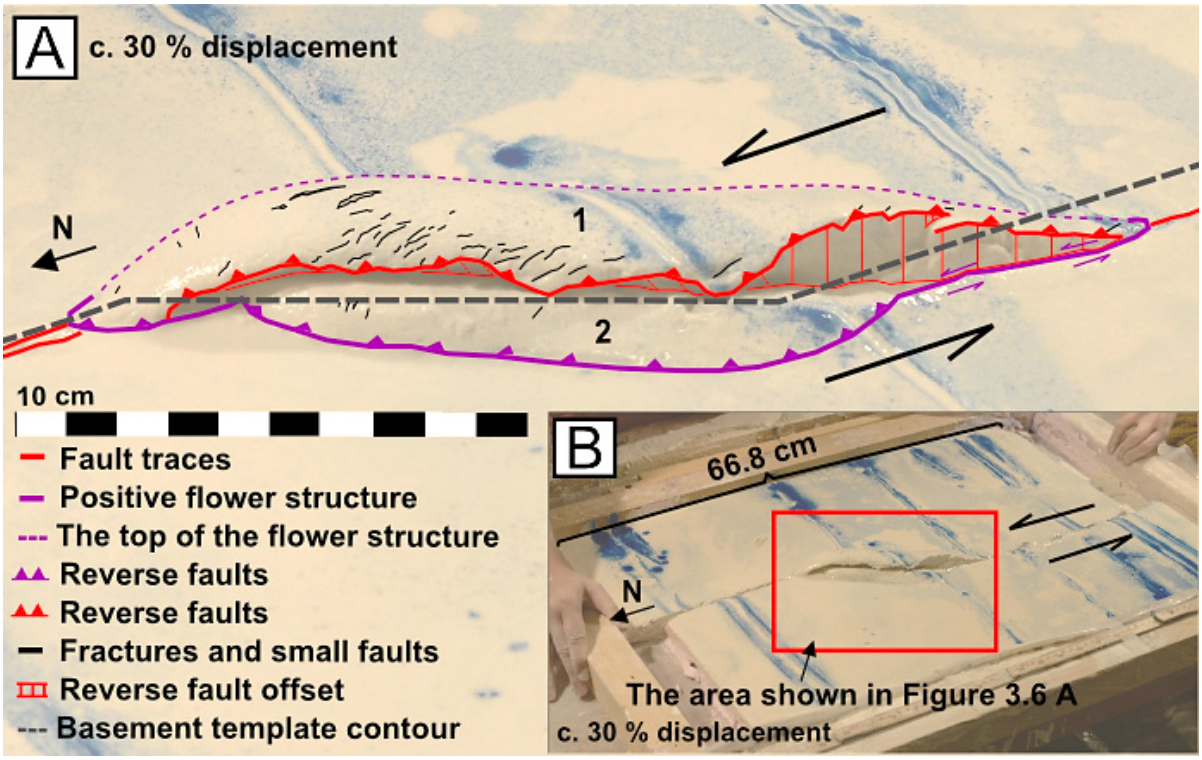


**Figure 3.6 A:** The flower structure after c. 30 % of the displacement (oblique view).
**B:** The red square portrays the area shown in Figure 3.6 A (oblique view).

The third fault block was relatively small, underlying the northern half of the second block (Figs. 3.7 A B). The reverse fault that separated fault blocks 4 and 5 was reactivated as a normal fault shortly after the formation of fault block 5. The fourth block represented the hanging wall (Figures 3.8 A and B show the flower structure before this normal fault displacement and Figure 3.9 A shows the flower structure after displacement). After the formation of all seven fault blocks, the three northernmost ones (fault blocks 5-7) rotated slightly clockwise towards the northeast as one unit, whilst the four southern blocks did not rotate (fault blocks 1-4) (Video 1, Experiment 32-14).

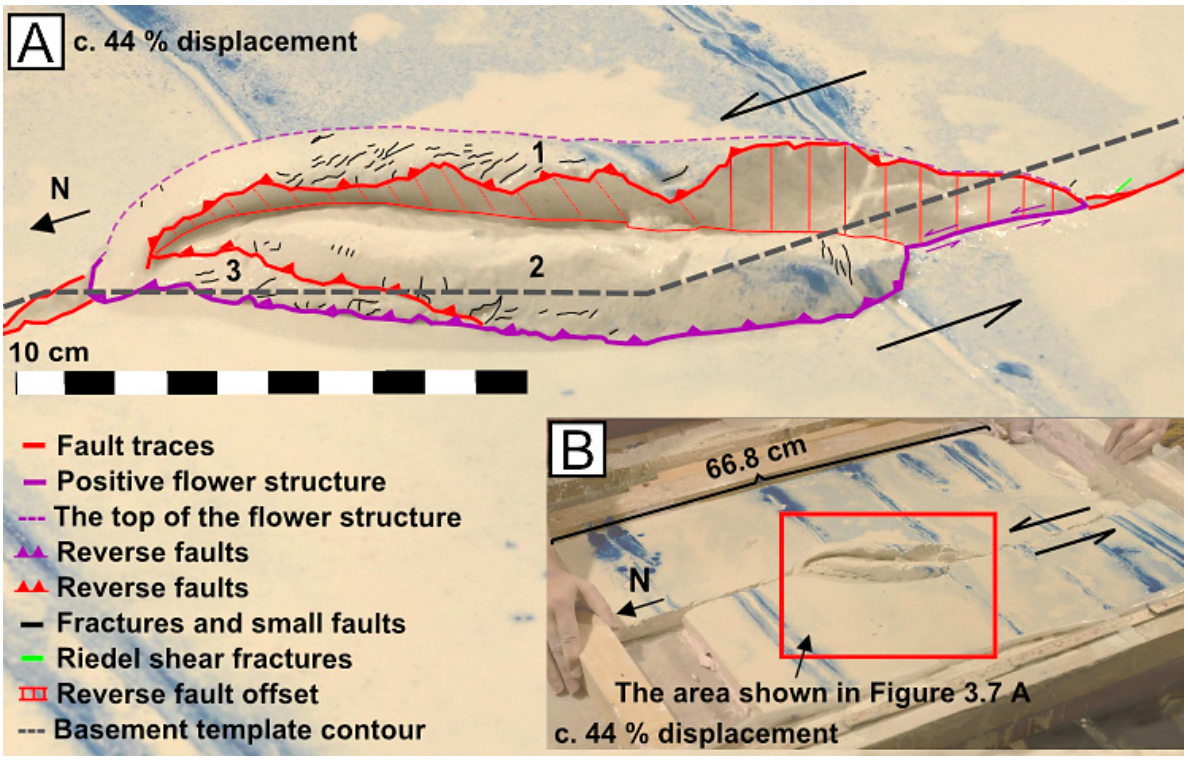


**Figure 3.7 A:** The flower structure c. 44 % into the displacement (oblique view).
**B:** The red square portrays the area shown in Figure 3.7 A (oblique view).

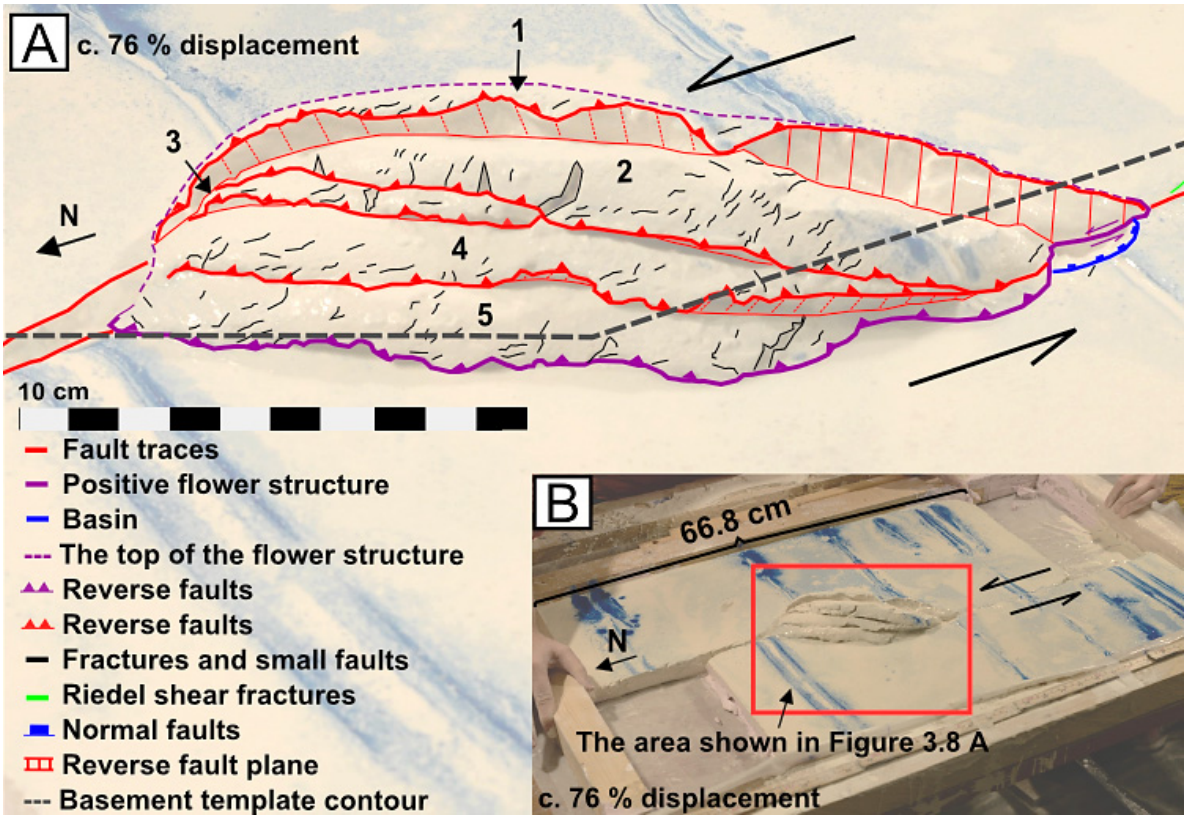


**Figure 3.8 A:** The flower structure c. 76 % into the displacement (oblique view).
**B:** The area lined in red represents the area shown in Figure 3.8 A (oblique view).

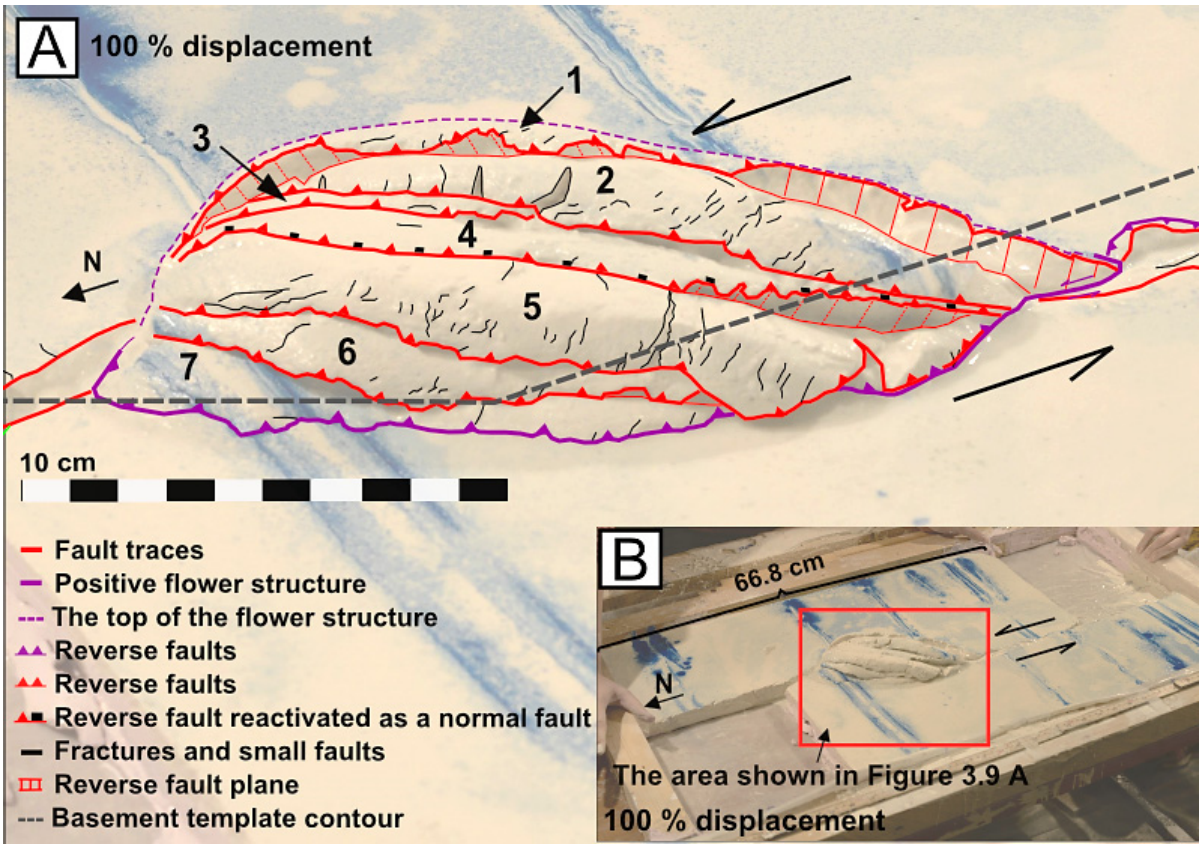


**Figure 3.9 A:** The flower structure after displacement. The fault blocks are numbered (oblique view).
**B:** The red square portrays the area shown in Figure 3.9 A (oblique view).

A small positive structure was located between the second and third marker stripe and the width of the fault trace varied in the southern half of the model, as shown in Figures 3.10 A and B. The deformation was more complex close to the major flower on the southern side. A few of the marker lines were slightly deflected towards the movement direction.

Riedel shear fractures were evident along the fault trace in the northern part of the model, particularly on the eastern fault block, as indicated in Figures 3.10 A and B. Some could be seen south of the flower structure, but they were not as many or as apparent as in the northern part. The angle between these and the main fault ranged between c. 10-19°. The fractures on top of the flower structure had the main orientations NW-SE and NE-SW, and there were also some oriented E-W (Figs. 3.10 A and B).

The model was 87.7 cm long after the experiment, making the total displacement 20.9 cm. The length of the flower structure was c. 21.5 cm in the finished model, and it had a maximum height of c. 4.5 cm. Fault blocks 1-6 in the flower structure all showed a sense of ductile deformation, as their edges folded slightly downwards (towards the northwest) when they moved upwards (Fig. 3.9 A). The positive flower formed with a similar angle to the basement template in the early stages of the

experiment, and eventually rotated slightly clockwise giving an overall angle of 30-35° relative to the main fault direction. The fault blocks constituting the flower structure had similar angles to the overall structure (Figs. 3.10 A and B).

The angles of the reverse fault planes gradually decreased upwards, as faults in flower structures are inclined to widen upwards (Fossen, 2010).

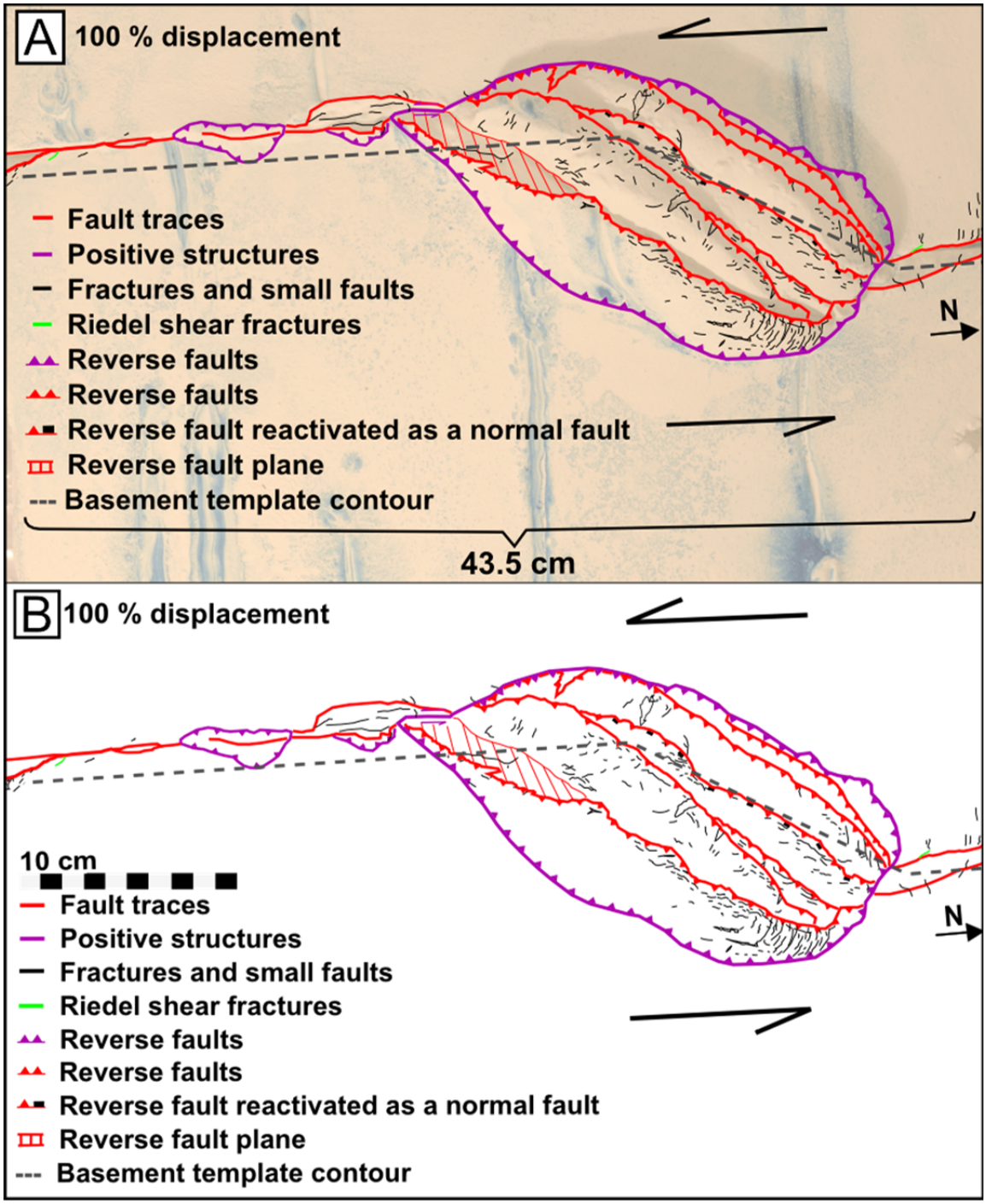


**Figure 3.10 A and B:** The final interpretation of experiment 32-14.

The area that was the most affected by edge effects is outlined in purple in Figure 3.11 and the red square portrays the area shown in Figures 3.10 A and B.

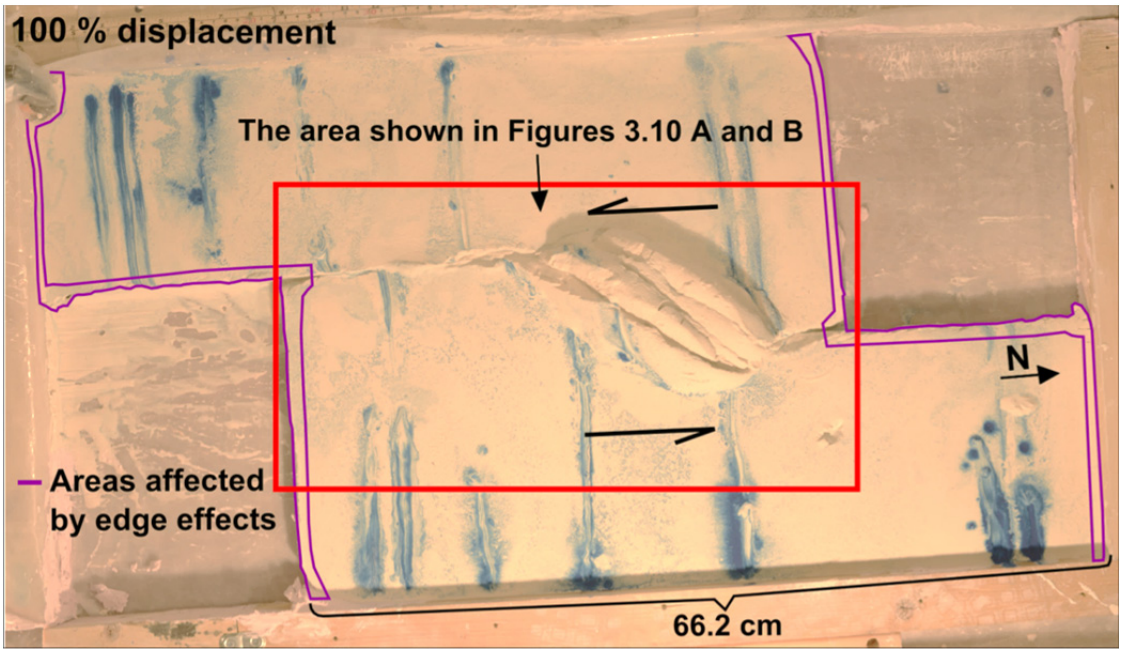


**Figure 3.11:** The red square portrays the areas shown in Figures 3.10 A and B and the areas lined in purple were the most affected by edge effects.

### 3.2.2 Experiment 34-14: 45° restraining bend

The basement template utilized in this experiment had a 45° restraining bend, leading to transpressional deformation (Fig. 3.13 A). The plaster was a bit too stiff when the movement was initiated, but the structures formed were still of good quality. Five sets of marker stripes were used as reference points in the description of this experiment; they were numbered from the southern edge of the model (Fig. 3.13 B). General information about the setup and duration of experiment 34-14 is found in Table 3.3 and a video of the experiment is found in Appendix A (Video 2).

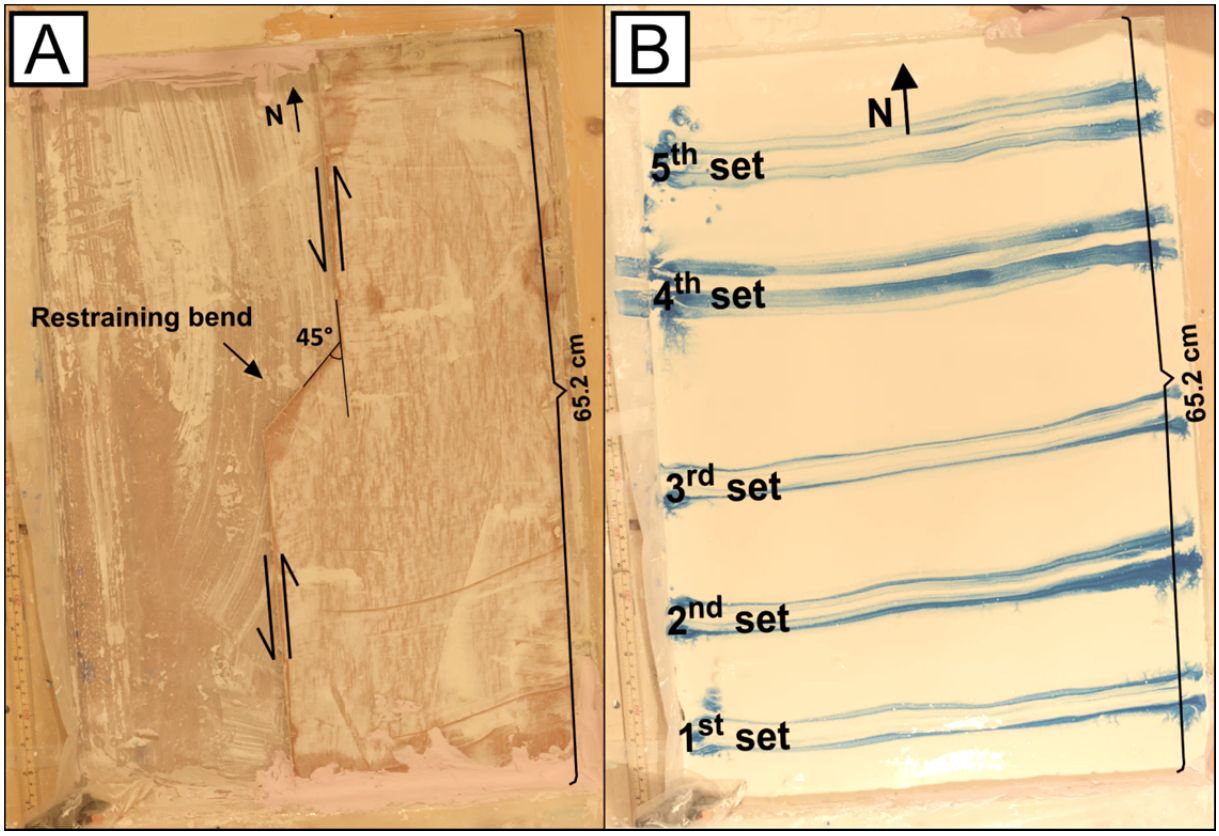


**Figure 3.12 A:** The basement template. **B:** Marker stripes applied to the plaster (numbered from the south).

**Table 3.3**

| | |
|---|---|
| Date of the experiment | 06.11.2014 |
| Plaster mixture | 10 liters of plaster and 6 liters of water |
| Plaster to water ratio | 1.66:1 |
| Duration | 16 seconds |
| Length of the short sides of the frame | 44 cm |
| Length of the long sides before and after displacement | Before displacement: 65.2 cm<br>After displacement: 89.9 cm |
| Total displacement | 24.7 cm |

**Table 3.3:** General information about the setup and duration of experiment 34-14 is given in this table.

Brittle deformation commenced after c. 8 % of the total displacement of 24.7 cm (Figure 3.13 B shows the model c. 11 % into the movement). Beginning fractures (very faint stripes) with the main orientations NNW-SSE and WSW-ENE formed through the southern half of the model. The first ones mentioned were synthetic relative to the main fault direction and were classified as riedel shear

fractures. The latter ones were characterized as riedel marked shears. The light reflection north of the third stripe-set showed that plaster started accumulating here, forming a pop-up structure (Fig. 3.13).

Two fault traces formed on both sides of the positive structure and they comprised NNW-SSE and some N-S oriented fractures. The location of these segments and the area of plaster accumulation are shown in Figure 3.13, c. 11 % into the movement. The southern fault trace developed earlier than the northern trace.

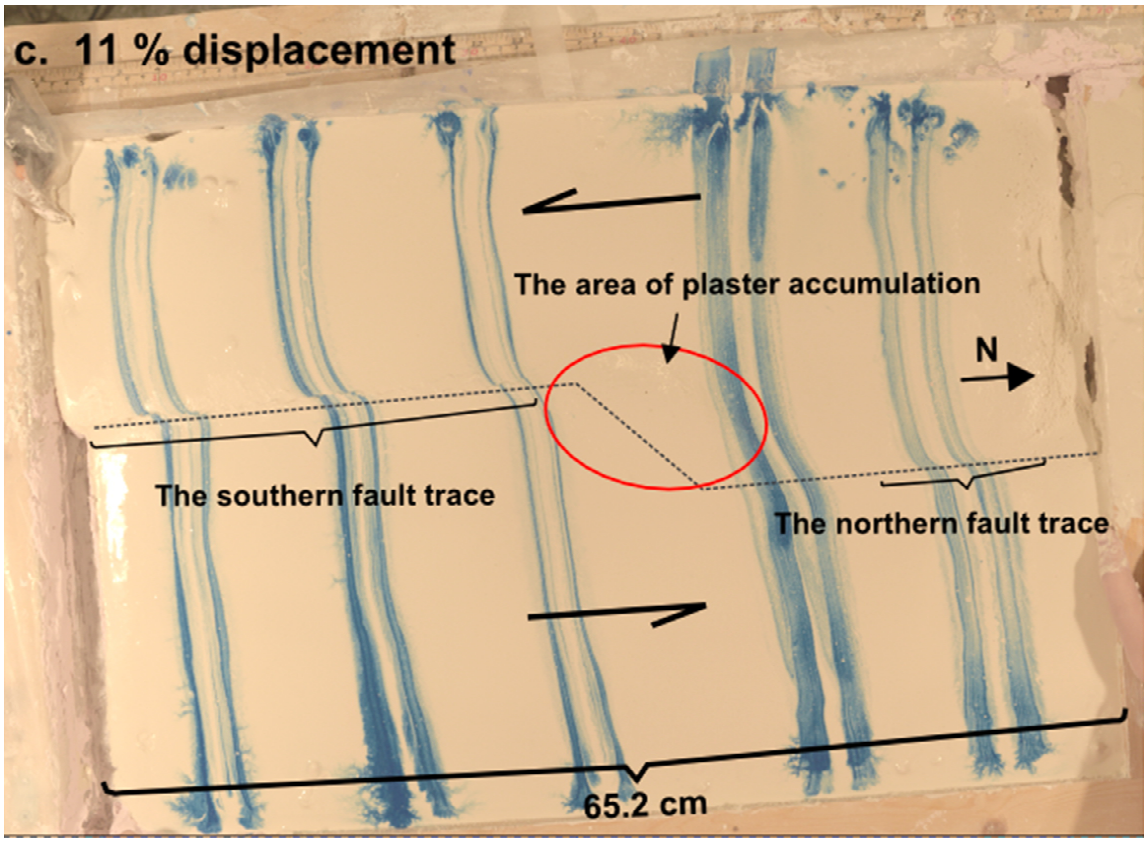


**Figure 3.13:** The model after c. 11 % of the displacement.

All the marker lines showed displacement c. 14 % into the movement. The western edge of the positive structure had become more defined and a hard-link between the two fault segments had thus formed. The western side of the structure moved upwards compared to the adjacent flat plaster, thus representing the hanging wall in a reverse fault. The south-eastern and eastern edge of the pop-up structure became distinct shortly after, and it was defined as a positive flower structure. Figures 3.14 A and B display the flower approximately 25 % into the movement.

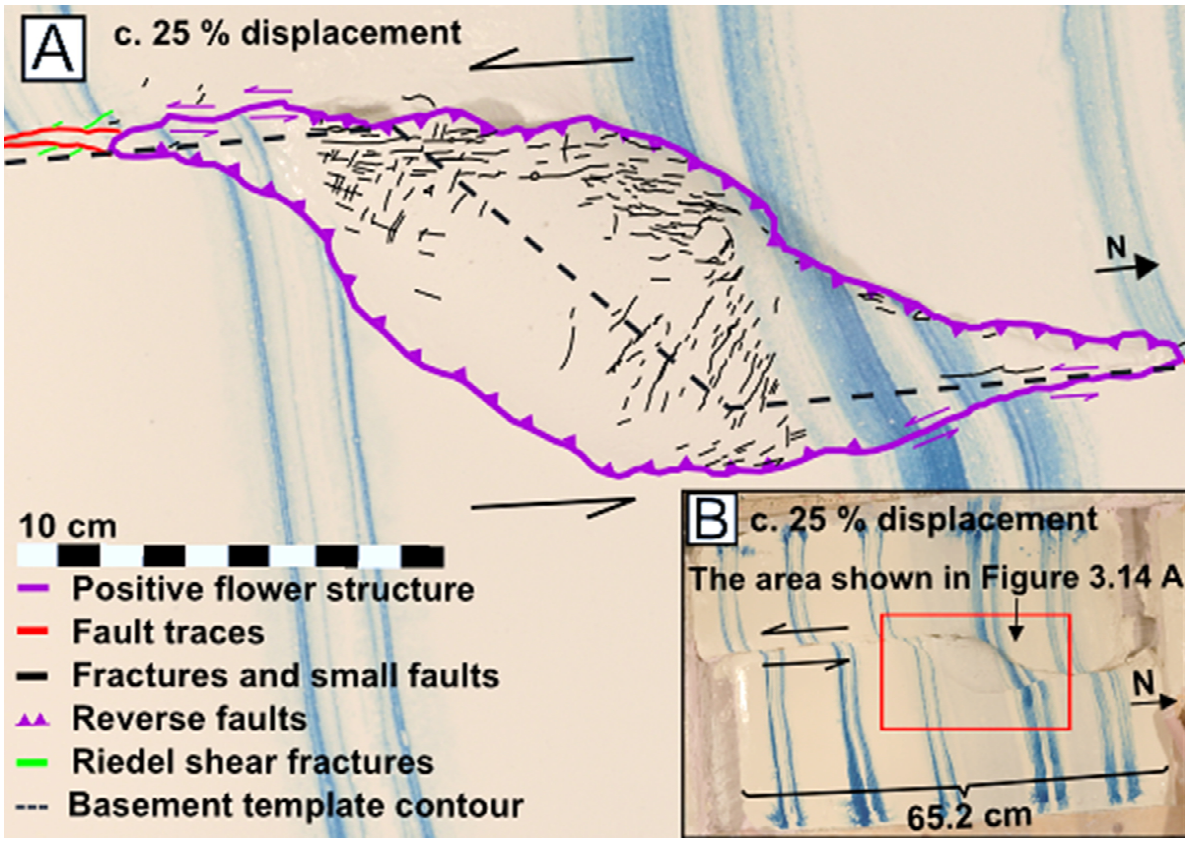


**Figure 3.14 A:** The positive flower structure c. 25 % into the displacement.
**B:** The red square portrays the area shown in Figure 3.14 A.

Between approximately 32 % and 100 % of the displacement four more fault blocks developed as part of the flower, and this structure thus comprised five fault blocks in total (Figs. 3.15 and 3.16). The northwestern outer rim of the flower was not as defined as the rest of the rim after displacement. A significant amount of reverse displacement was evident on its western edge.

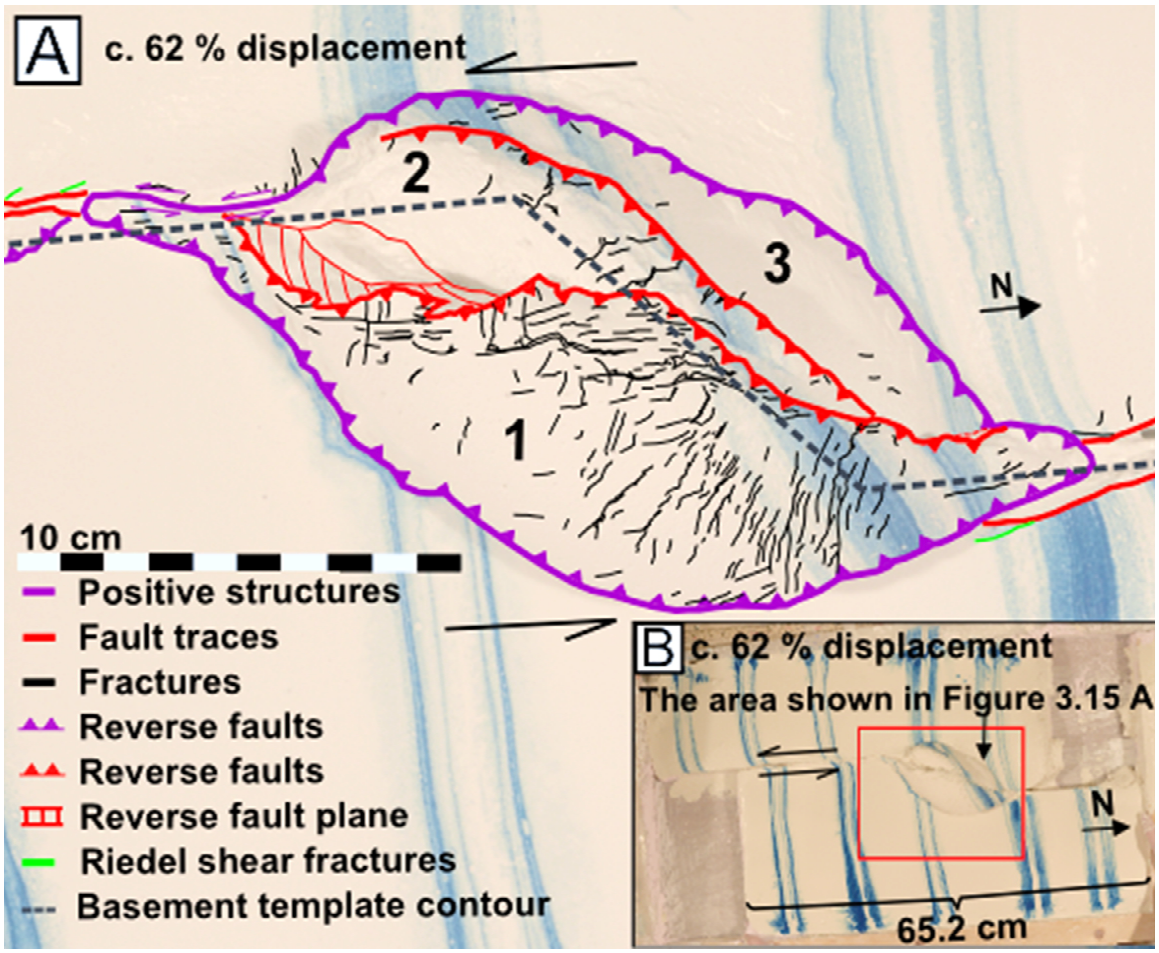


**Figure 3.15 A:** The flower structure c. 62 % into the displacement.
**B:** The area outlined in red represents the area shown in Figure 3.15 A.

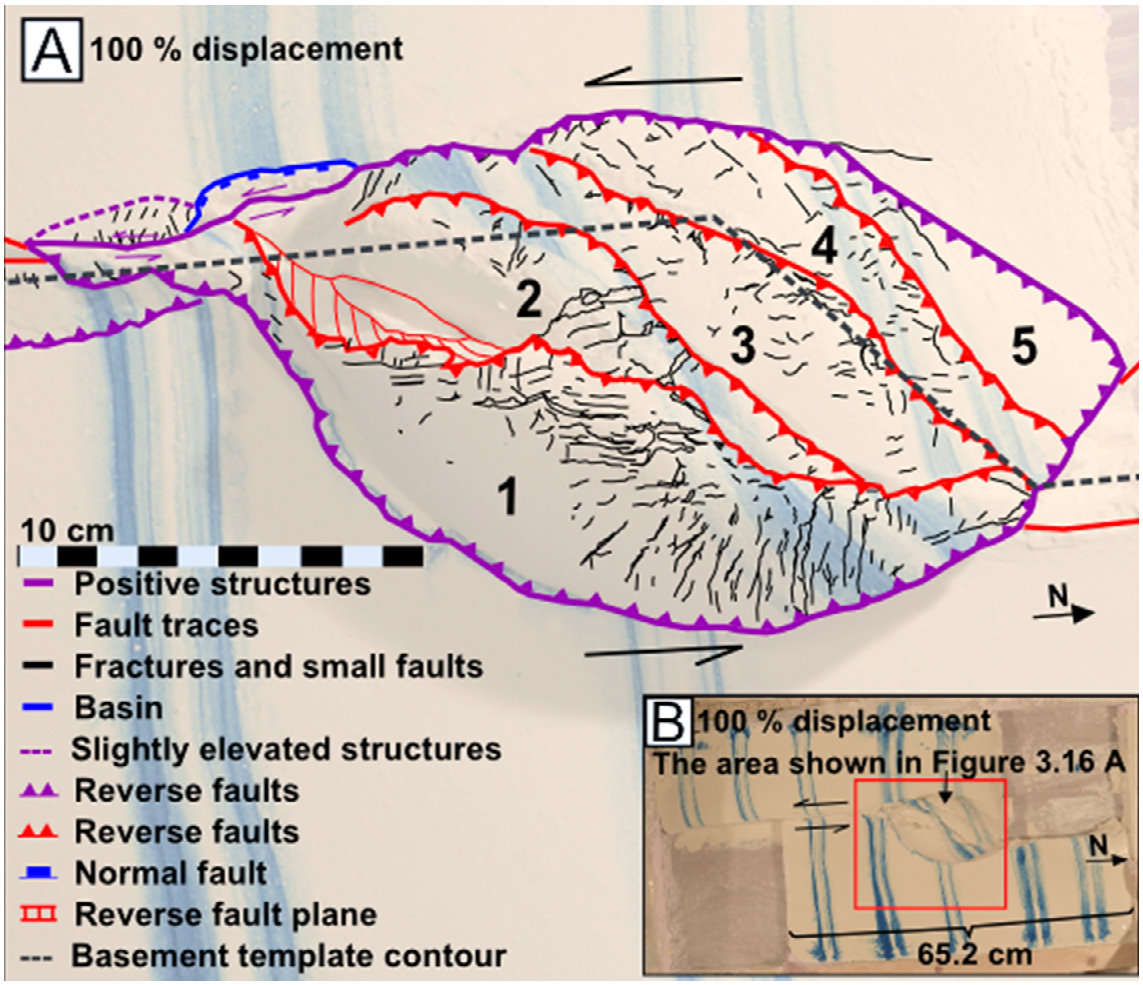


**Figure 3.16 A:** The flower structure after displacement.
**B:** The red square portrays the area shown in Figure 3.16 A.

The fault trace south of the flower structure developed with a degree of normal displacement; the eastern fault block had moved downwards compared to the western block and thus defined the hanging wall (Figs. 3.17 A and B; These figures make the fault south of the flower appear wide, but this is only due to the normal displacement). A relatively shallow and narrow basin had formed at the southwestern edge of the flower structure. Some small positive structures had developed in the southern half of the model, particularly in the area closest to the flower structure, as shown in Figures 3.17 A and B. All the marker stripes showed varying degrees of deflection towards the movement direction.

The flower structure had fractures with a big variety of orientations: N-S, NNE-SSW, WSW-ENE, NW-SE and NE-SW (Fig. 3.16 A). Some riedel shear fractures were evident in the finished model, the angle between these and the main fault ranged between c. 15-20° (shown in green in Figs. 18 A and B). The length of the model was 89.9 cm after the experiment, bringing the total displacement to 24.7 cm.

The positive flower structure had a length of approximately 21.5 cm and it had a maximum height of 5 cm (relative to the flat plaster surface). The overall angle of this structure relative to the main fault was c. 20°, and the angles between the fault blocks constituting this structure and the main fault ranged from c. 20° in the south to 40-50° in the north. The reverse faults separating the fault blocks became less steep further upwards in the flower structure.

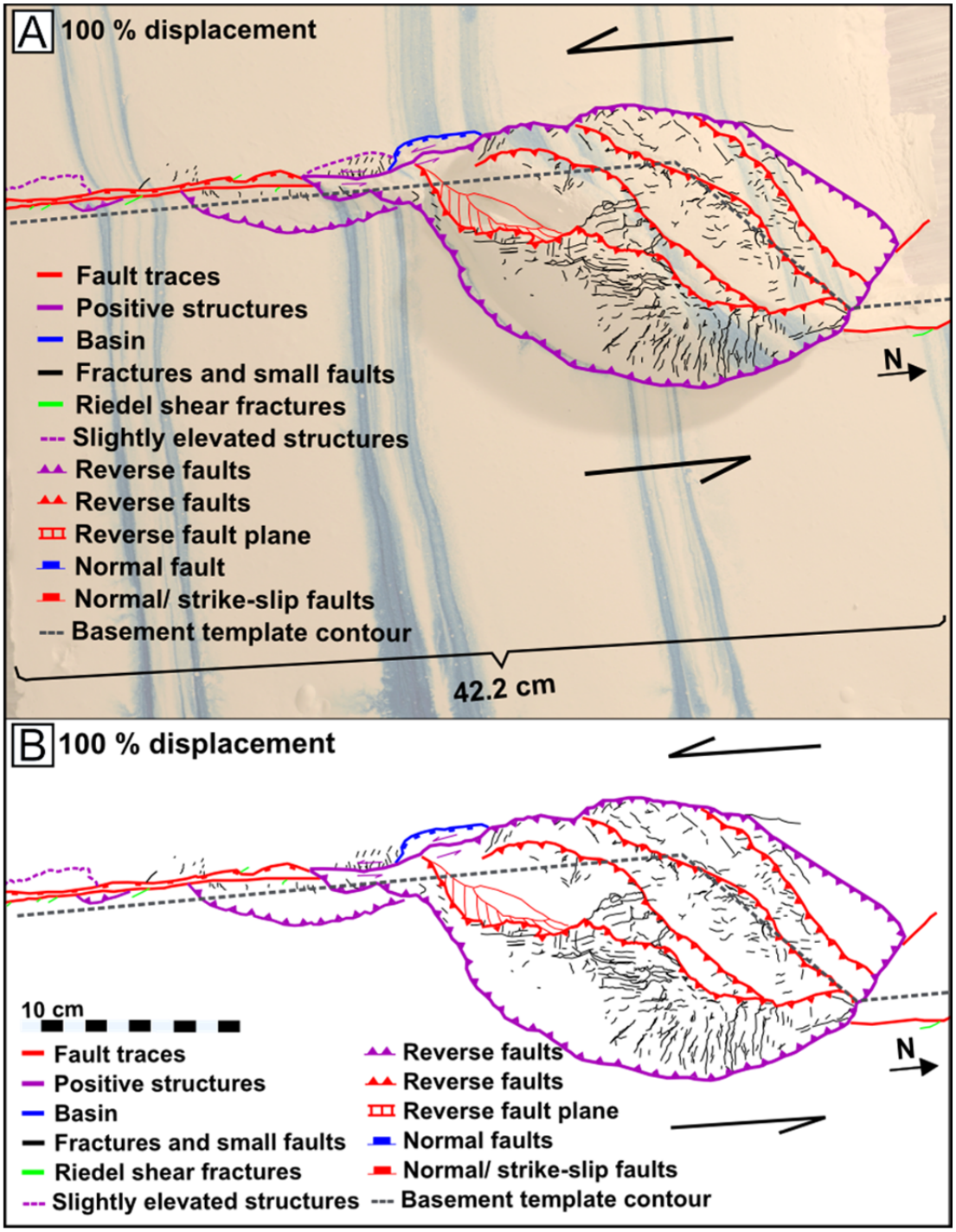


**Figure 3.17 A and B:** The final interpretation of experiment 34-14.

The area portrayed in Figures 3.17 A and B  is outlined in red in Figure 3.18 and the areas that were the most affected by edge effects in this experiment are outlined in purple.

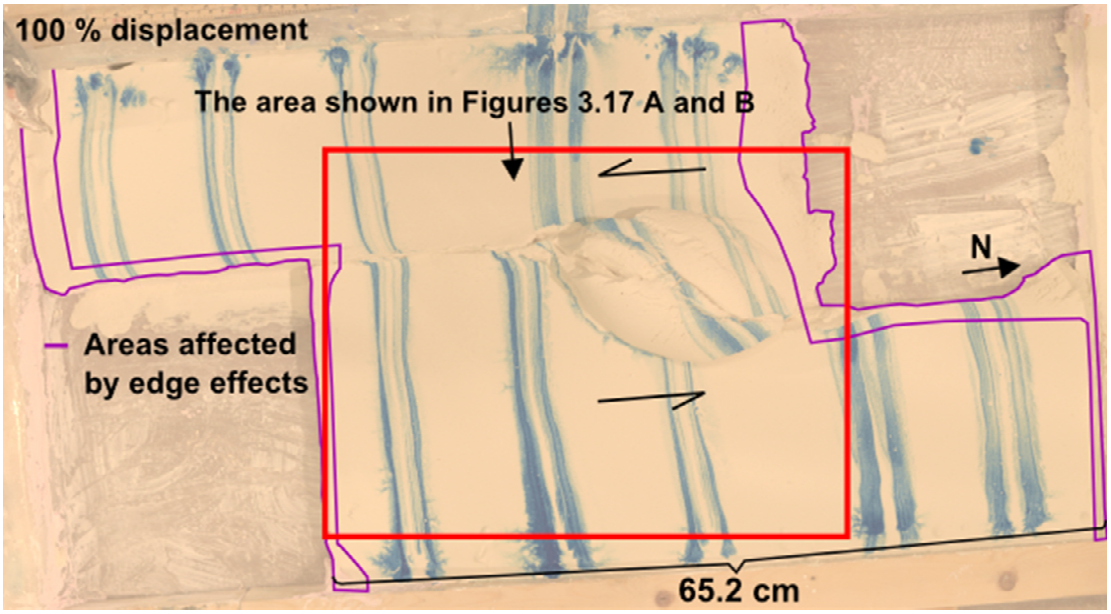


**Figure 3.18:** The red square portrays the areas shown in Figures 3.17 A and B and the areas lined in purple were the most affected by edge effects.

### 3.2.3 Experiment 36-14: 60° restraining bend

The basement template used in this experiment comprised a 60° restraining bend, causing transpressional deformation (Fig. 3.19 A). The plaster consistency was ideal when deformation was initiated. Five sets of marker stripes were applied to this plaster model, and these were used as reference points in the description, with the first set being the southernmost one (Fig. 3.19 B). General information about the setup and duration of experiment 36-14 is found in Table 3.4 and a video of the experiment is found in Appendix A (Video 3).

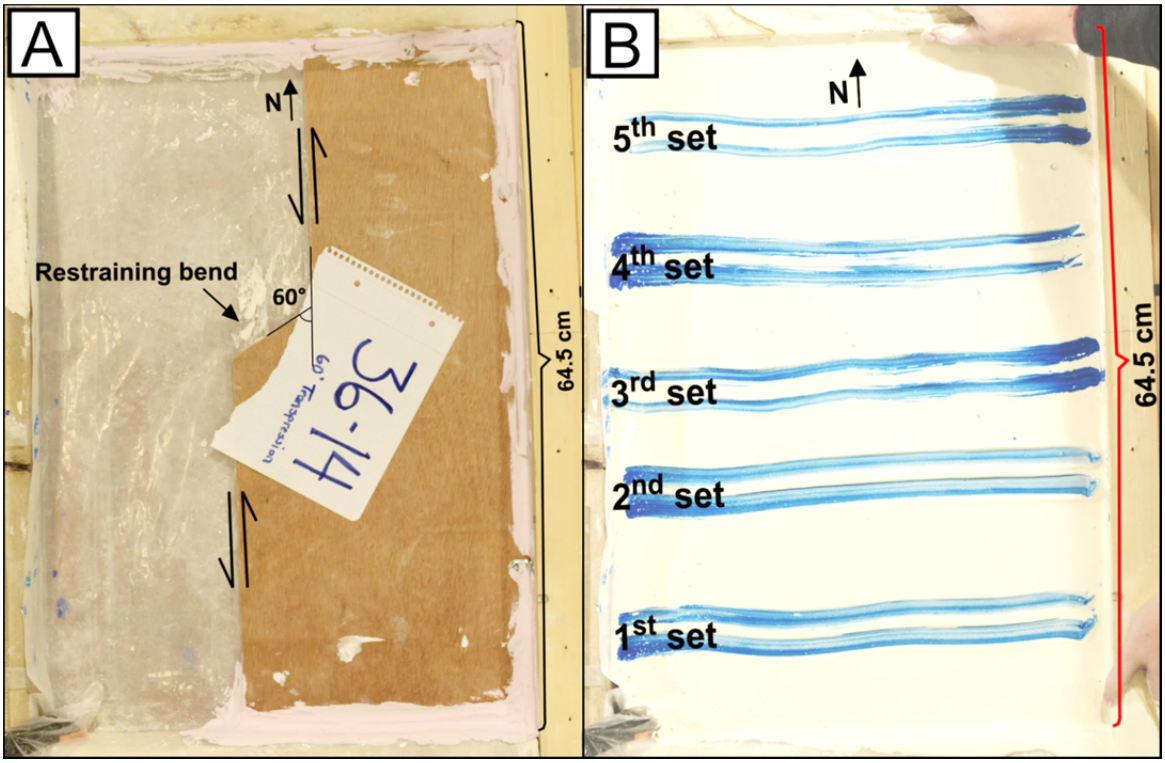


**Figure 3.19 A:** The basement template. **B:** Marker stripes applied to the plaster (numbered from the south).

**Table 3.4**

| | |
|---|---|
| Date of the experiment | 02.12.2014 |
| Plaster mixture | 8 liters of plaster and 4.8 liters of water |
| Plaster to water ratio | 1.66:1 |
| Duration | 21 seconds |
| Length of the short sides of the frame | 45 cm |
| Length of the long sides before and after displacement | Before displacement: 64.5 cm<br>After displacement: 88.5 cm |
| Total displacement | 24 cm |

**Table 3.4:** General information about the setup and duration of experiment 36-14 is given in this table.

Brittle deformation commenced in the southernmost part of the model after c. 9 % of the total movement of 24 cm. Beginning fractures were (very faint stripes) oriented WSW-ENE and some had the orientation NNW-SSE (barely noticeable). The most visible ones were characterized as riedel marked shears, and the faint ones were synthetic and classified as riedel shear fractures. Plaster had started accumulating north of the third stripe-set, forming a pop-up structure (Fig. 3.20). This was

evident from the reflection of light in this area. Displacement became evident in the south shortly after, and the fault trace in the southern area extended northwards to the third stripe-set (Fig. 3.20). The northern fault trace became visible after slightly more movement.

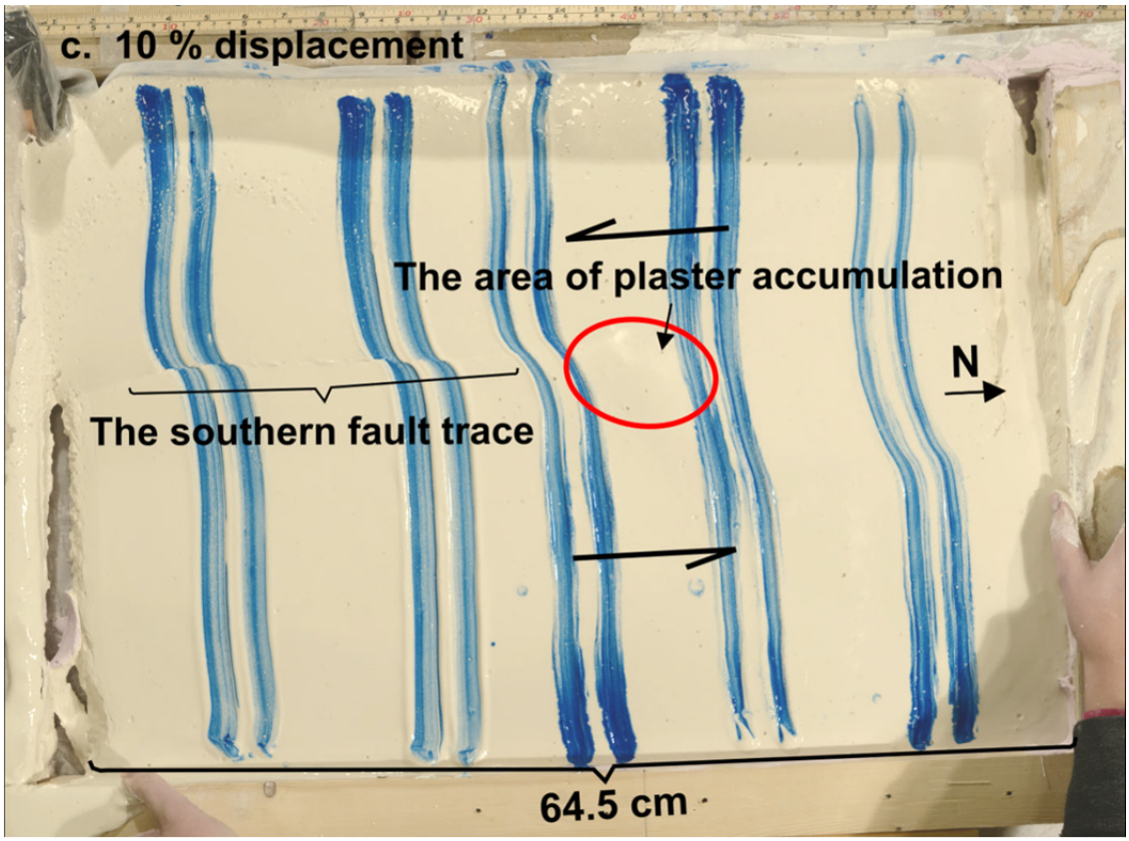


**Figure 3.20:** The model c. 10 % into the displacement. The area outlined in red represents the area of plaster accumulation and the southern fault trace is pointed out.

Circa 22 % into the movement the eastern edge of the pop-up structure was defined and a hard-link between the two fault traces had formed. With slightly more movement the entire outer rim of the structure was defined making this a flower structure. Figure 3.21 illustrates the positive flower after c. 37 % of the movement, before new fault blocks were added to this. As the flower structure moved northwards it rotated slightly clockwise towards the northeast, up until new fault blocks started developing (further mentioned below).

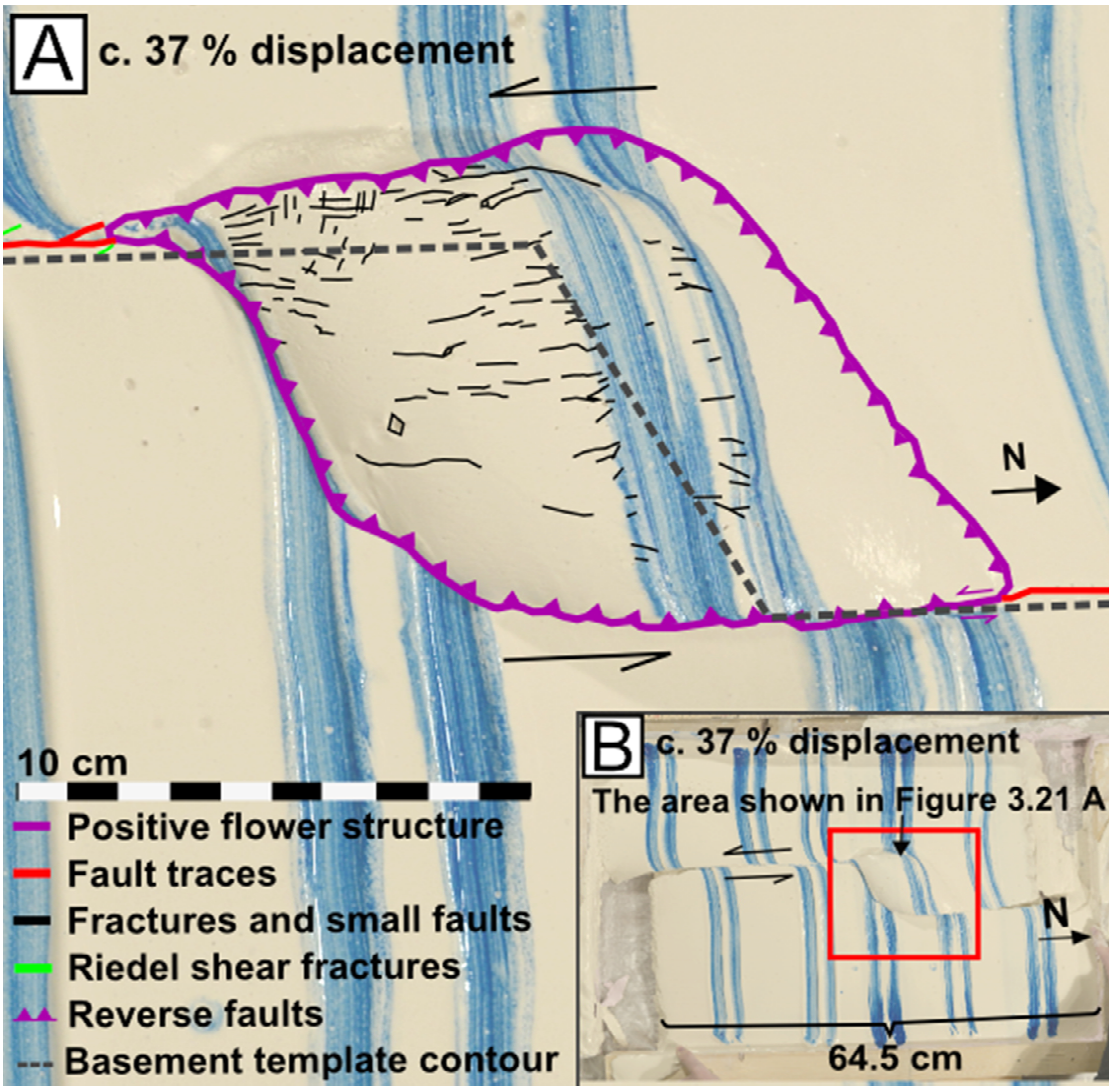


**Figure 3.21 A:** The flower structure c. 37 % into the displacement.
**B:** The red square portrays the area shown in Figure 3.21 A.

Between c. 47 % and 100 % of the displacement two more fault blocks formed as parts of the flower structure (Figs. 3.22 and 3.23). Towards the end of the experiment the positive flower seemed to get steeper on the eastern side. The northern tip of the flower structure rotated slightly counterclockwise towards the northwest when the structure came closer to the northern edge of the model (Fig. 3.23).

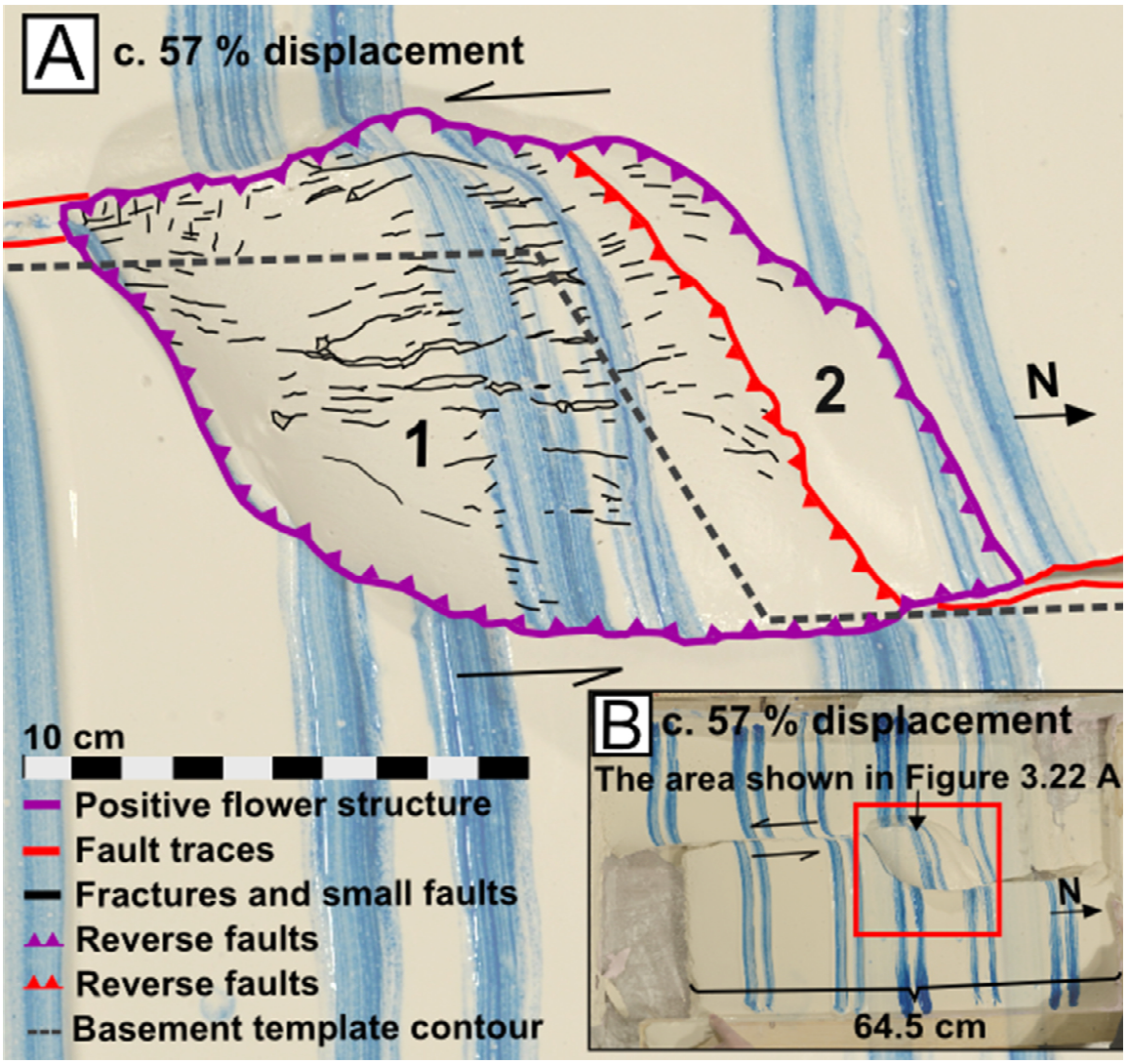


**Figure 3.22 A:** The flower structure c. 57 % into the displacement.
**B:** The red square portrays the area shown in Figure 3.22 A.

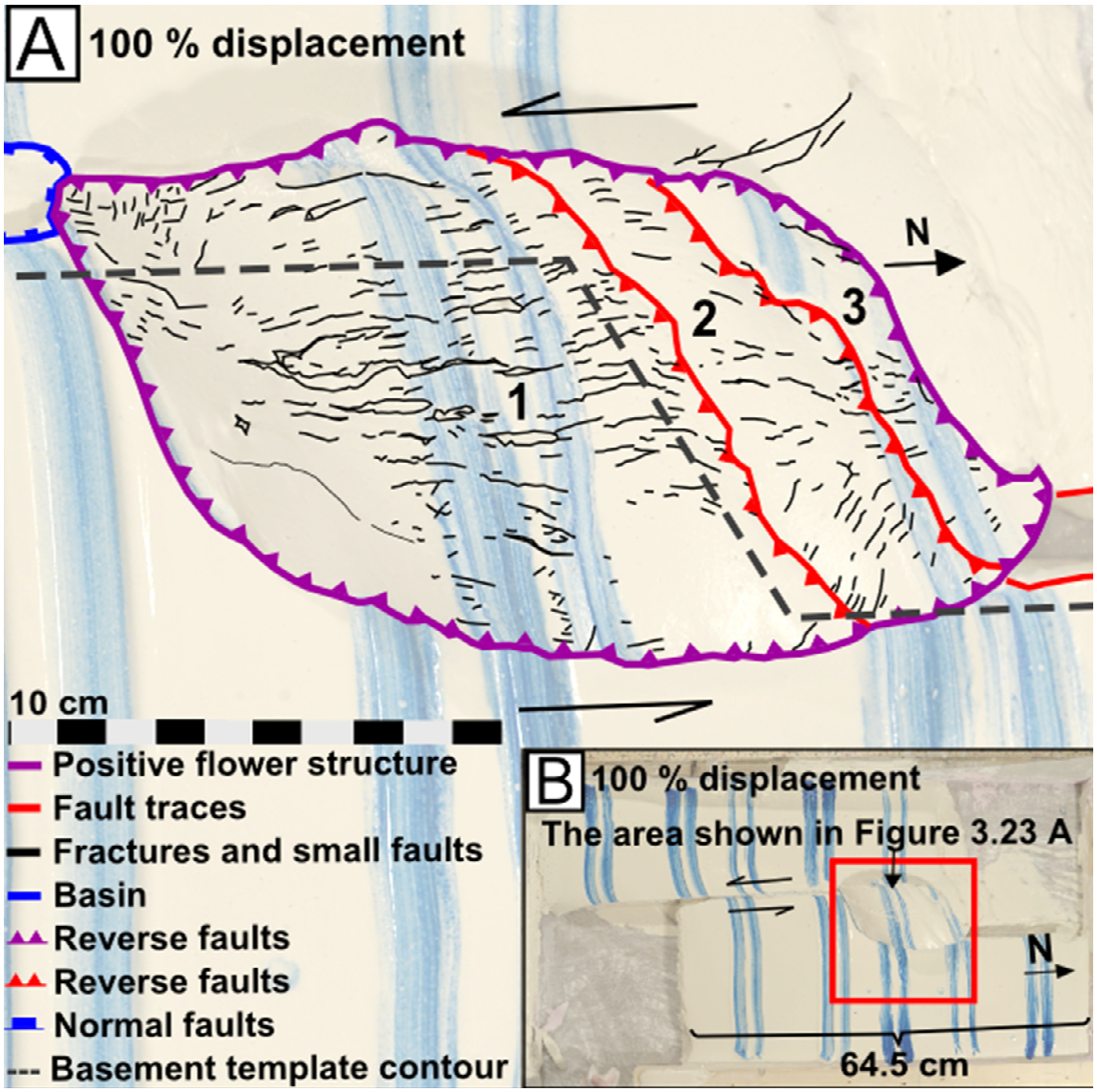


**Figure 3.23 A:** The flower structure after displacement.
**B:** The red square portrays the area shown in Figure 3.23 A.

Small structures had formed along the fault in the southern half of the model. An elongated basin was located just south of the flower structure. Further south of this basin a small positive structure and a very small basin had formed. The main fault had a degree of normal displacement in addition to the dominating strike-slip movement in the southernmost area, where the eastern fault block had moved down relative to the western side and thus represented the hanging wall (Figs. 3.24 A and B). Deflection of the plaster towards the movement was evident on the majority of the marker stripes, as shown in Figures 3.24 A and B.

A few riedel shear fractures were evident along the fault trace on the eastern fault block, the angle between these and the main fault ranged between c. 14-18°. The fractures on top of the flower

structure had the orientations NNE-SSW, NNW-SSE, NW-SE and N-S. The two newer fault blocks were less affected by fracturing than the oldest block.

The model was 88.5 cm long after the experiment, giving a total displacement of 24 cm. The flower structure was 20 cm in length, and the maximum height was c. 4 cm relative to the flat plaster surface. The overall angle of this feature was approximately 20° relative to the main fault, and it comprised fault blocks angled c. 45-50° (Figs. 3.24 A and B).

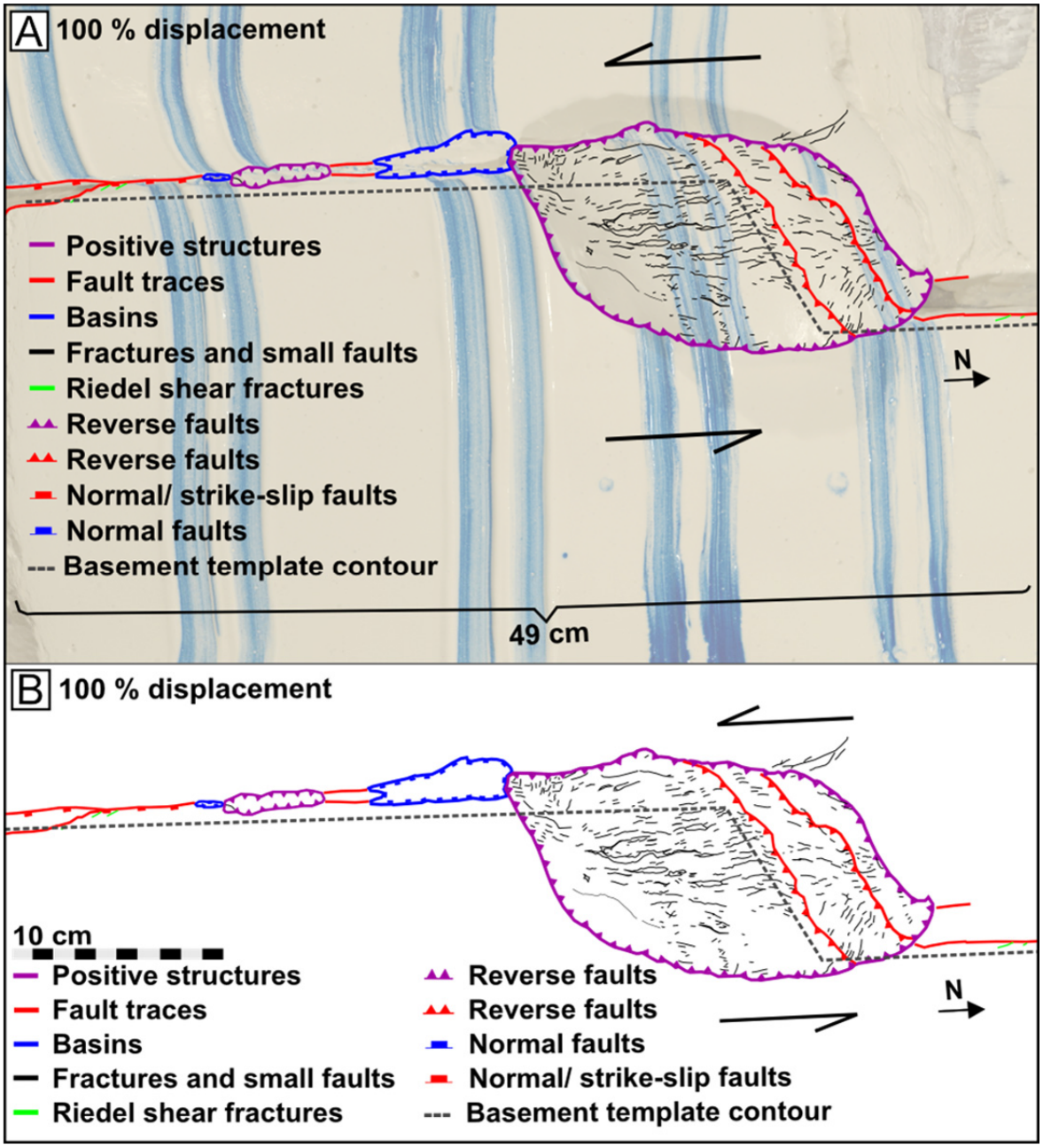


**Figure 3.24 A and B:** The final interpretation of model 36-14.

The areas outlined in purple in Figure 3.25 portray the areas that were affected the most by edge effects. The area outlined in red in this figure represents the area shown in Figures 3.24 A and B.

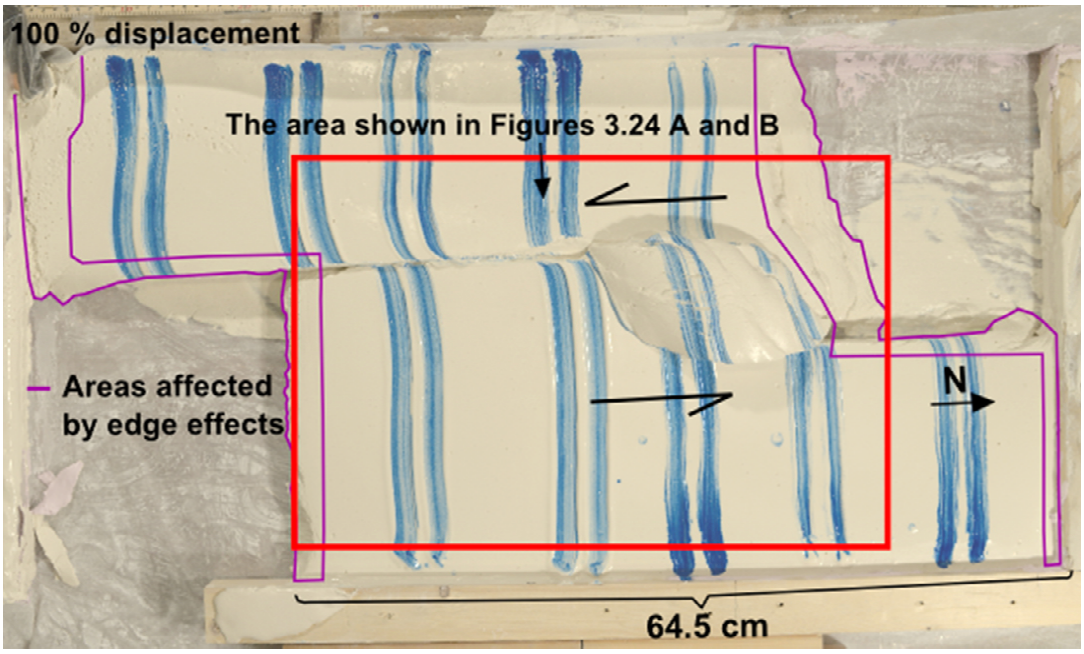


**Figure 3.25:** The red square portrays the areas shown in Figures 3.24 A and B and the areas lined in purple were the most affected by edge effects.

## 3.3 Transtensive experiments

Experiment 40-14, 39-14 and 37-14 resulted in models containing pull-apart basins formed by transtensional bends of 30°, 45° and 60° angles, respectively. These experiments were performed for gaining insight into the structural influence pertaining to different releasing bend angles.

### 3.3.1 Experiment 40-14: 30° releasing bend

The basement template used in this model comprised a 30° releasing bend as shown in Figure 3.26 A, and transtensional deformation occurred. The plaster consistency was quite stiff when poured into the frame and the structures that formed were of good quality. Five sets of marker stripes were applied to the plaster and were used as reference points in the description with the first set being the southernmost one (Fig. 3.26 B). General information about the setup and duration of experiment 40-14 is found in Table 3.5 and a video of this experiment is found in Appendix A (Video 4).

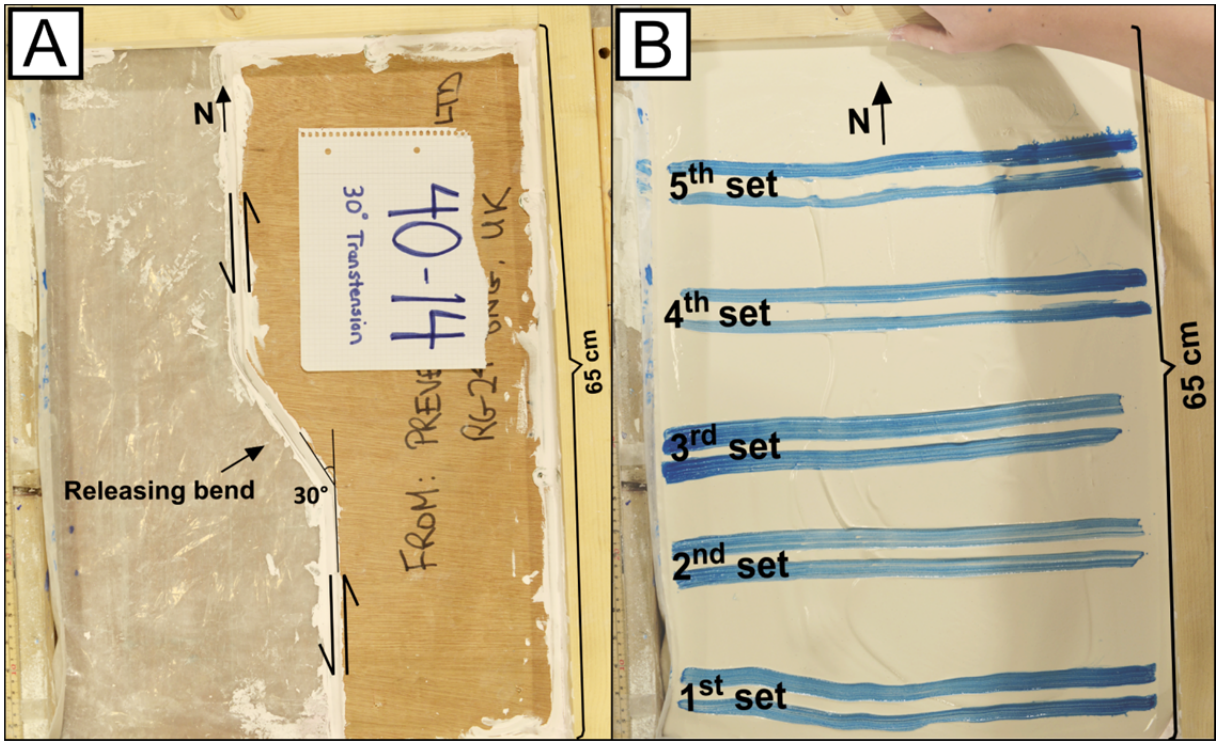


**Figure 3.26 A:** The basement template. **B:** Marker stripes applied to the plaster.

**Table 3.5**

| | |
|---|---|
| Date of the experiment | 03.12.2014 |
| Plaster mixture | 8 liters of plaster and 4.8 liters of water |
| Plaster to water ratio | 1.66:1 |
| Duration | 13 seconds |
| Length of the short sides of the frame | 45 cm |
| Length of the long sides before and after displacement | Before displacement: 65 cm<br>After displacement: 78 cm |
| Total displacement | 13 cm |

**Table 3.5:** General information about the setup and duration of experiment 40-14 is given in this table.

Ductile deformation dominated for the first c. 18 % of the total movement of 13 cm. After approximately 10 % of the motion plaster started sinking in the area of the third set of marker stripes. Riedel shear fractures developed (very faint at this stage) with the orientation NNW-SSE, these were synthetic relative to the main fault direction. Other beginning fractures were oriented WSW-ENE and NE-SW, thus forming a conjugate set with the other fractures. These were the most

visible north of the third stripe-set and they were classified as riedel marked shears. The fractures became more visible after c. 42 % of the displacement as shown in Figures 3.27 A and B.

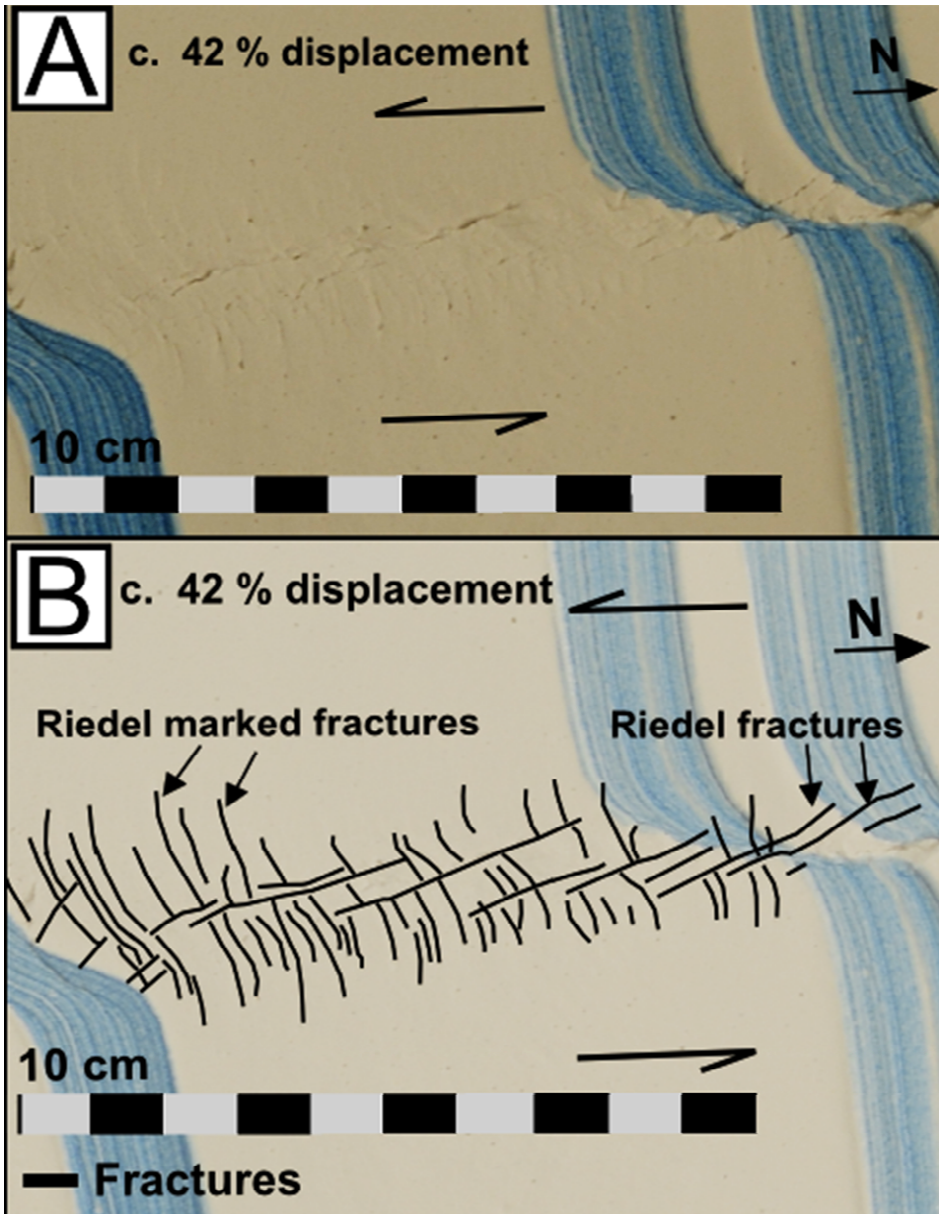


**Figure 3.27 A:** Riedel shears and antithetic fractures c. 42 % into the displacement.
**B:** The interpretation of the area shown in Figure 3.27 A (the location of these structures is outlined in red in Figure 3.28).

The model was moved quite abruptly, and when c. 42 % of the movement was reached a fault trace had formed in the northern half of the model and southwards through half of the releasing bend (Fig. 3.28). The fault trace in the south was less developed when it came to its extent and continuity. Although the two fault traces comprised several fault segments (they were not fully continuous) they were overlapping in the area of the releasing bend and the faults were therefore soft-linked, as can

be seen in Figure 3.28. This figure also showed where the southernmost part of the northern fault trace had opened 0.5-1 cm, forming a rift/ a narrow pull-apart basin.

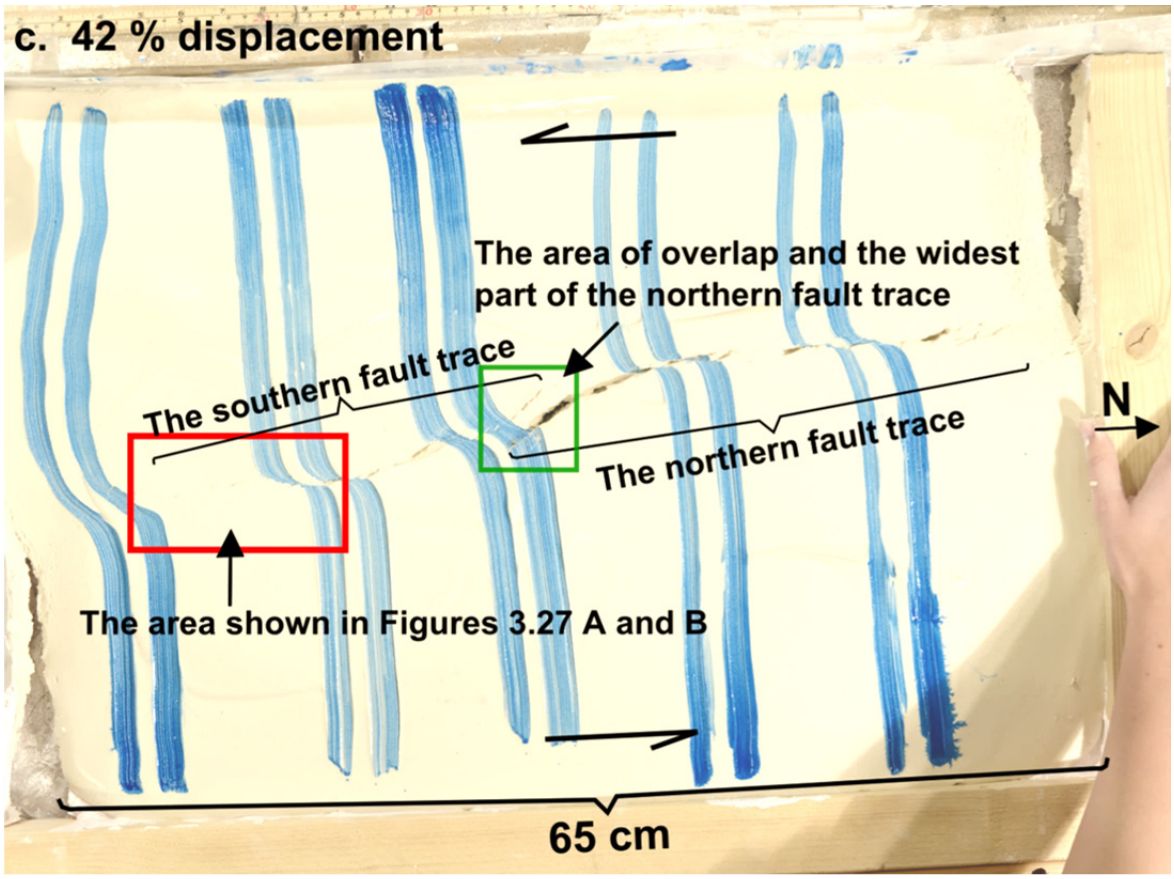


**Figure 3.28:** The model after c. 42 % of the displacement. The red square portrays the area shown in Figure 3.27 A and B. The green square shows the location of the overlap between the two fault traces and shows the widest area of the northern fault trace.

With slightly more movement the fault cut through the majority of the southernmost area as well. The plaster in between the overlapping fault segments was cut by an oblique transfer fault c. 49 % into the movement, thus connecting the two main fault segments and forming a hard-link (Figs. 3.29 A and B). The tips of the two fault segments were left as inactive branches. A relay ramp formed where the northern fault segment ended in an inactive branch constituting a part of the eastern basin wall. The ramp had a relatively gentle dip northwestwards into the basin (it did not have a high amount of normal displacement). A small and a large basin had developed south of the pull-apart basin (Figs. 3.29 A and B).

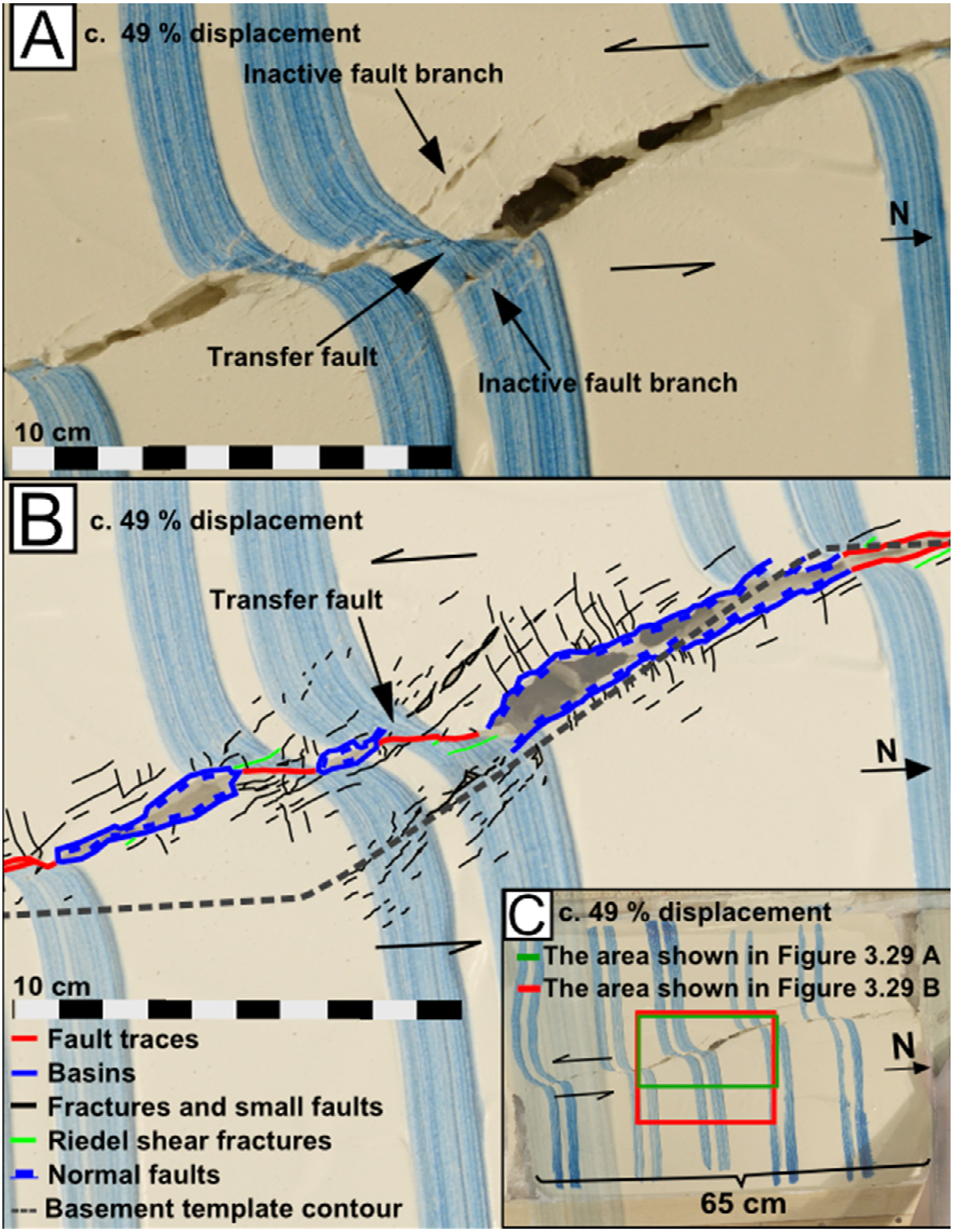


**Figure 3.29 A:** The transfer fault that connected the two fault traces c. 49 % into the displacement. **B:** Interpretation of the area shown in Figure 3.29 A. **C:** The green square portrays the area shown in Figure 3.29 A and the area outlined in red is the area illustrated in Figure 3.29 B.

The two basins south of the pull-apart basin grew and these three basins eventually linked up. This was very apparent when c. 75 % of the movement was reached (Figs. 3.30 A and B).

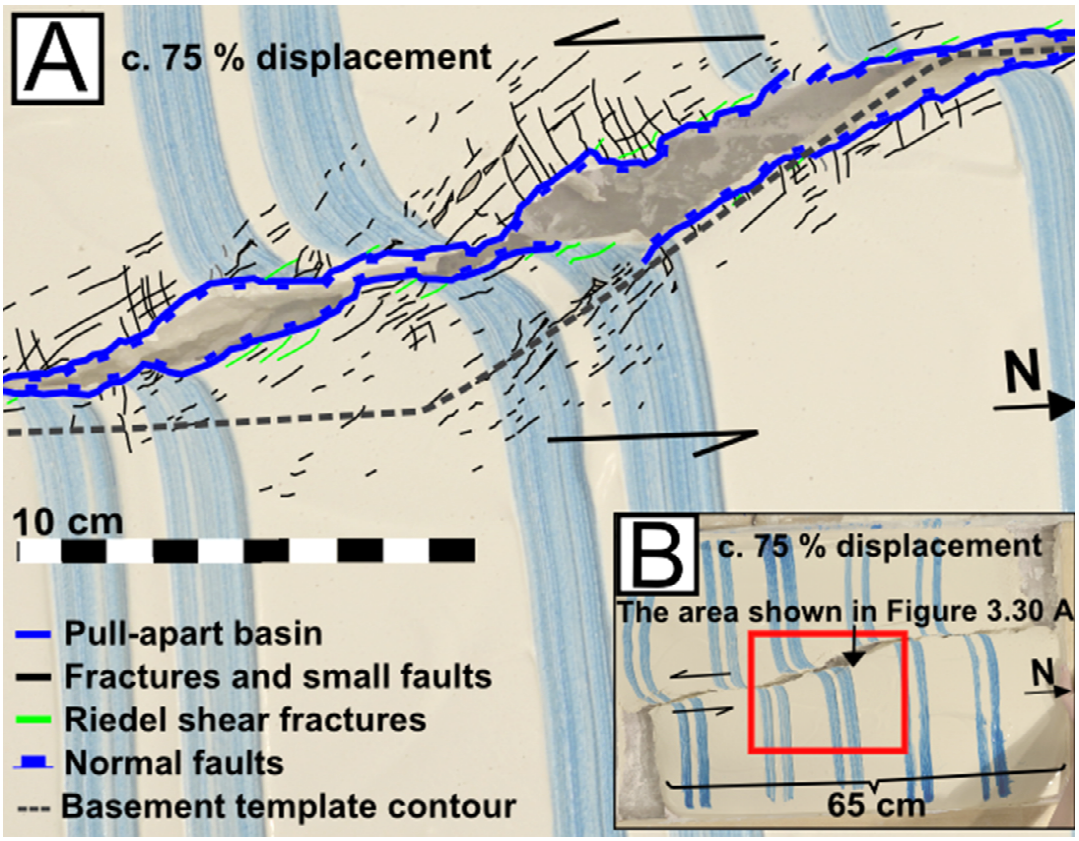


**Figure 3.30 A:** The pull-apart basin area c. 75 % into the displacement, when the two basins had connected. **B:** The red square shows the area portrayed in Figure 3.30 A.

The pull-apart basin was approximately 4 cm at the widest and 28 cm in length after displacement. The overall angle of the basin was quite hard to measure because of its shape, but a rough estimate would be between 13-20°. The area where the previously separate basins had connected was quite narrow compared to the overall width of the pull-apart basin. A significant amount of fractures affected the area to the east and west of the pull-apart; these were oriented similarly to this structure (Figs. 3.31 A and B). Both the riedel shear fractures as well as the riedel marked shears were visible in the finished model. The angle between the riedel shears and the main fault ranged between c. 16-20° and the riedel marked fractures had angles of c. 74-78° relative to the main fault.

As the experiment was moved quite far the fault plane overall ended up quite wide, as can be seen in the figures below.

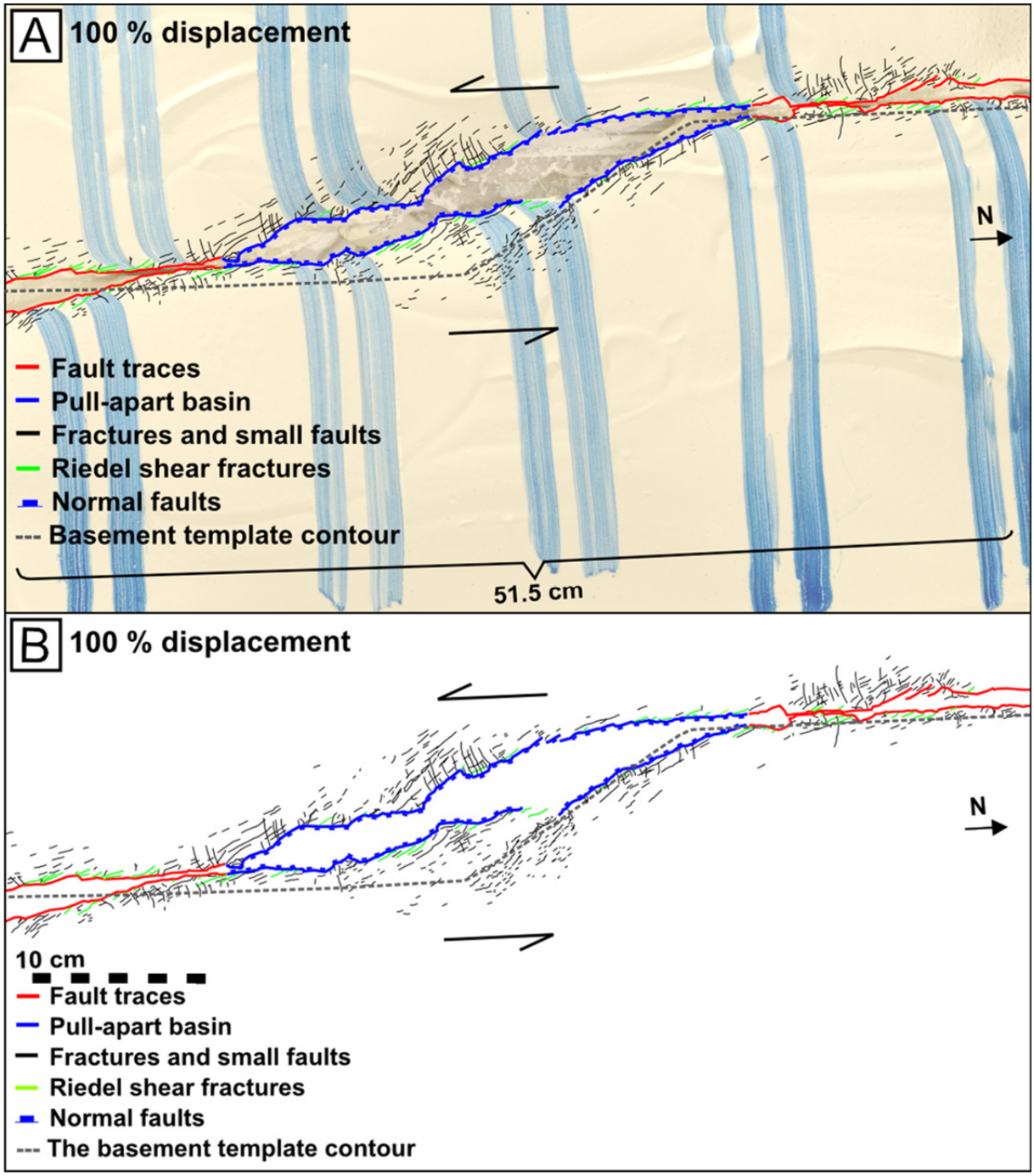


**Figures 3.31 A and B:** The final interpretation of experiment 40-14.

The area affected the most by edge effects is outlined in purple in Figure 3.32 and the red square portrays the area shown in Figures 3.31 A and B.

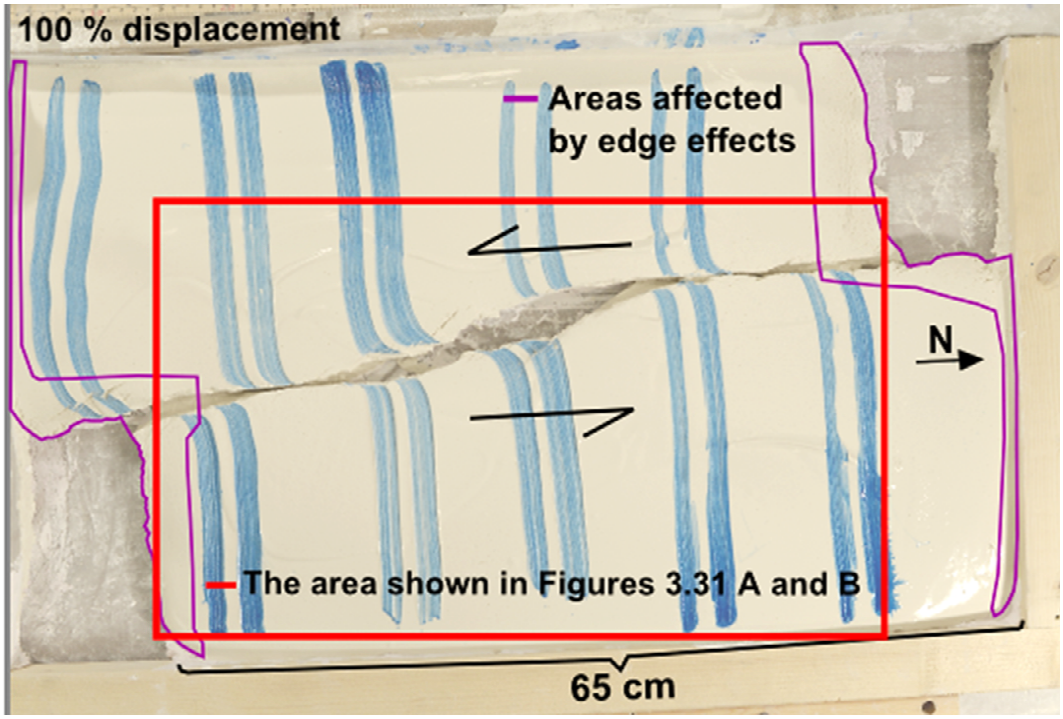


**Figure 3.32:** The areas that were the most affected by edge effects are outlined in purple and the red square portrayed the area shown in Figures 3.31 A and B.

### 3.3.2 Experiment 39-14: 45° releasing bend

The basement template used in this experiment comprised a 45° releasing bend, leading to transtensional deformation (Fig. 3.33 A). The plaster mixture was poured into the frame when it was quite stiff and the structures that formed were of good quality. The five sets of marker stripes applied to the plaster were used as points of reference when describing the experiment; the first set was located furthest to the south (Fig. 3.33 B). General information about the setup and duration of experiment 39-14 is found in Table 3.6 and a video of this experiment is found in Appendix A (Video 5).

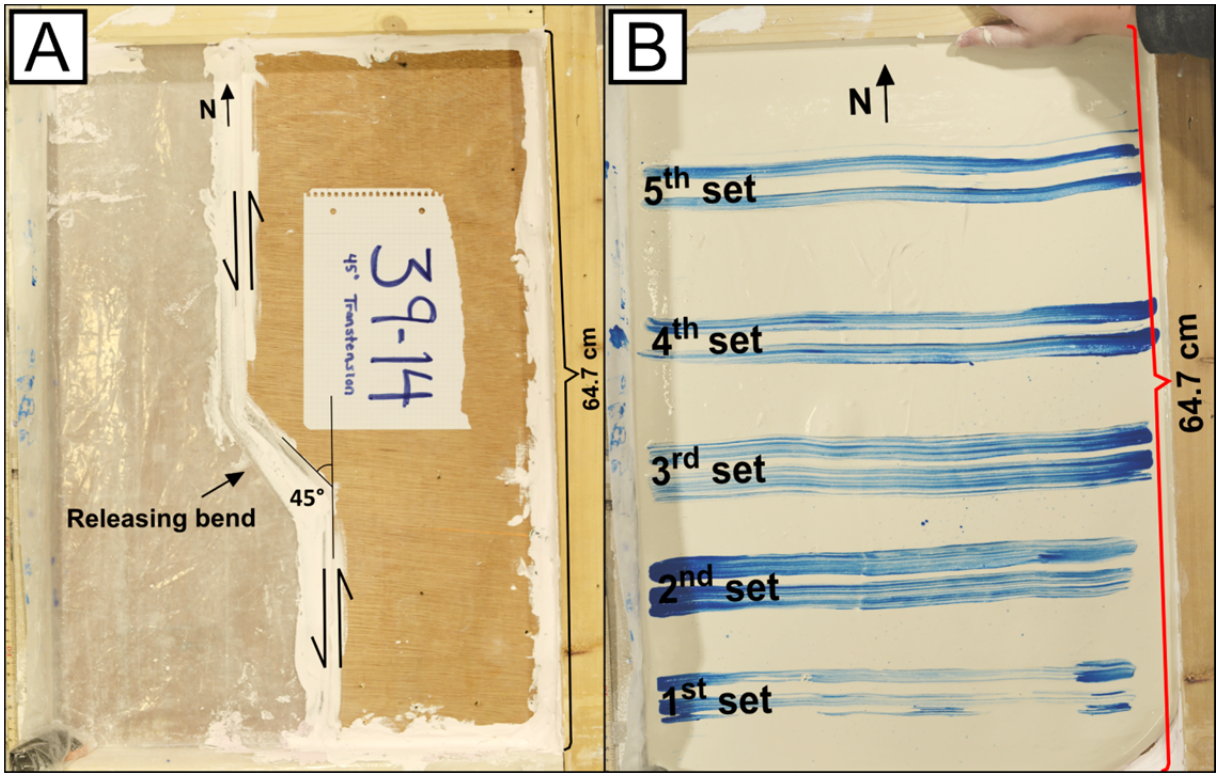


**Figure 3.33 A:** The basement template. **B:** Marker stripes applied to the plaster (numbered from the south).

**Table 3.6**

| | |
|---|---|
| Date of the experiment | 02.12.2014 |
| Plaster mixture | 8 liters of plaster and 4.8 liters of water |
| Plaster to water ratio | 1.66:1 |
| Duration | 13 seconds |
| Length of the short sides of the frame | 45 cm |
| Length of the long sides before and after displacement | Before displacement: 64.7 cm<br>After displacement: 75.1 cm |
| Total displacement | 10.4 cm |

**Table 3.6:** General information about the setup and duration of experiment 39-14 is given in this table.

Ductile deformation dominated up until 25 % of the total movement of 10.4 cm. Plaster started sinking north of the third stripe-set after approximately 10 % of the displacement. A few beginning fractures formed along the middle part of the model apart from the northernmost area, with the orientation WSW-ENE. These were characterized as riedel marked fractures. Faint fractures with the orientation NNW-SSE formed north of the third stripe-set. These were classified as riedel shear

fractures and were synthetic relative to the main fault trend. Some displacement was evident in the southernmost area.

Normal faults and more fractures had formed in the area of the third stripe-set c. 34 % into the displacement. These revealed the location of the releasing bend, as shown in Figure 3.34. A fault trace had formed north of the releasing bend and another one had developed through the southern half of the model; these comprised several NNW-SSE fractures (Fig. 3.34).

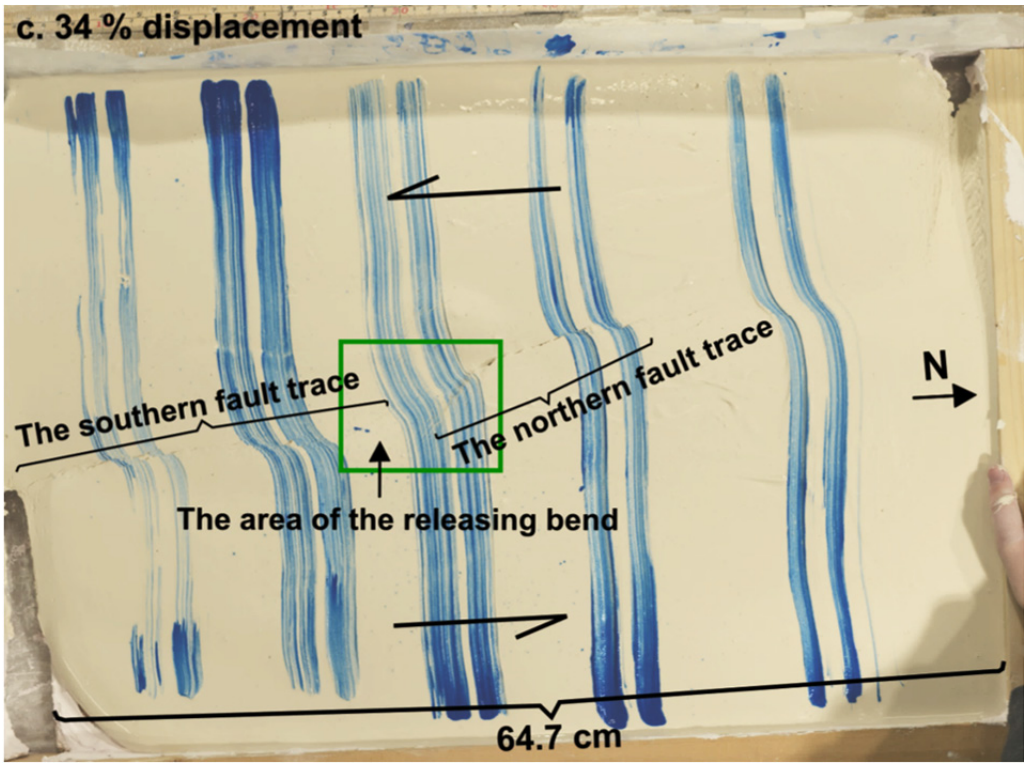


**Figure 3.34:** The model after c. 34 % of the displacement. The area of the releasing bend is outlined in green and the extent of the fault traces is shown.

Circa 50 % into the displacement a pull-apart basin had started forming just south of the releasing bend, Figures 3.35 A and B show this basin after c. 58 % of movement. A large relay ramp had formed, dipping northwestwards into the basin from the eastern fault block (Figs. 3.35 A and B). The northern fault trace was not completely continuous in the area of the releasing bend, but the northern and southern fault segments were overlapping and therefore soft-linked at this stage. Two basins had developed south of the pull-apart basin (Figs. 3.35 A and B).

The fault became wider north of the pull-apart basin, which made the basin really long and narrow towards the north shortly after its formation. The lower part of the relay ramp was heavily fractured, and it eventually broke off of the upper part when an oblique transfer fault formed and linked the

two main fault segments (Figs. 3.35 A and B). After c. 79% of the movement the two basins were joined (Figs. 3.36 A and B).

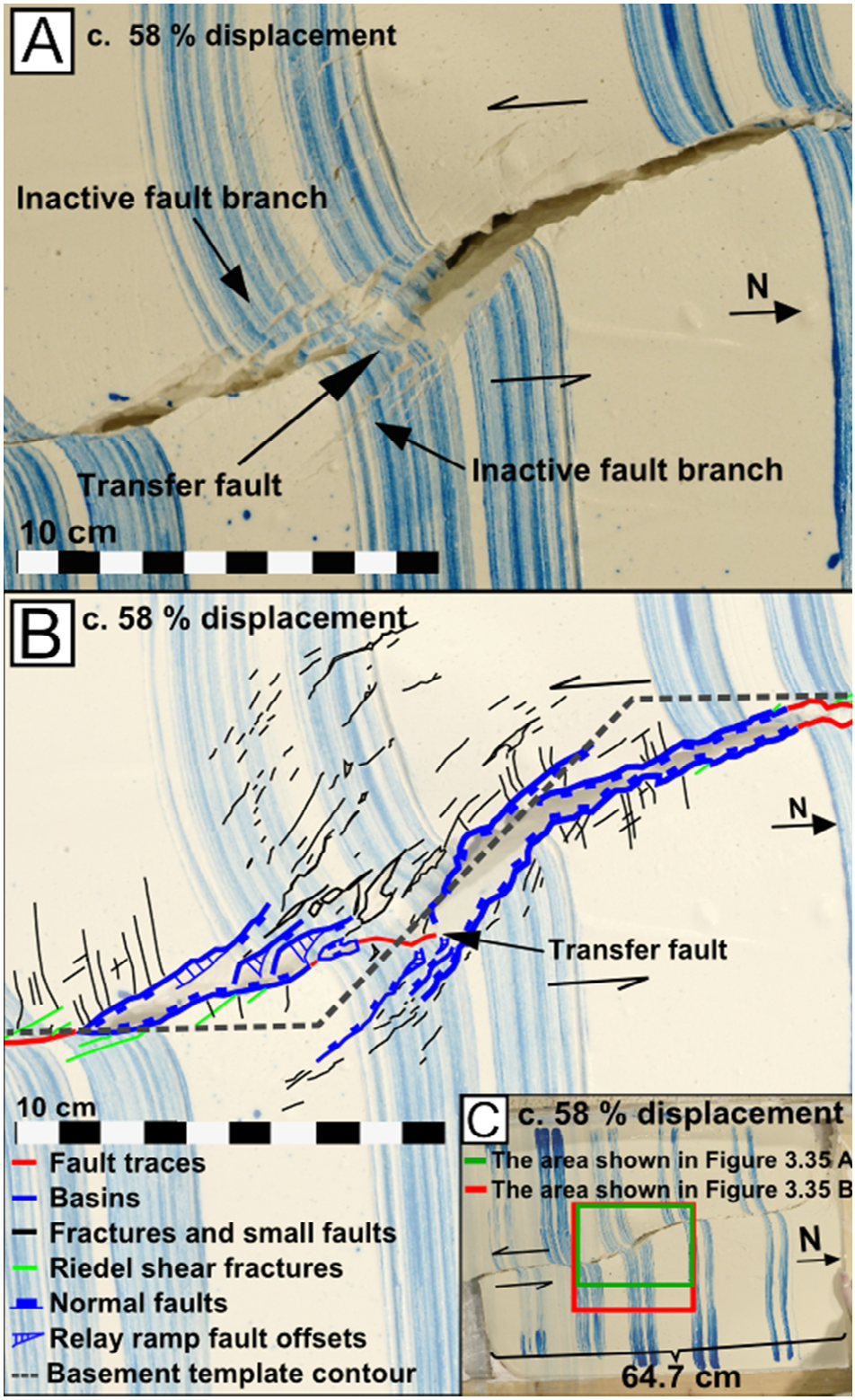


**Figure 3.35 A:** The releasing bend area c. 58 % into the displacement. **B:** Interpretation of The area shown in Figure 3.35 A. **C:** The area outlined in green represents the area shown in Figures 3.35 A and the red square portrays the area shown in Figure 3.35 B.

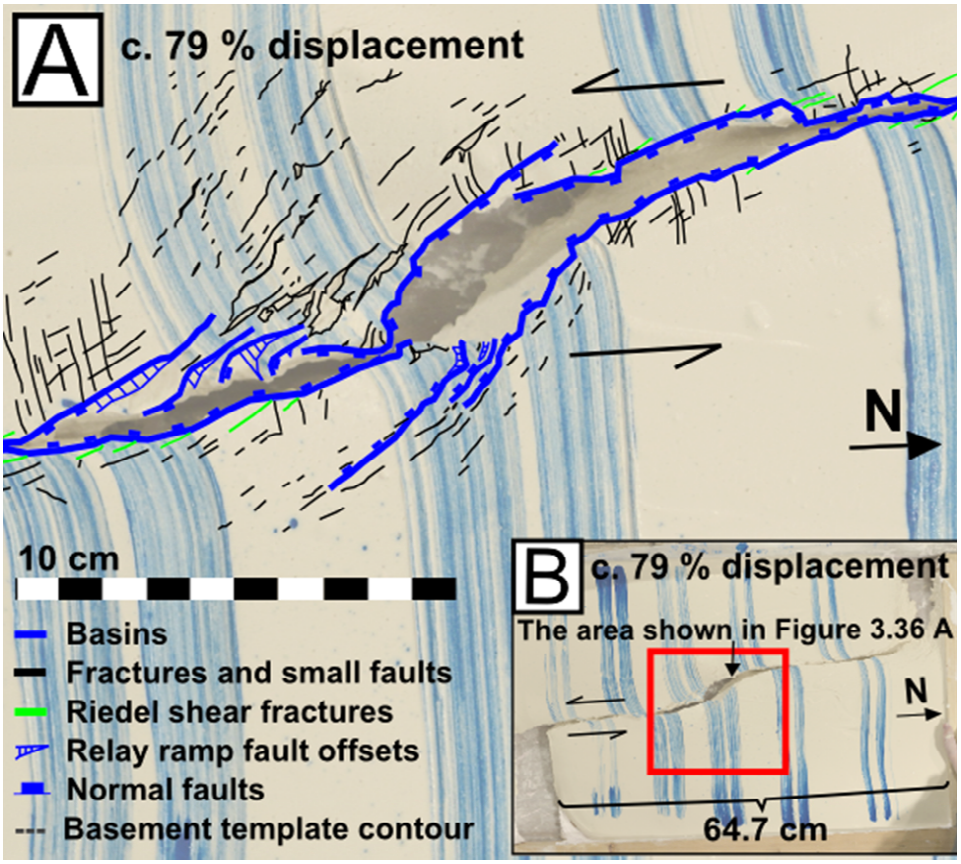


**Figure 3.36 A:** The pull-apart basin area c. 79 % into the displacement.
**B:** The red square shows the area portrayed in Figure 3.36 A.

The fault trace became more continuous in the southern part of the model. A positive structure with a length of c. 3 cm had formed in the area of the second stripe-set. A small basin had formed north of the pull-apart basin, as shown in Figures 3.37 A and B.

The pull-apart basin had a length of 23.5 cm after displacement and it was 4 cm at the widest. The angle of this structure was hard to estimate due to the basin's shape, but overall it was less than 20° from the main fault trend. The area around the basin comprised a lot of fractures and normal faults, particularly the western fault block; these structures had a similar orientation to the pull-apart basin. The riedel-shears and the riedel marked fractures were visible in the finished model. The angle between the riedel fractures and the main fault ranged between c. 9-17°, and the angle between the riedel marked fractures and the main fault was between c. 76-80°.

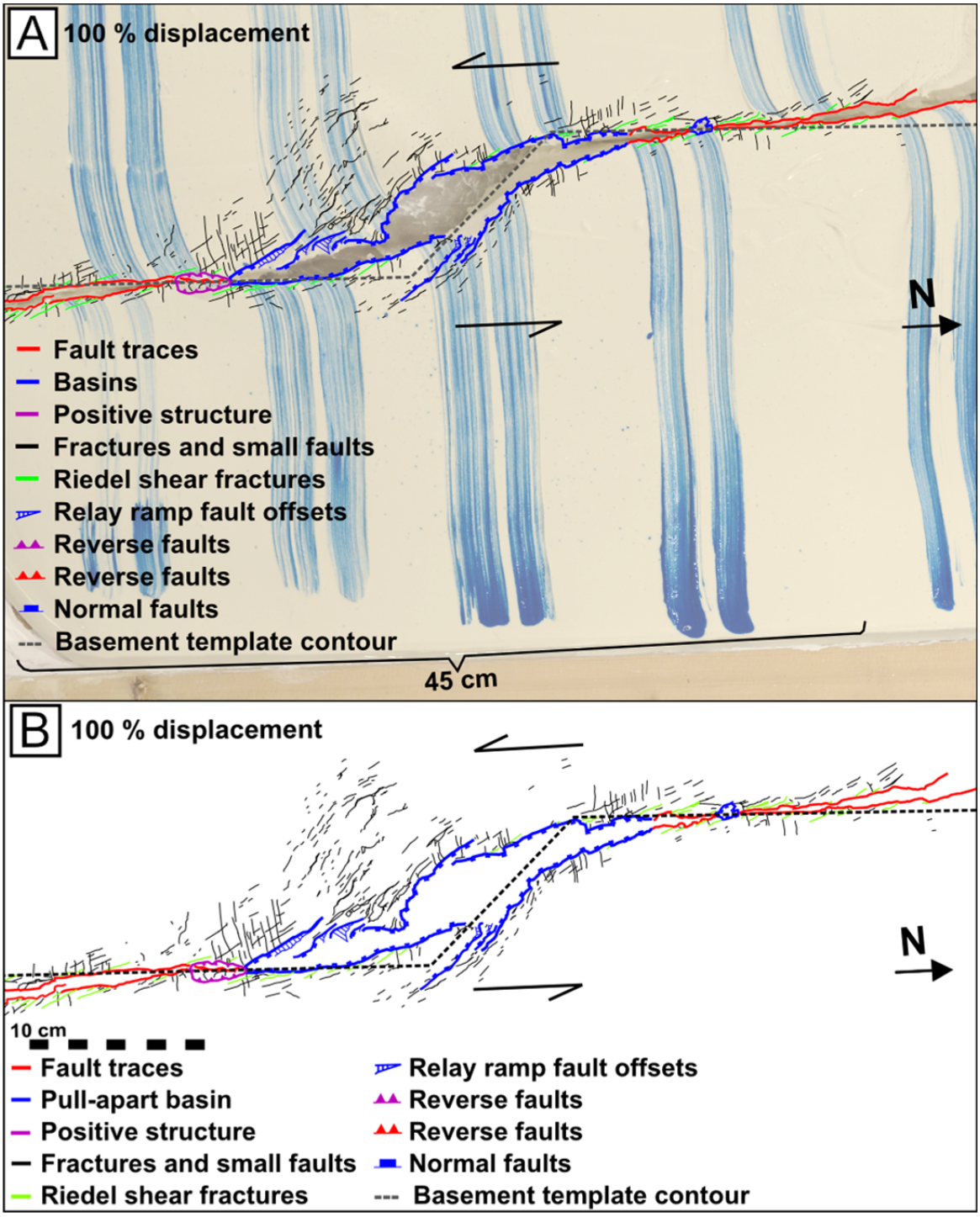


**Figure 3.37 A and B:** The final interpretation of experiment 39-14.

The areas that were the most affected by edge effects are outlined in purple, in Figure 3.38, and the red square portrays the area shown in Figures 3.37 A and B.

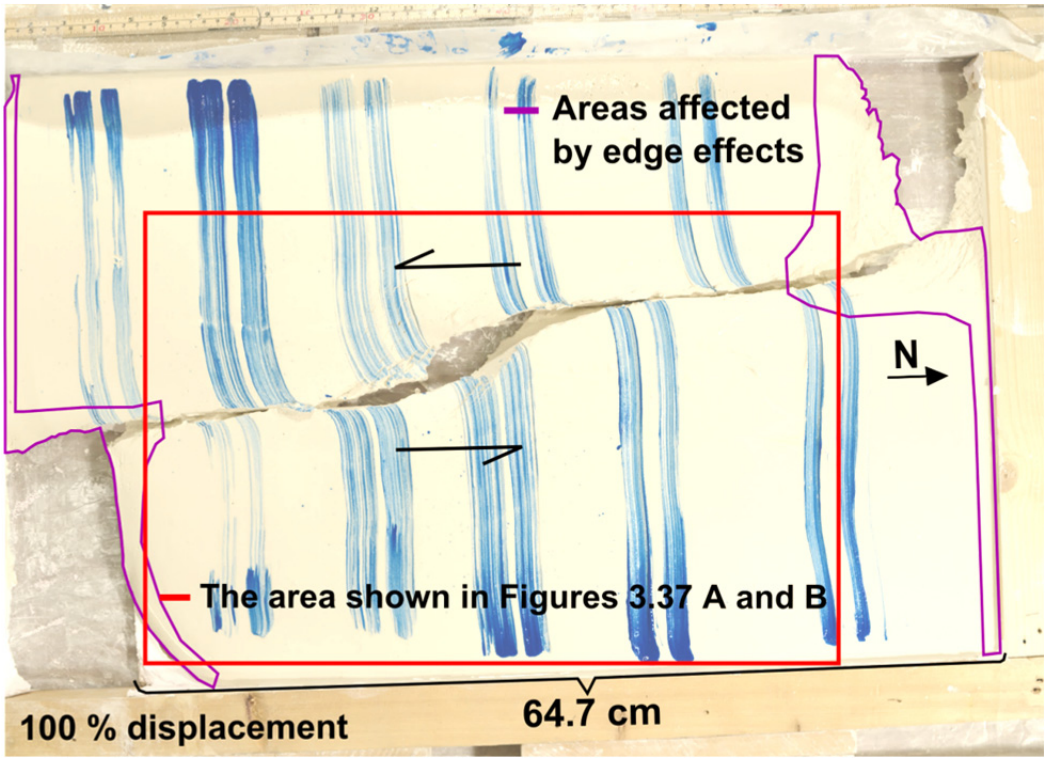


**Figure 3.38:** The areas that were the most affected by edge effects are outlined in purple and the red square portrays the area shown in Figures 3.37 A and B.

### 3.3.3 Experiment 37-14: 60° releasing bend

The basement template utilized for this experiment had a 60° releasing bend, resulting in transtensional deformation (Fig. 3.39 A). The plaster mixture was quite stiff when poured into the frame and the structures that formed were of good quality. Four sets of marker stripes were applied to this model, and these were used as reference points in the description, with the first set furthest south (Fig. 3.39 B). General information about the setup and duration of experiment 37-14 is found in Table 3.7 and a video of this experiment is found in Appendix A (Video 6).

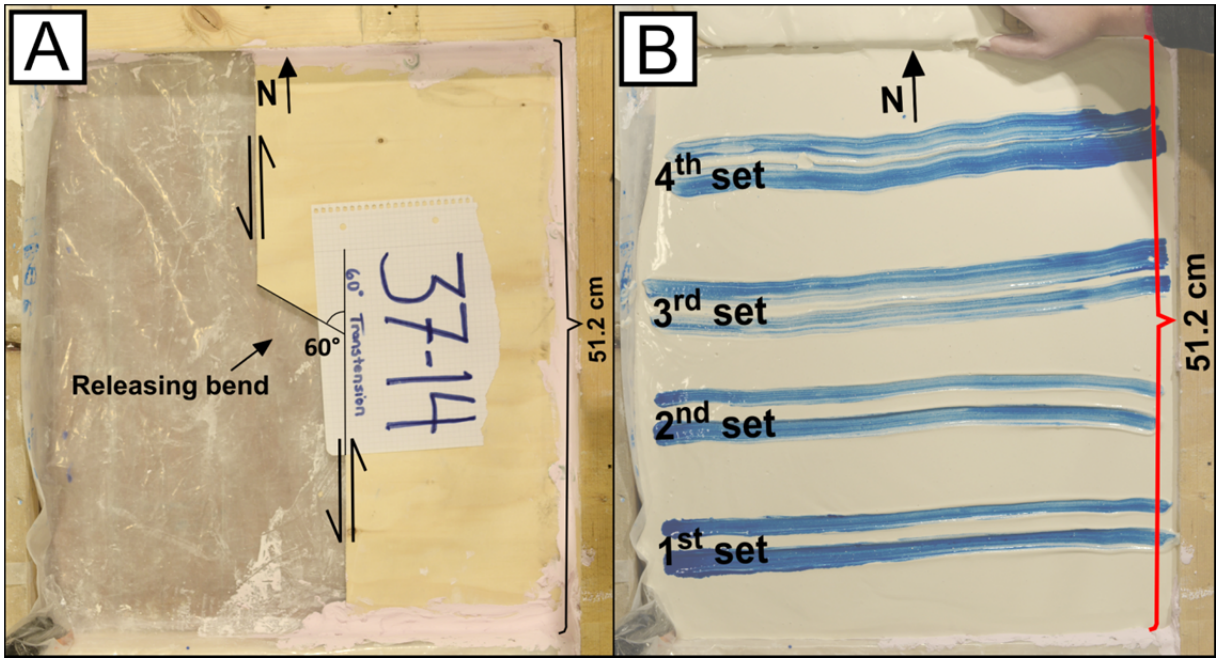


**Figure 3.39 A:** The basement template. **B:** Marker stripes applied to the plaster (numbered from the south).

**Table 3.7**

| | |
|---|---|
| Date of the experiment | 02.12.2014 |
| Plaster mixture | 6 liters of plaster and 3.6 liters of water |
| Plaster to water ratio | 1.66:1 |
| Duration | 12 seconds |
| Length of the short sides of the frame | 44.5 cm |
| Length of the long sides before and after displacement | Before displacement: 51.2 cm<br>After displacement: 60.2 cm |
| Total displacement | 9 cm |

**Table 3.7:** General information about the setup and duration of experiment 37-14 is given in this table.

Ductile deformation (folding of the marker layers) dominated up until c. 26 % of the total displacement of 9 cm. After 9 % of the movement plaster started sinking in the area of the third stripe-set. Beginning fractures (faint stripes) oriented NNW-SSE and WSW-ENE formed between the third and fourth stripe-set. The first ones were characterized as riedel shears and these were synthetic relative to the direction of the main fault. The latter ones were defined as riedel marked shears, and the fractures formed conjugate sets. Other fractures with a NW-SE orientation were

generated on the third stripe-set, on the eastern fault block. Some displacement was evident in the northernmost area.

A fault trace developed in the northern part of the model, making the contour of the basement template more prominent (Fig. 3.40). The fault trace in the southern half of the model was segmented; it developed quickly after the formation of the northern fault trace. After c. 28 % of the movement the northern fault curved southeastward and linked up with the NW-SE oriented fractures, as illustrated in Figure 3.40.

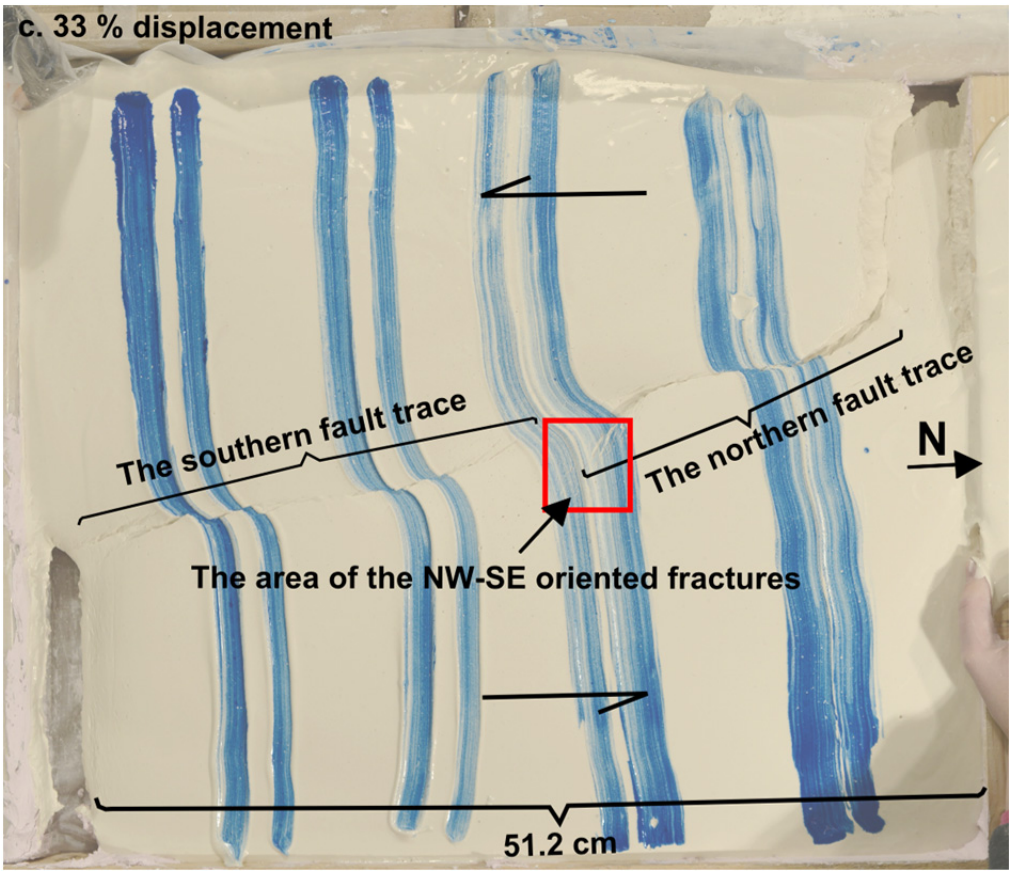


**Figure 3.40:** The model after c. 33 % of the displacement. The fault traces are shown as well as the area of the NW-SE oriented fractures.

Approximately 50 % into the displacement a pull-apart basin had started developing in the releasing bend area (Figs. 3.41 A and B). The two main fault traces were soft-linked at this stage. A narrow basin was located south of the pull-apart basin. With more movement the plaster that constituted the northern part of the basin sunk in further, thus making the basin deeper, and it extended towards the north. A relay ramp dipped northwestwards into the basin, as shown in Figure 3.41.

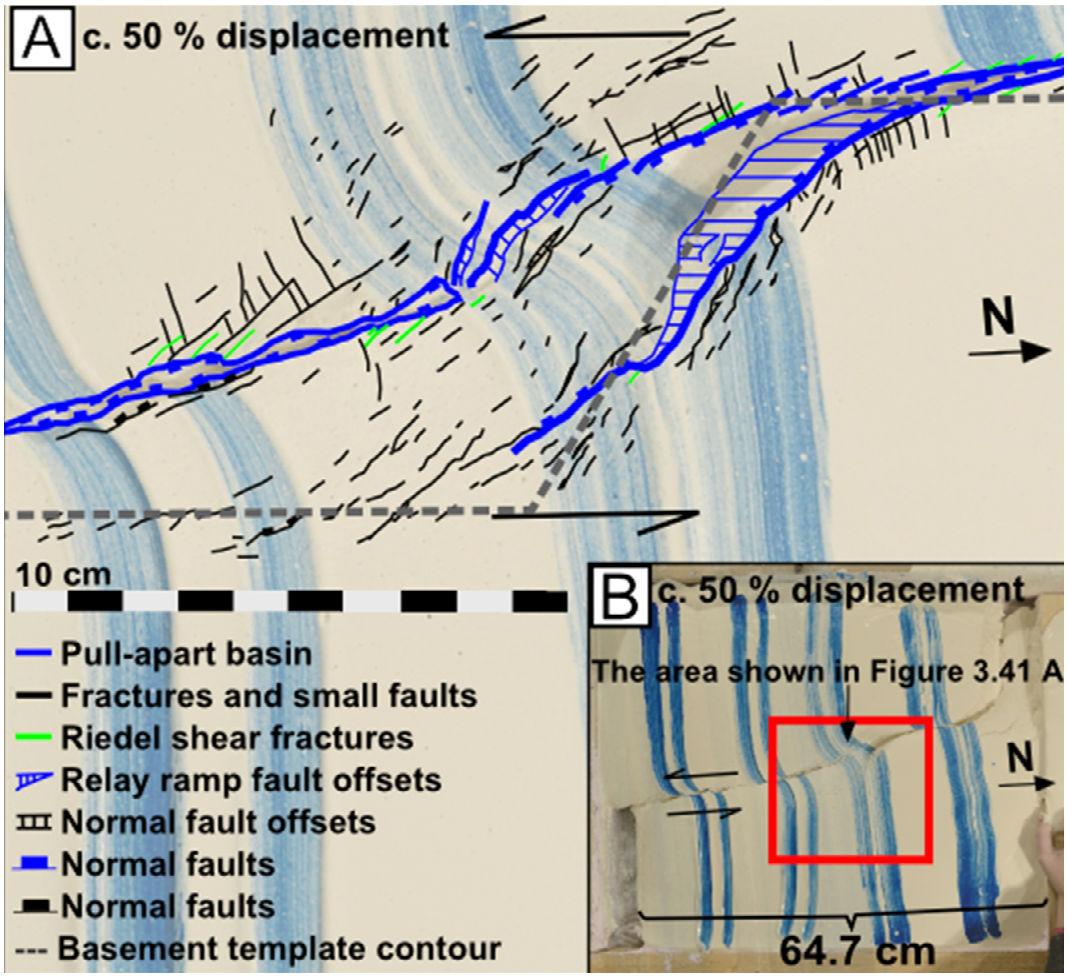


**Figure 3.41 A:** The area of the releasing bend c. 50 % into the displacement.
**B:** The area outlined in red represents the area shown in Figure 3.41 A.

With increased displacement the pull-apart basin opened towards the northern edge of the model. The fault was relatively wide in the northern area when 70 % of the movement was completed. The smaller basin was very narrow and eventually opened up towards the southern edge.

From approximately 81 % of the displacement and onwards the lower part of the relay ramp in the pull-apart basin started breaking off and moving southwards with the western fault block. The upper part of this structure was fixed to the eastern fault block and thus moved northwards (Figs. 3.42 A and B). An oblique transfer fault split the relay ramp into two parts and this fault connected the two main fault segments, thus making them hard-linked (Figs. 3.42 A and B).

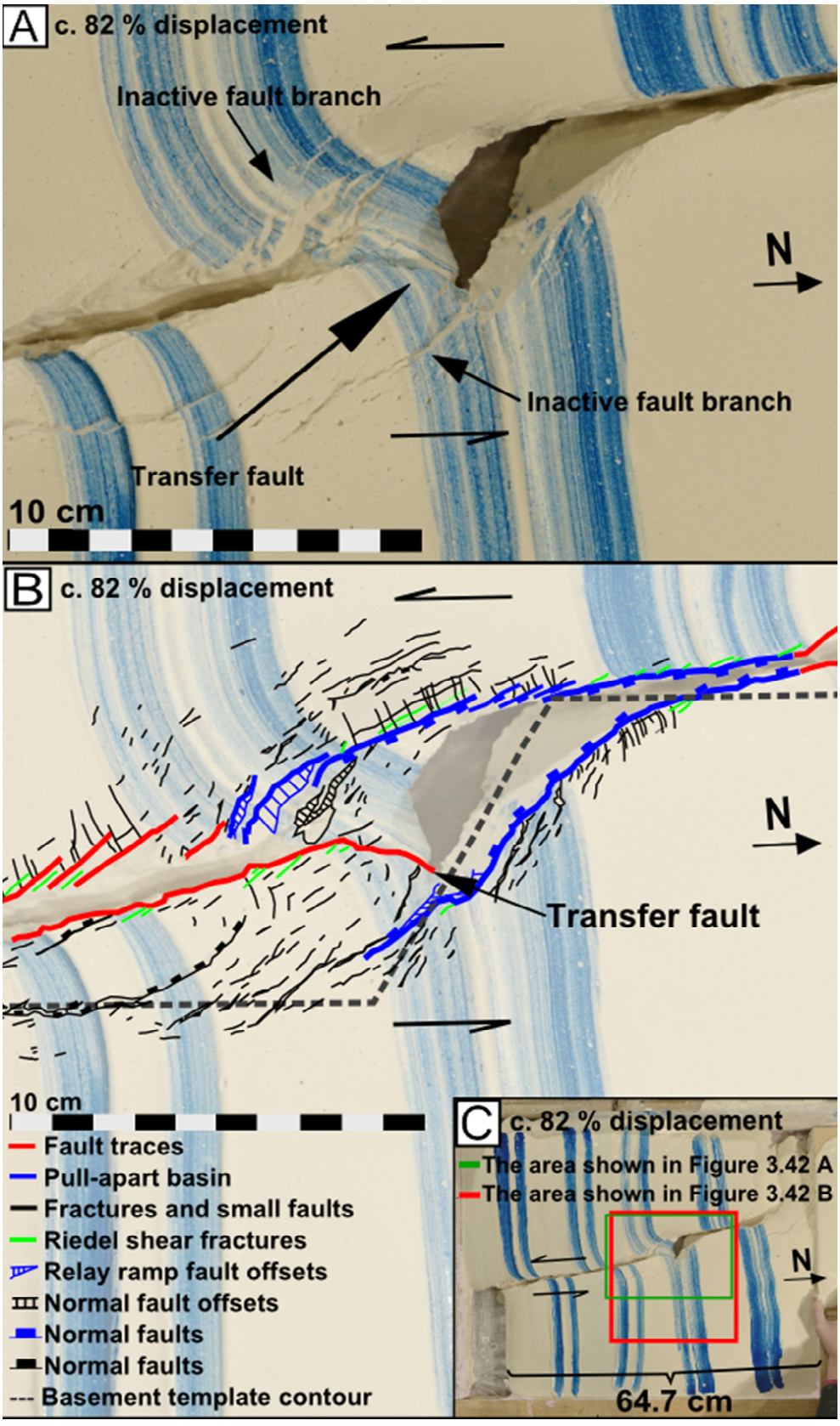


**Figure 3.42 A:** The releasing bend area c. 82 % into the displacement.
**B:** Interpretation of the area shown in Figure 3.42 A.
**C:** The green square portrays the area shown in Figure 3.42 A and the area lined in red represents the area shown in Figure 3.42 B.

The western part of the relay ramp was located between the two basins. Because this part was at a lower level compared to the plaster layer one could say that the two basins had connected and that this particular area was a shallower part of the basin (Figs. 3.43 A and B).

The pull-apart basin had a length of c. 18.5 cm after displacement and it was 5 cm at its widest. The angle of the basin relative to the main fault was hard to estimate due to its shape, but the northern wall was at a higher angle (relative to the main fault trend) compared to the basins in the other transtensive models. The area to the east and the west of the basin contained fractures and normal faults that were relatively parallel to the basin (Figs. 3.43 A and B). The angle between the riedel fractures and the main fault ranged between c. 10-18° and the riedel marked fractures had an angle of c. 78-83° to the main fault trend. The fault became wide through the entire model, as it was moved quite far.

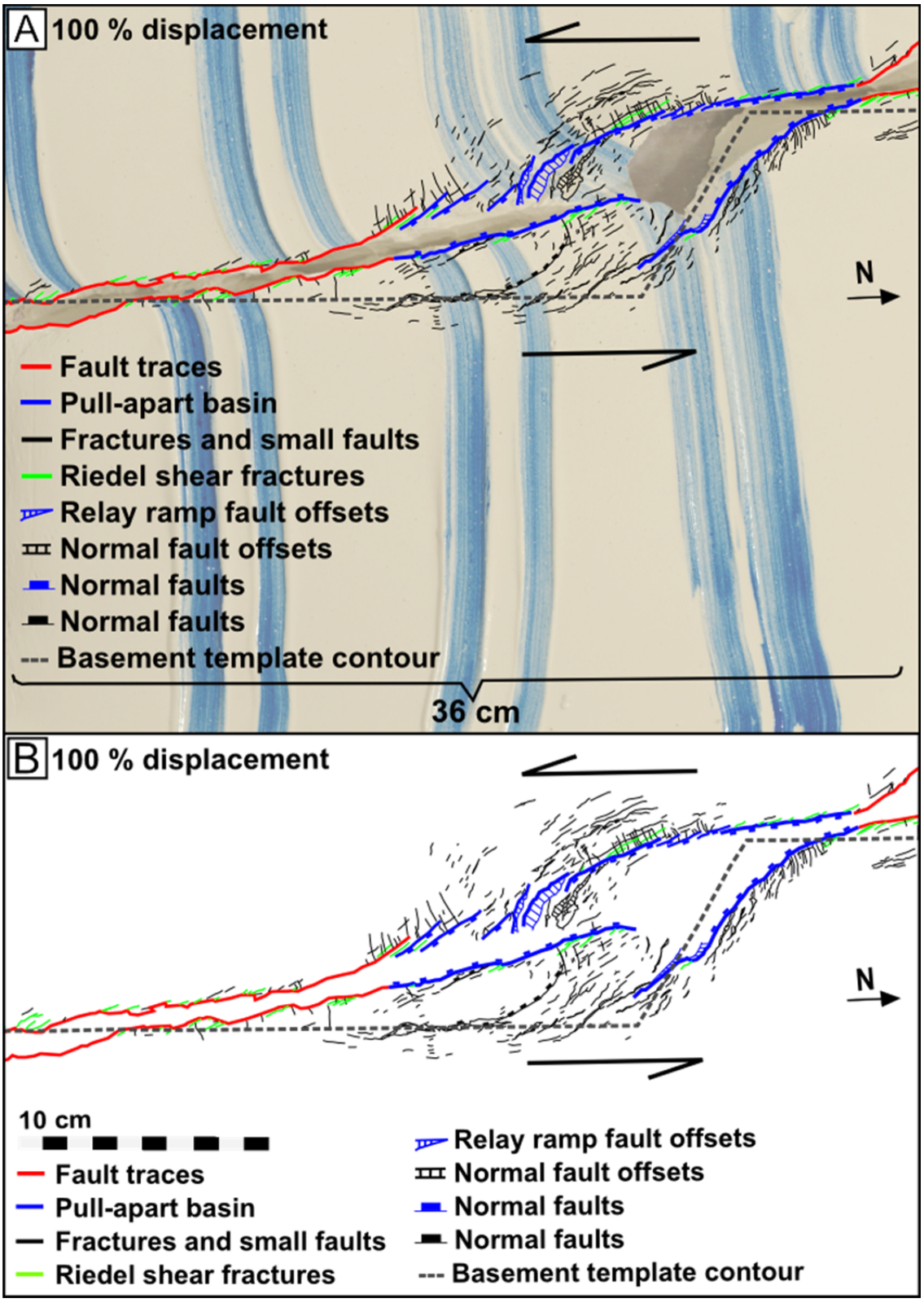


**Figure 3.43 A and B:** The final interpretation of experiment 37-14.

The areas outlined in purple in Figure 3.44 represent the places where the edge effects have made the biggest impact in this model. The red square portrays the areas shown in Figures 3.43 A and B.

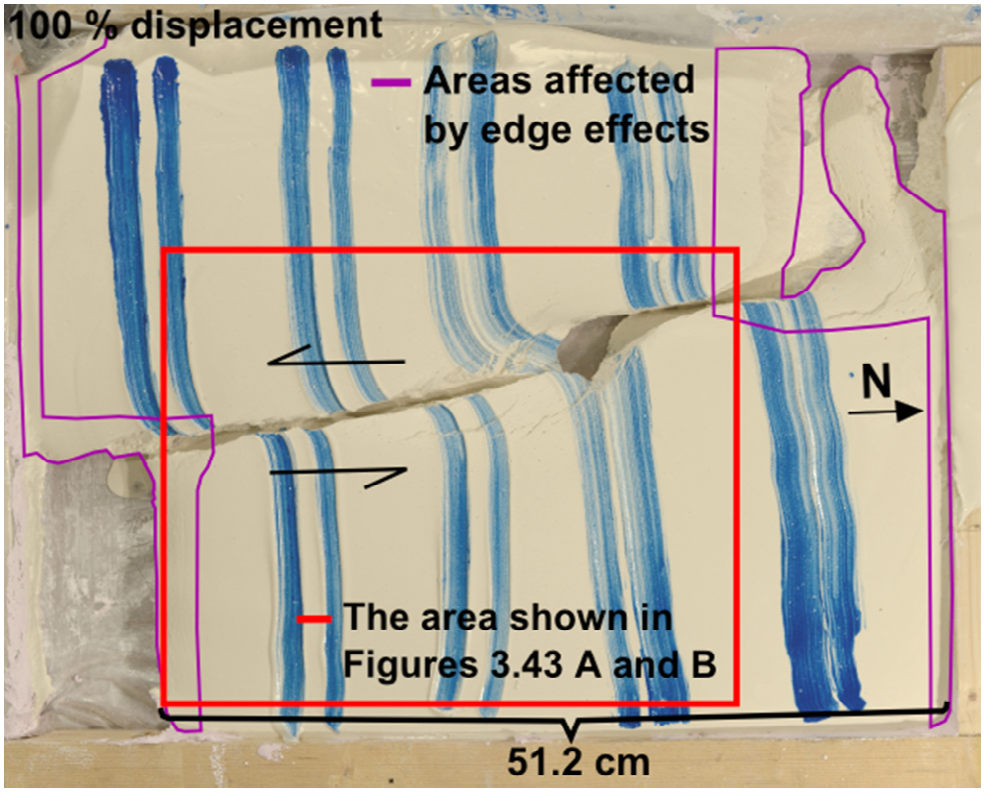


**Figure 3.44:** The areas that were the most affected by edge effects are outlined in purple and the red square shows the area portrayed in Figures 3.43 A and B.

## 3.4 Experiments with a combination of transtension and transpression

The basement templates used in the following two experiments (19-14 and 08-13) had a more complex geometry compared to the basement templates used for the six experiments described above. The finished model of experiment 19-14 comprised three main structures that represented transpressional and transtensional deformation. Experiment 08-13 was transtension-dominated, but also contained a small convergent structure.

### 3.4.1 Experiment 19-14

The purpose of this study was to reproduce deformation associated with a naturally occurring subsurface fault system, and to see the development of structures by using a similar basement template to the one in nature. To simplify the description of the development, this report refers to irregularity X and Y in the basement geometry (Fig. 3.45 A). The mixture was poured into the frame quite early, resulting in disruption of the marker stripes (Fig. 3.45 B). At the time of deformation it had the right consistency. General information about the setup and duration of experiment 19-14 is found in Table 3.8 and a video of this experiment is found in Appendix A (Video 7).

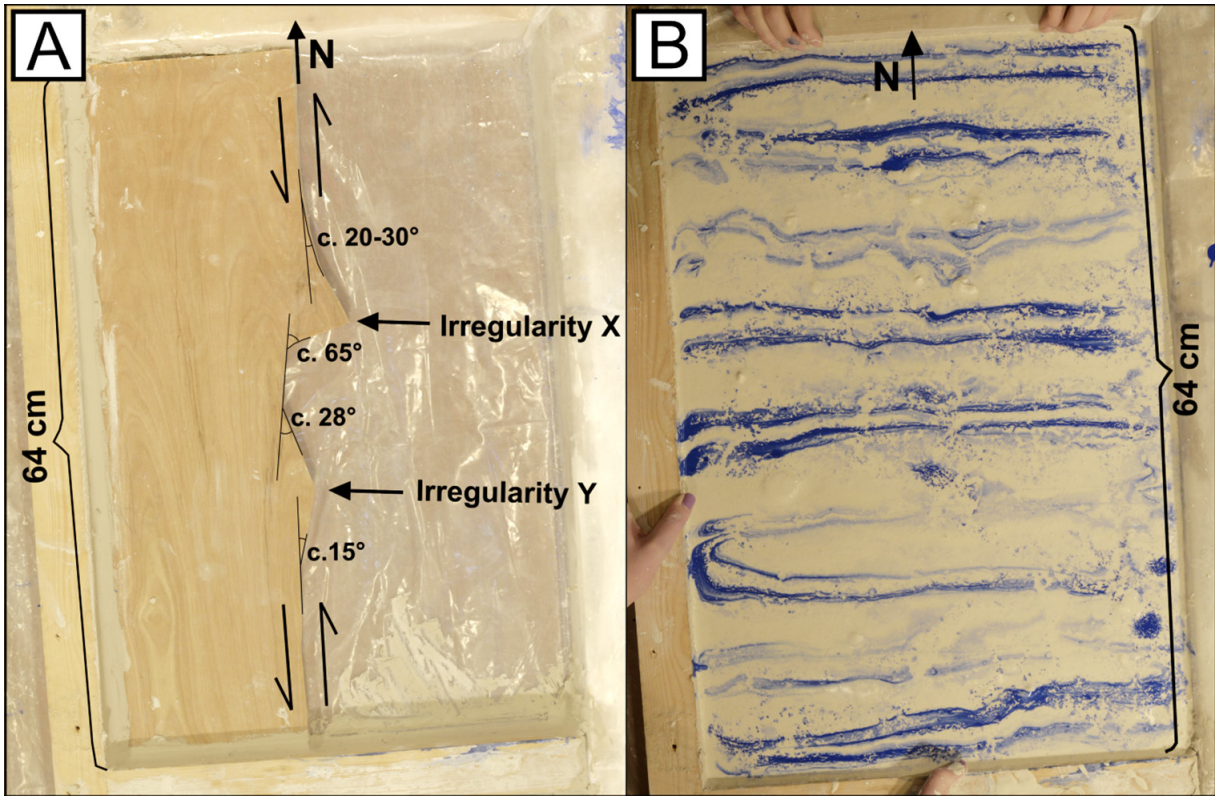


**Figure 3.45 A:** The basement template. **B:** Marker stripes disrupted by water percolation.

**Table 3.8**

| | |
|---|---|
| Date of the experiment | 19.02.2014 |
| Plaster mixture | 8.8 liters of plaster and 6 liters of water |
| Plaster to water ratio | 1.46:1 |
| Duration | 16 seconds (significant movement for 9 seconds) |
| Length of the short sides of the frame | 43 cm |
| Length of the long sides before and after displacement | Before displacement: 64 cm<br>After displacement: 70 cm |
| Total displacement | 6 cm |

**Table 3.8:** General information about the setup and duration of experiment 19-14 is given in this table.

Brittle deformation commenced from the beginning of movement in the northern part of the model, with the expansion of fractures located at heterogeneities (lumps) in the plaster mixture. These fractures were present before deformation started and one of these gradually opened north of irregularity X as the western fault block was moved southwards relative to the eastern block. With continued displacement this structure evolved into a pull-apart basin bounded by the walls of the

tensile fracture and the main fault. Towards the end of the experiment a tensile fracture on the basin's southern side opened further and caused a change in shape (this started happening c. 72 % into the displacement). Figure 3.46 A shows the basin c. 25 % into the movement, after 1.5 cm displacement. The next image (Fig. 3.46 B) illustrates the basin c. 58 % into the displacement (equivalent to 3.5 cm) and Figure 3.46 C shows the basin at its final stage, after 6 cm displacement.

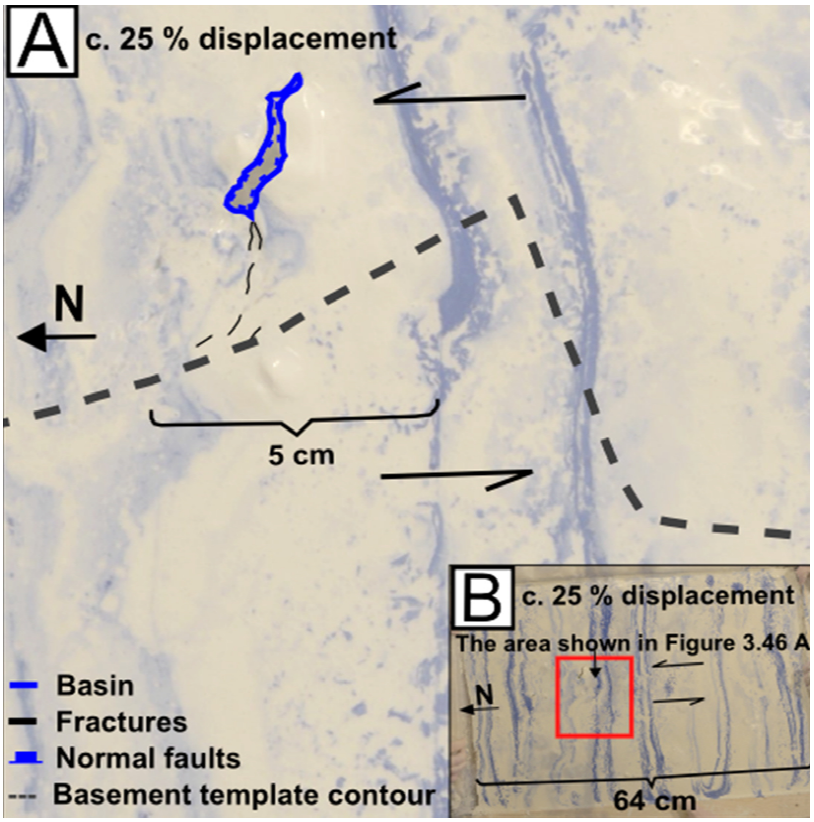


**Figure 3.46 A:** The basin c. 25 % into the displacement.
**B:** The red square portrays the area shown in Figure 3.46 A.

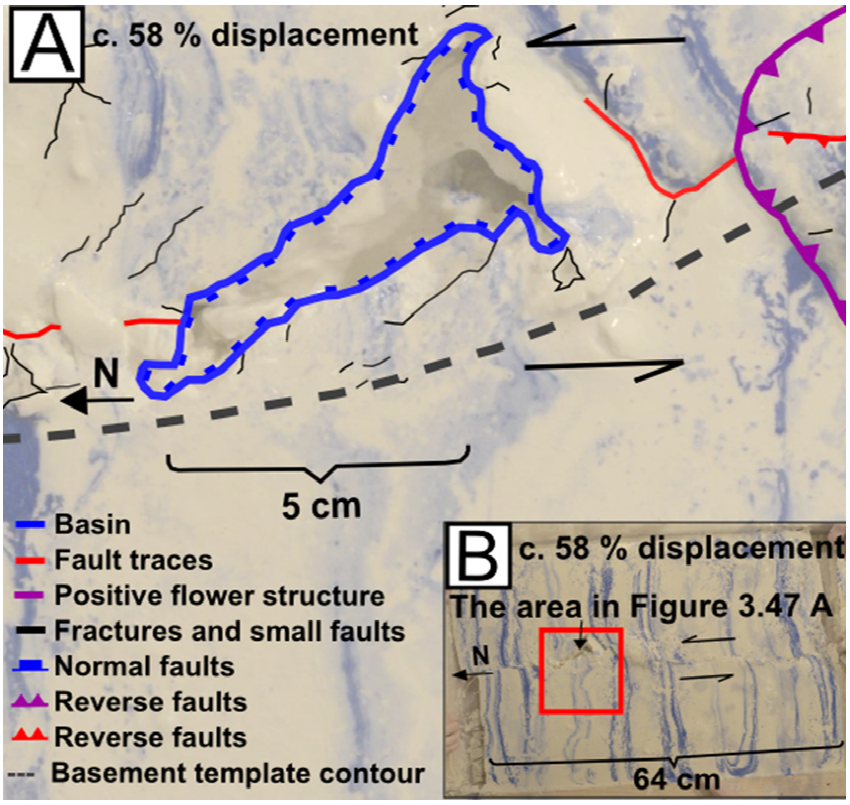


**Figure 3.47 A:** The basin c. 58 % into the displacement.
**B:** The area lined in red represents the area shown in Figure 3.47 A.

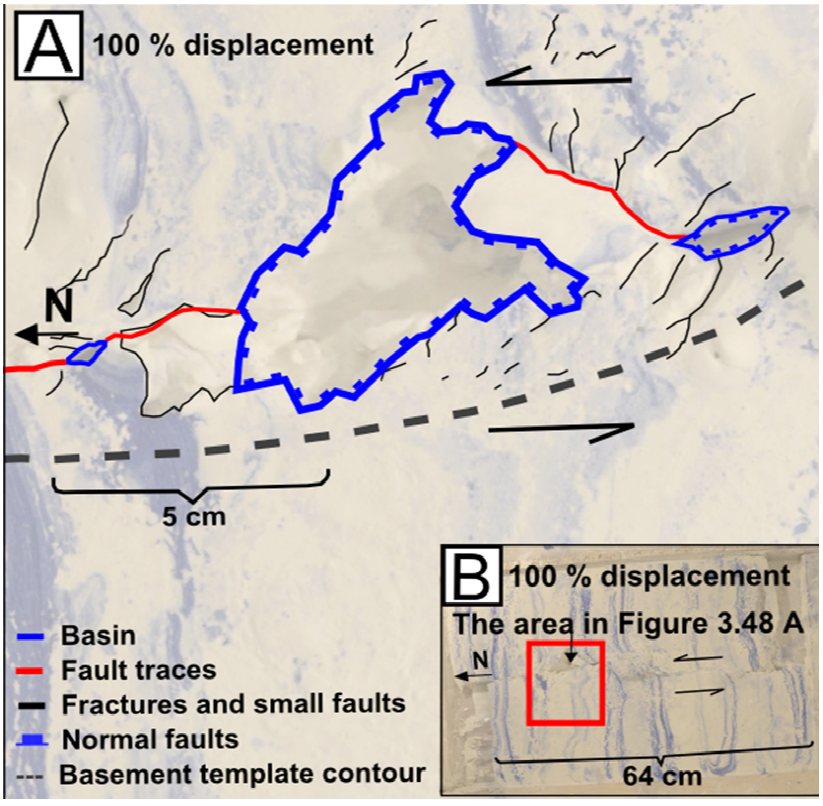


**Figure 3.48 A:** The pull-apart basin after displacement.
**B:** The area lined in red illustrates the area shown in Figure 3.48 A.

Plaster started accumulating south of irregularity X approximately 13 % into the motion, and a pop-up structure formed. Shortly after, a fault trace formed in the northern part of the model and extended southwards to just south of the basin. All the stripes north of irregularity X showed significant displacement after c. 30 % movement. The pop-up structure, classified as a positive flower structure, grew throughout the experiment, particular on its eastern side (Figs. 3.49 A and B, 3.50 A and B, and 3.51 A and B).

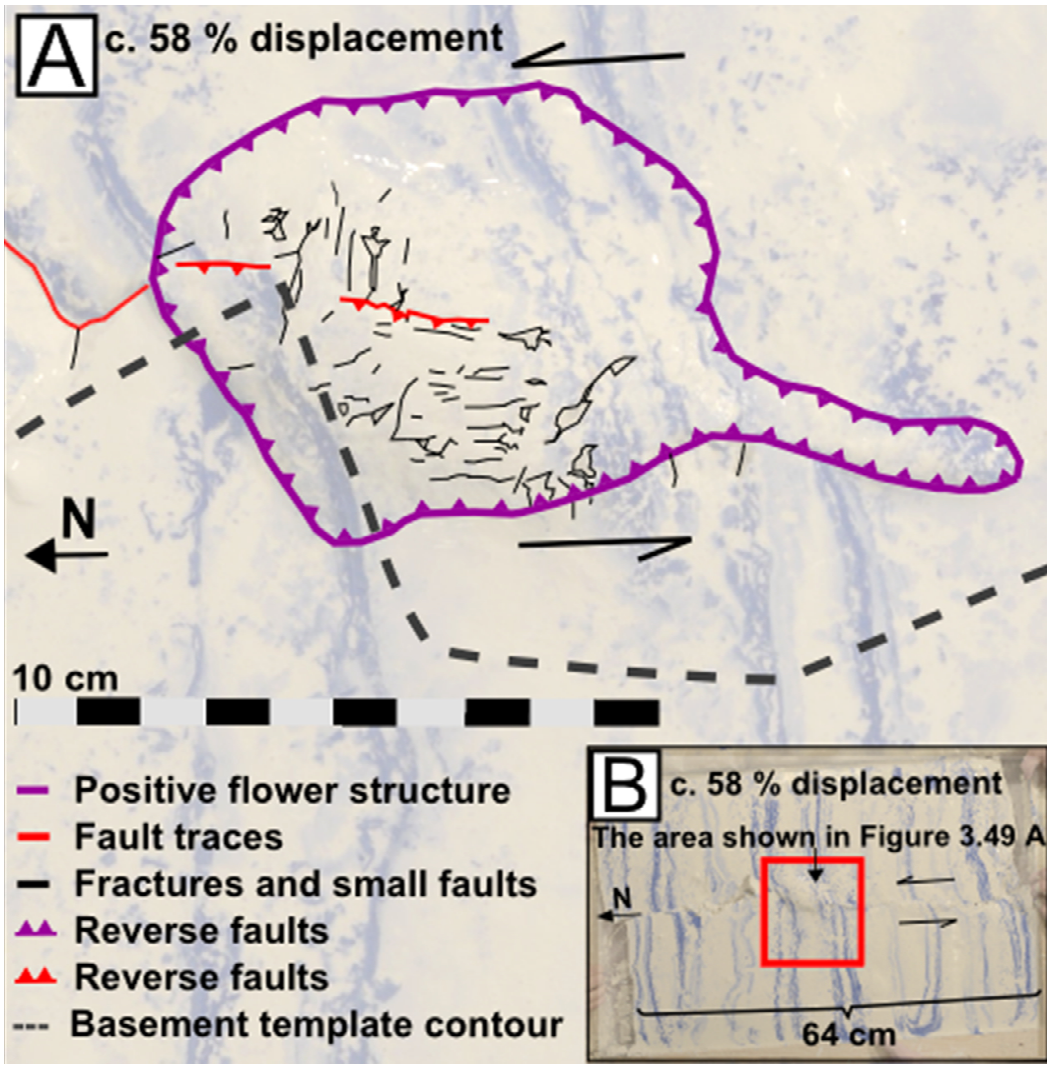


**Figure 3.49 A:** The flower structure c. 58 % into the displacement.
**B:** The area lined in red illustrates the area shown in Figure 3.49 A.

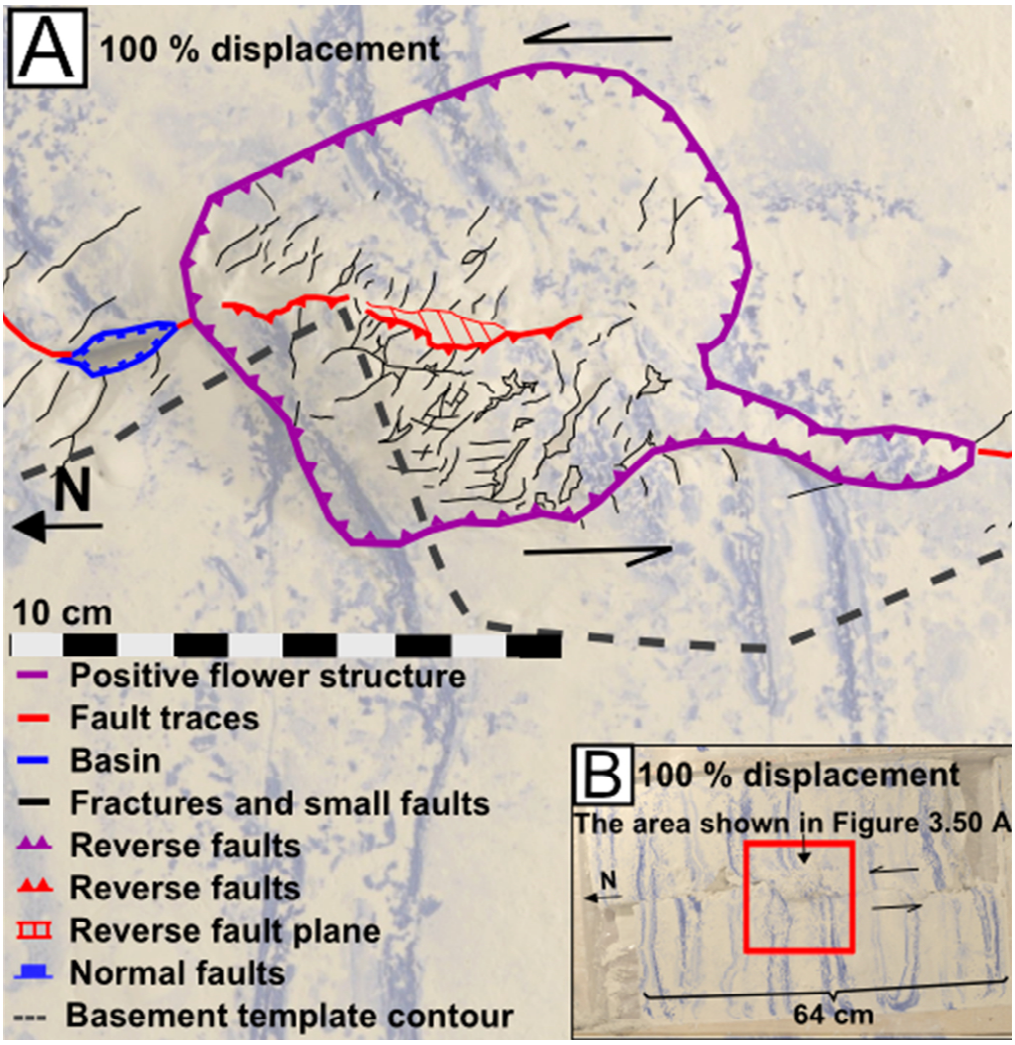


**Figure 3.50 A:** The positive flower structure after displacement.
**B:** The area lined in red shows the area illustrated in Figure 3.50 A.

After c. 30 % of the movement another pop-up structure started developing south of irregularity Y in the basement template. The light reflection and the fractures concentrated in this area made the plaster accumulation evident. A fault trace (oriented N-S) became visible between the two positive structures shortly after, and fractures with the orientation NNW-SSE were located along the fault trace in this area. These fractures were classified as riedel shear fractures. As the displacement increased these structures became more pronounced. The positive structure in the southern area, also classified as a flower structure, was smaller than the one that formed first. Figures 3.51 A and B and 3.52 A and B show this structure circa 58 % into the displacement and after displacement, respectively.

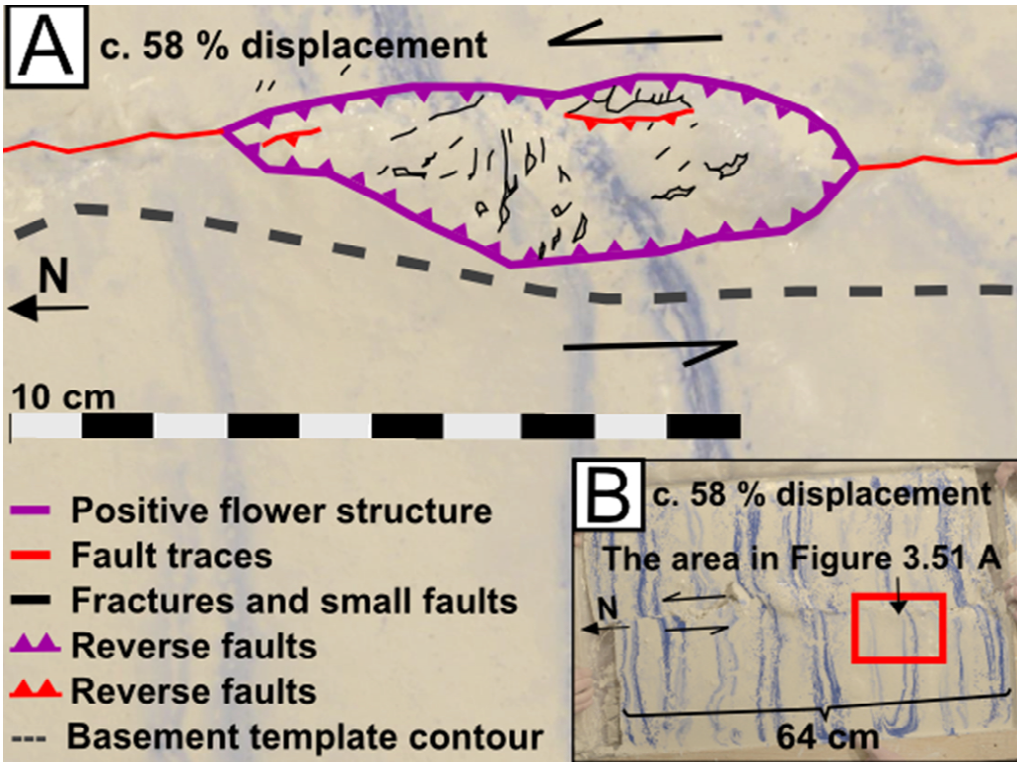


**Figure 3.51 A:** The small flower structure c. 58 % into the displacement.
**B:** The red square shows the area portrayed in Figure 3.51 A.

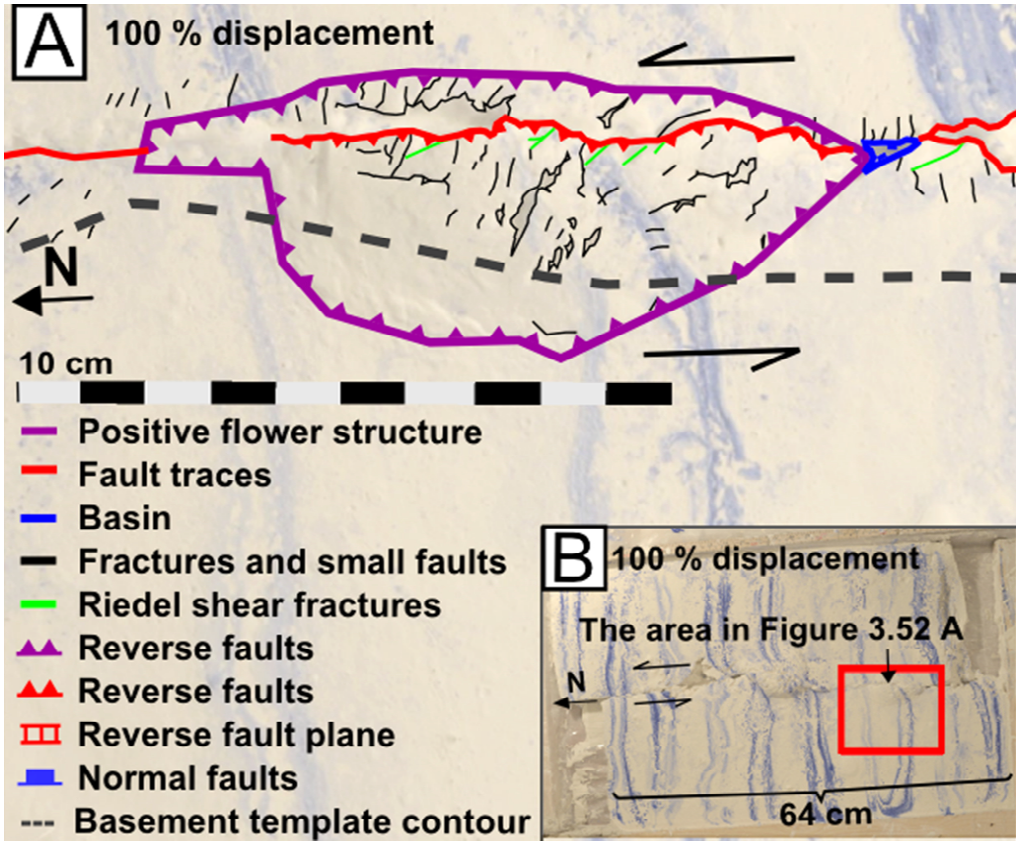


**Figure 3.52 A:** The small positive flower structure after displacement.
**B:** The red square shows the area in Figure 3.52 A.

The fractures on top of the major flower structure had various orientations, but the majority of the fractures were oriented NW-SE and N-S (Fig. 3.50 A). On the southern side the positive structure ended in a thinned, elongated tail-like form. One could see that the positive structure expanded significantly on its eastern side from c. 60 % movement and onwards, and to a smaller degree on its western side. The plaster built up to a higher angle on the southern side and west of this feature.

The fractures on top of the small flower structure had the main orientations NW-SE, NNW-SSE (Fig. 3.52 A). The western side of this structure formed with a higher angle than the eastern side, and the structure was largest on the western fault block side. Expansion occurred with the smaller flower structure as well, but to a less extent.

Fractures formed in other parts of the model as well, shown in Figures 3.53 A and B of the finished model. The total displacement in this experiment measured approximately 6 cm, making the length of the model 70 cm. The major flower structure was c. 13 cm long, and had a maximum height of c. 2.2 cm. The small flower structure was c. 11 cm long and c. 0.9 cm at its highest. The basin was c. 6.2 cm in the longest direction. The angle between the riedel shear fractures that were evident in the finished model and the main fault ranged between c. 20-30°.

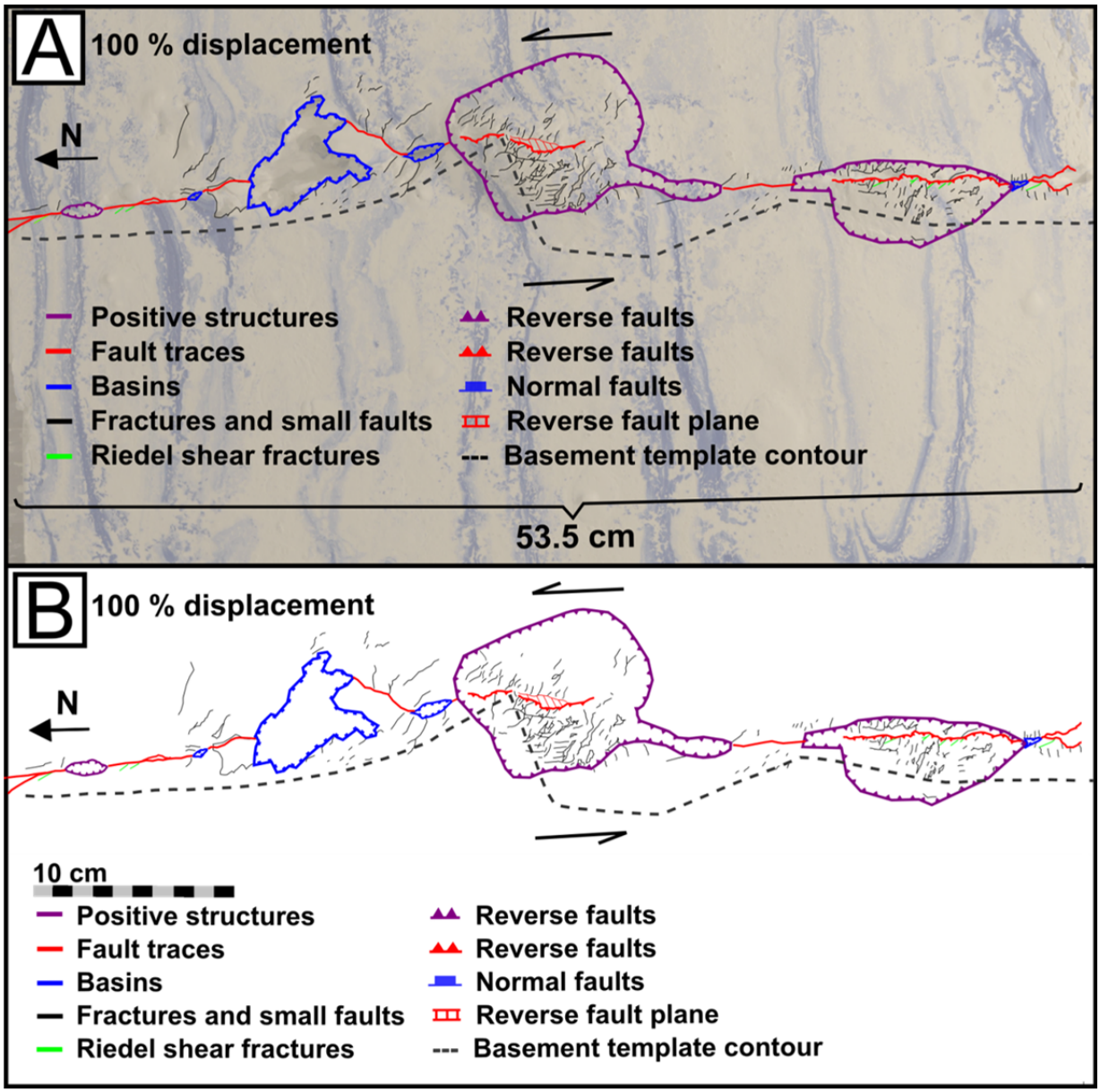


**Figures 3.53 A and B:** The final interpretation of experiment 19-14.

Figure 3.54 shows the areas that were affected the most by the edge effects in this experiment. The red square shows the area portrayed in Figures 3.53 A and B.

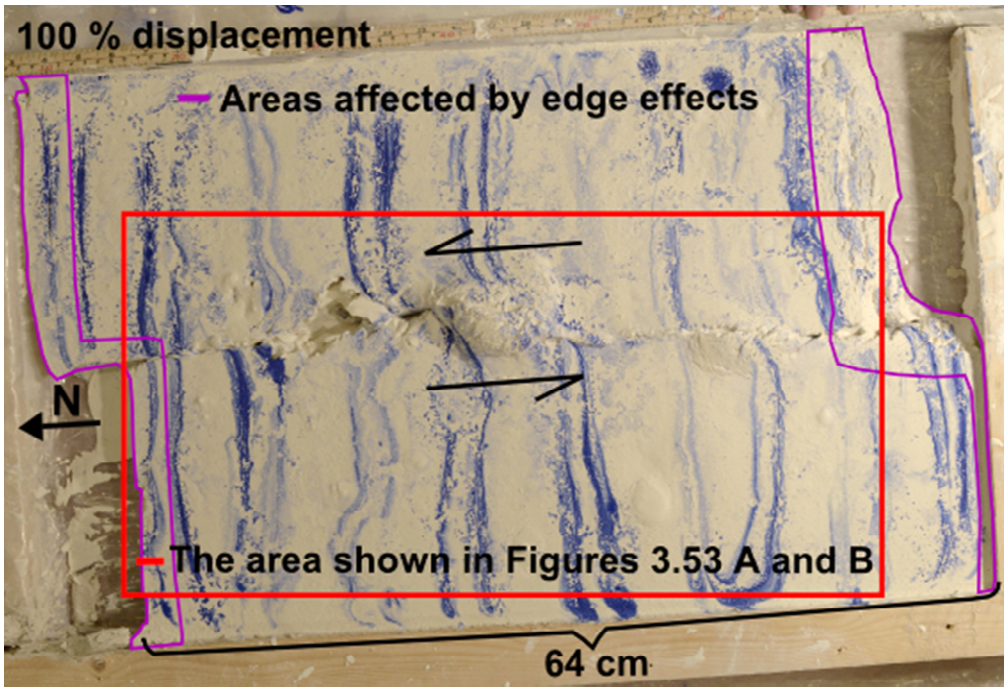


**Figure 3.54:** The red square shows the area portrayed in Figures 3.53 A and B and the areas outlined in purple are the areas that were the most affected by edge effects.

### 3.4.2 Experiment 08-13

The setup for this experiment was different than for the other experiments. The frame was restricting on all sides, as described in chapter 2 (methods).The basement template used in this experiment contained a large releasing bend and a small irregularity/ paired releasing and restraining bend (Fig. 3.55 A). The plaster mixture was of the right consistency when the deformation was initiated. The marker stripes were applied using a rag and were therefore very uneven (Fig. 3.55 B). Because of this the stripes were not used as reference points in the description. General information about the setup and duration of experiment 08-13 is found in Table 3.9, and a video of this experiment is found in Appendix A (Video 8).

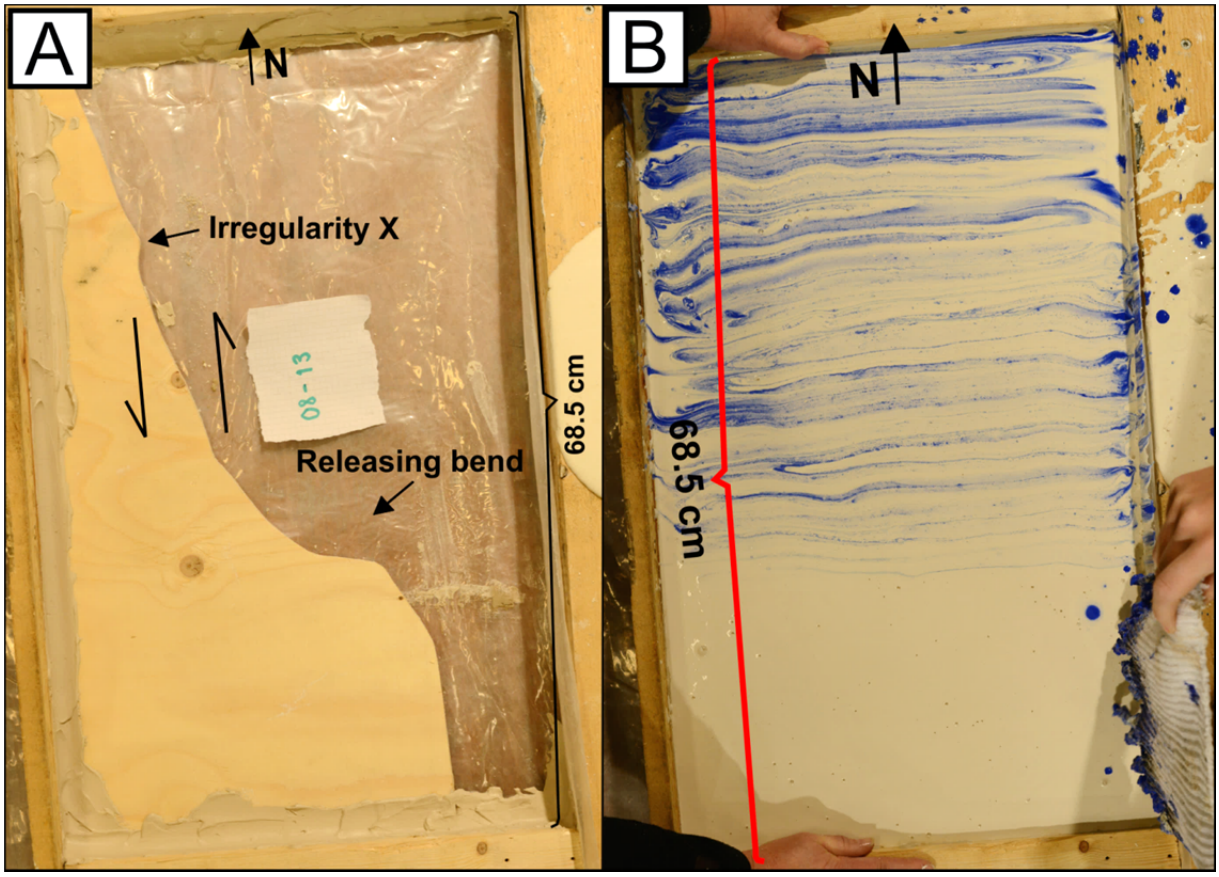


**Figure 3.55 A:** The basement template. **B:** Application of marker stripes using a rag.

**Table 3.9**

| | |
|---|---|
| Date of the experiment | 13.11.2013 |
| Plaster mixture | 9 liters of plaster and 6 liters of water |
| Plaster to water ratio | 1.5:1 |
| Duration | 15 seconds |
| Length of the short sides of the frame | 42 cm |
| Length of the long sides | 68.5 cm |
| Total displacement | Approximately 3.8 cm |

**Table 3.9:** General information about the setup and duration of experiment 08-13 is given in this table.

Brittle deformation started c. 11 % into the total displacement of 3.8 cm, when a small fracture oriented NW-SE formed in the middle part of the model, in the area of the releasing bend. Many more tensile fractures formed in this area with orientations similar to the underlying releasing bend, as shown in Figures 3.56 A and B which portray this area c. 21 % into the movement. With further

displacement many fractures expanded in width. Some large fractures developed with a high degree of normal displacement as they were expanding; Figures 3.57 A and B illustrate this normal faulting c. 47 % into the movement. The north-eastern fault block defined the hanging wall, and thus sloped downwards towards the south-western footwall block. The area thus contained a large basin, which will be referred to as a rift basin/ pull-apart basin in the continued description. The northern edge of this basin became noticeable with further displacement (after 47 % of the movement).

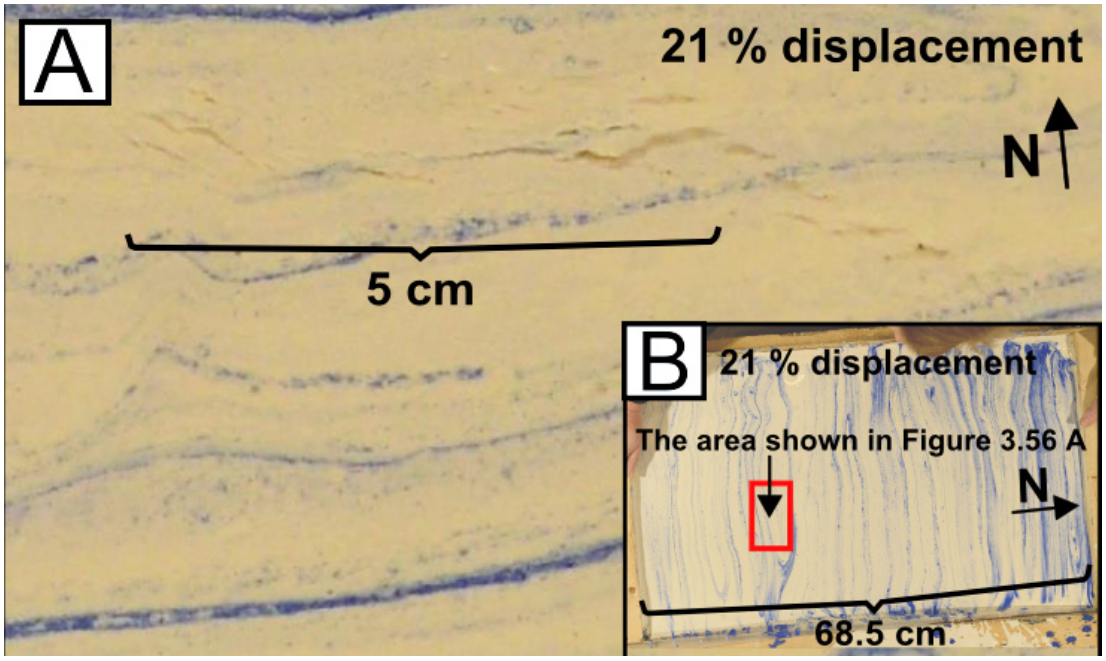


**Figure 3.56 A:** The area of the releasing bend shortly after c. 21 % of the displacement.
**B:** The area in the red square is the area shown in Figure 3.56 A.

Approximately 34 % into the movement WSW-ENE aligned fractures had formed just south of the rift basin and these were classified as riedel marked shears. Further south fractures characterized as riedel shears were oriented NNW-SSE, synthetic to the main fault trend (Figs. 3.57 A and B). Northwest of the rift basin very pronounced normal faults eventually formed. These were subparallel structures located next to one another, as illustrated in Figure 3.57 A. Strike-slip fault traces consisting of several segments had formed northwest and southeast of the releasing bend area c. 47 % into the movement (Fig. 3.57 A).

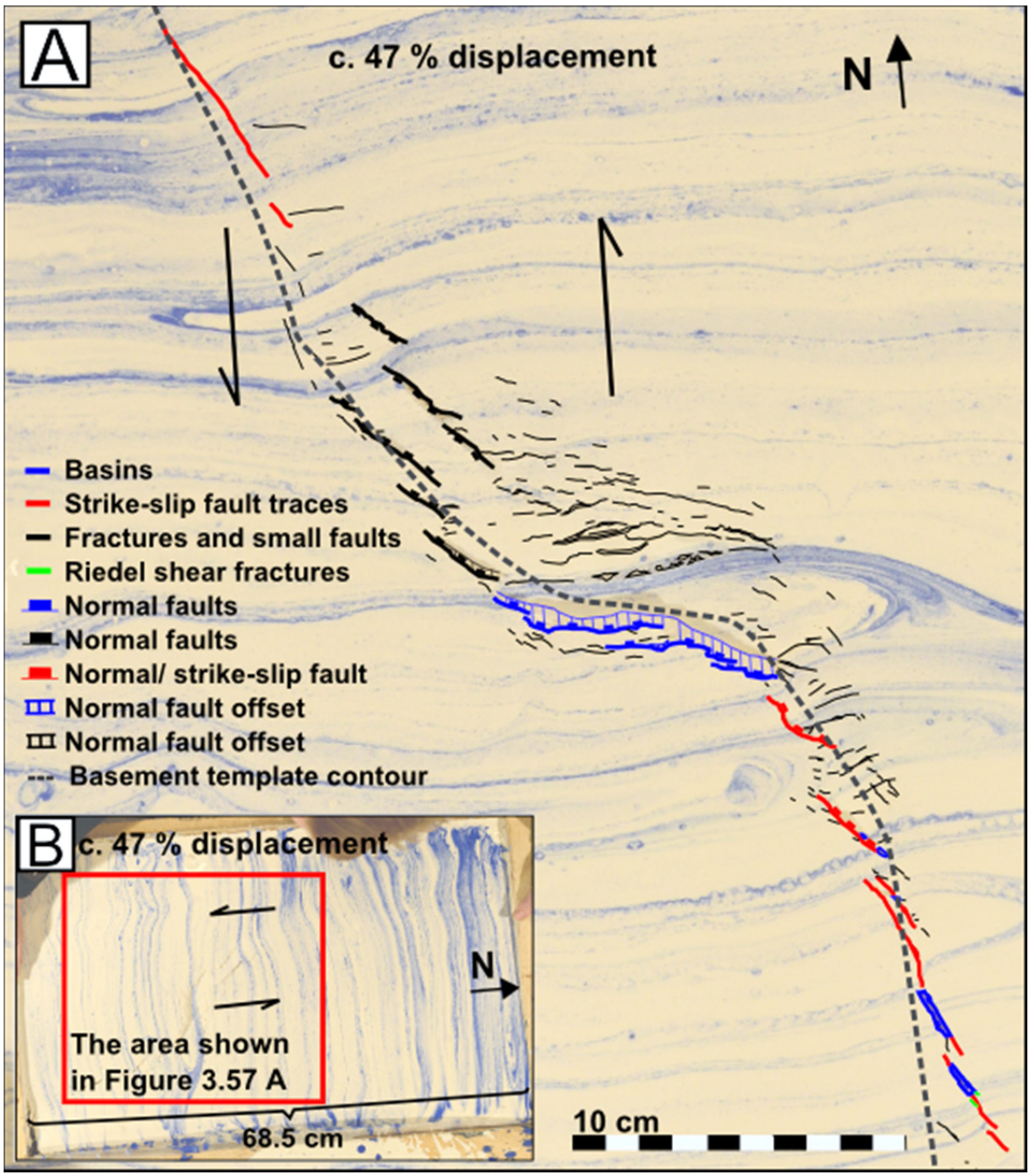


**Figure 3.57 A:** Experiment 08-13 c. 47 % into the displacement.
**B:** The area lined in red represents the area illustrated in Figure 3.57 A.

After c. 55 % of the movement the southern fault trace was close to continuous. Four small basins had formed in the southern area where fractures had expanded. A part of the plaster comprising the northern side of the rift basin had partly detached from the north-eastern fault block, due to this part being down-faulted relative to the western side of the basin (Fig. 3.58 A).

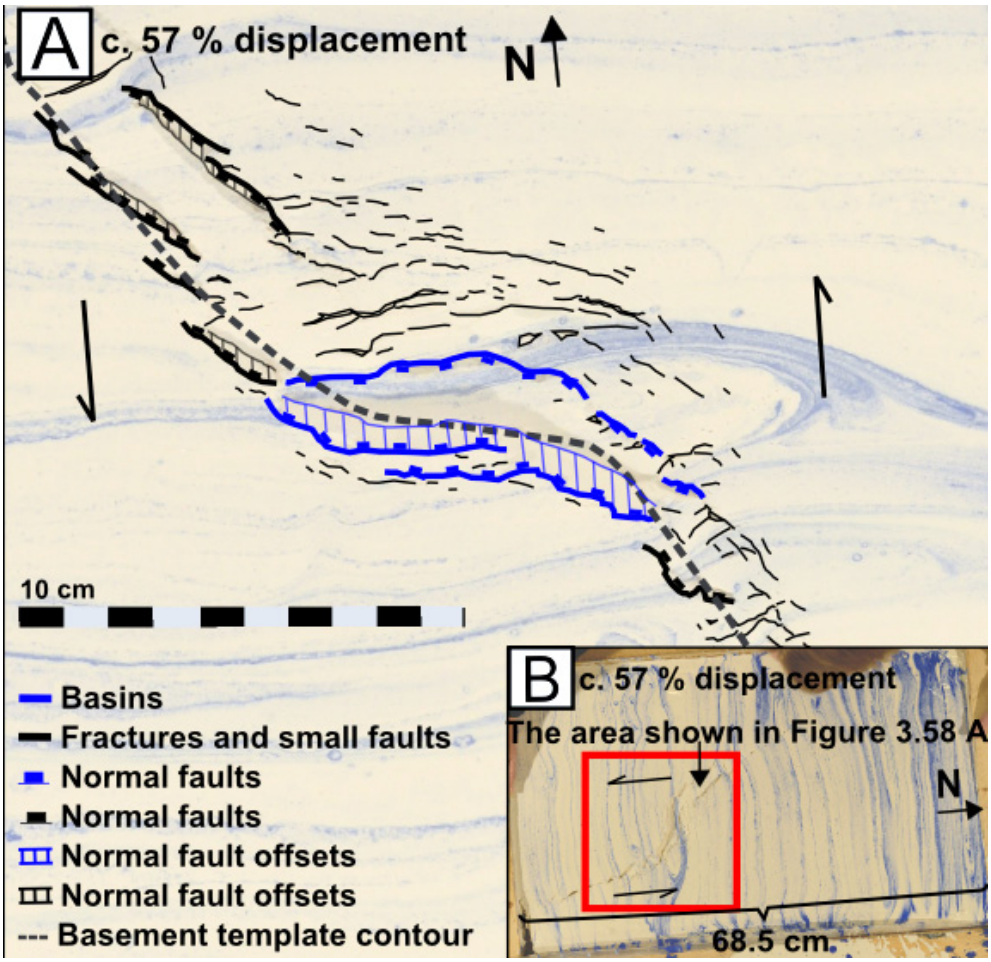


**Figure 3.58 A:** The releasing bend area c. 57 % into the displacement.
**B:** The red square shows the area illustrated in Figure 3.58 A.

When c. 70 % of the motion was reached the rift basin had expanded in width. More fault segments had developed northwest of the parallel normal faults; these were also subparallel and located next to one another. Towards the end of movement one of these fault segments expanded and a basin formed, as shown in Figures 3.59 and 3.60.

Some of the smaller basins in the southern area linked together and three basins were present in the finished model (Figs. 3.59 and 3.60). The northern area also held two small basins after displacement, one of which was mentioned above (as the previous normal fault). The plaster between the parallel fault segments showed normal displacement (as the hanging wall) relative to the two main fault blocks. Because this area was connected to the pull-apart basin, the extent of the basin became much greater when this area sunk, as illustrated in Figures 3.59 and 3.60. The maximum width of the basin was c. 3.6 cm after displacement and the length of the basin was c 28 cm (including the area northwest of the large pull-apart basin).

A small positive structure had formed in the north, just south of irregularity X in the basement template. Several fractures of significant extent were located east and southeast of the flower structure (Figs. 48 and 49). Riedel shear fractures were evident in the southern half of the model and a few antithetic fractures could be seen further north. The angle between the riedel shears and the main fault varied between c. 11-20°, and the antithetic fractures had an angle of c. 60-70°, because these latter structures were curved this is a rough estimate.

The north-eastern fault block was the most affected by transtension, in the area of the bend; a lot of tensile fractures had developed here, as illustrated in the figures below (Figs. 3.59 and 3.60). This model was displaced less than the other experiments described, namely 3.8 cm. Several of the marker stripes were deflected towards the movement direction, the ones located in the middle of the model were the most affected. The finished model displayed several relay ramp structures sloping into the large basin from the north-eastern from both fault blocks and ramp structures had formed in two of the small southern basins (Figs. 3.59 and 3.60).

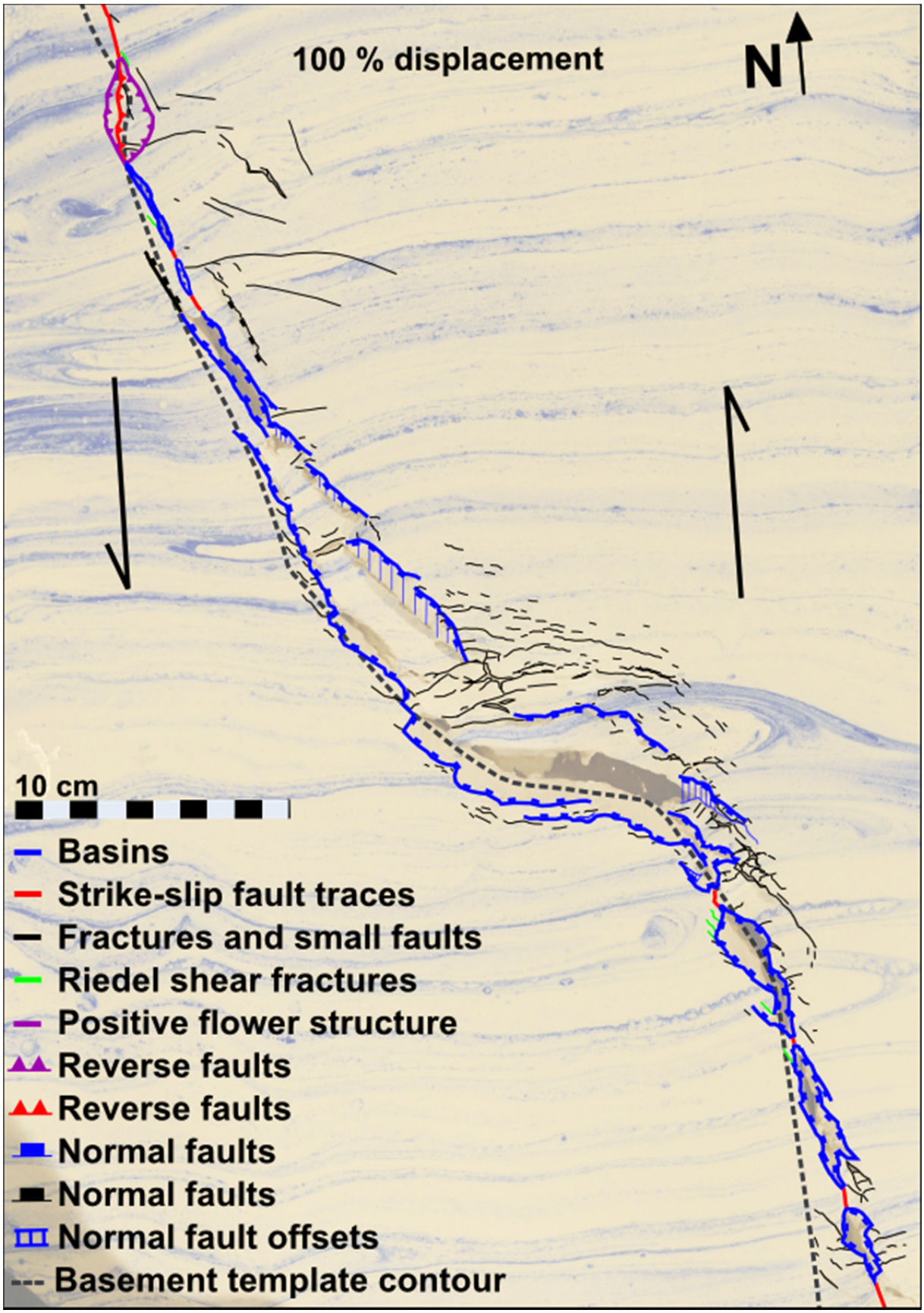


**Figure 3.59:** The final interpretation of experiment 08-13.

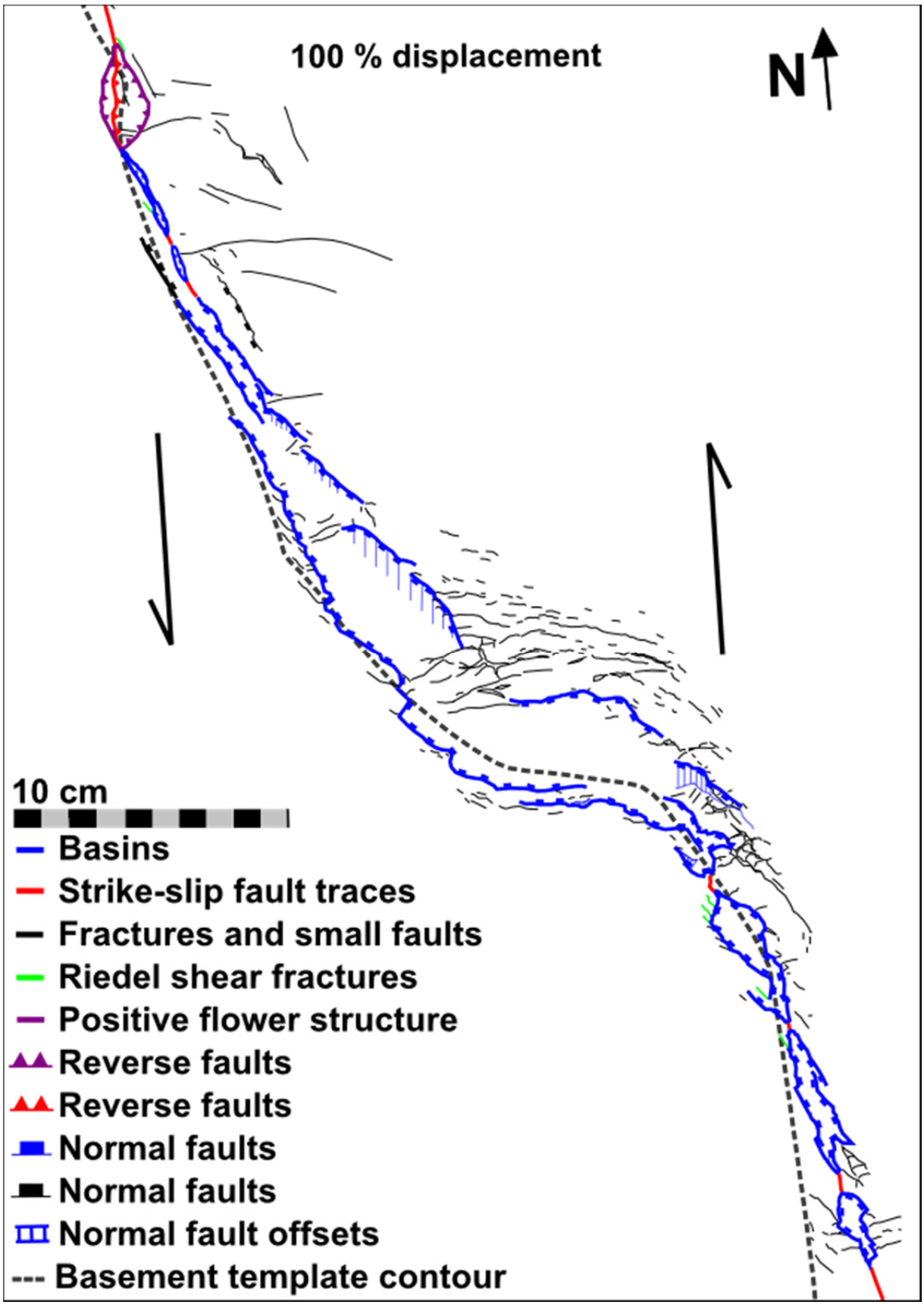


**Figure 3.60:** The final interpretation of experiment 08-13.

The areas that were affected the most by edge effects are pointed out in Figure 3.61. Because the frame used in this experiment was restricting on both of the short sides a lot of plaster accumulated in the northern area. The red square outlines the area shown in Figures 3.59 and 3.60.

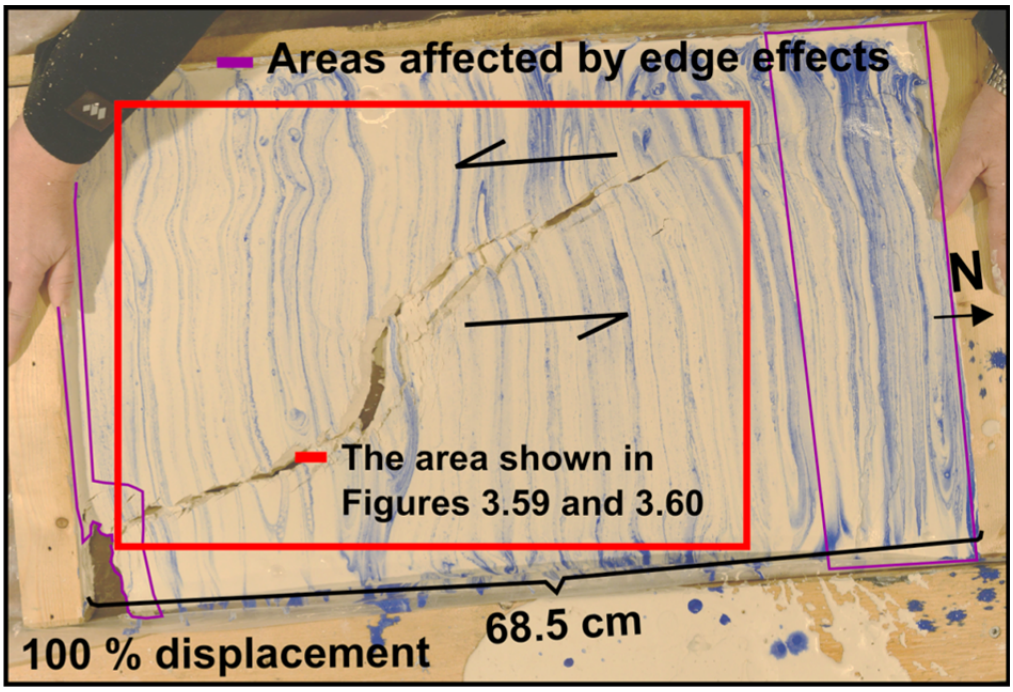


**Figure 3.61:** The red square shows the area portrayed in Figures 3.59 and 3.60 and the areas lined in purple were affected the most by edge effects. A lot of plaster accumulated in the northern area due to the restricting frame.

# 4 Discussion

## 4.1 Introduction

The main aim for this analogue modeling study has been to gain insight into the geometry and evolution of structures formed as a result of differently angled releasing and restraining bends in the basement configuration of strike-slip faults. In this chapter, the results from this study are discussed, and compared with natural strike-slip fault systems as well as with other analogue modeling studies focusing on strike-slip deformation.

All of the experiments described in this thesis emulated sinistral fault settings. For strike-slip faults in general, and thus for the main faults in the eight experiments described, $\sigma_1$ is horizontal with an angle to the main fault direction, making the fault blocks move along each other (Fossen, 2010). This is illustrated in Figure 4.1.

According to Christie-Blick and Biddle (1985) there are four main factors that control the nucleation and growth of structures along a continental strike-slip fault. The influence of transpressive and transtensive deformation along a fault is one important factor. Another element is the amount of displacement along a fault. The characteristics of the materials being deformed is a third key factor, and the fourth is the presence and location of previously formed structures along a fault. These factors have affected the models made in this study and some will be discussed in the following sub-chapters, with a particular focus on transpressive and transtensive deformation.

## 4.2 Transpressive experiments

A comparison between the transpressive experiments (32-14, 34-14, 36-14 and 19-14) has been done. The model with the two irregularities in the basement geometry (19-14) had very different experimental conditions from the other models, and was therefore compared to the other models at the end of the section “Positive flower structures”.

**Positive flower structures**

The width of the bends in the three models with simple restraining bends (32-14, 34-14 and 36-14) was 7 cm (normal to the main fault orientation). Brittle deformation on the model surface commenced before 10 % of the displacement was reached for all these experiments. The plaster mixtures used in these experiments were of the same consistencies when deformation commenced,

and the condition of the plaster mixture can therefore largely be disregarded when comparing the experiments.

The positive flower structures that formed in the experiments with 30°, 45° and 60° angles had very different characteristics. Seven fault blocks constituted the flower in the model with the most gently angled bend (30°) after a total displacement of 20.9 cm (Fig. 3.9 A). These were oriented similarly to the releasing bend in the underlying basement template and to the overall orientation of the flower structure relative to the main fault trend (Figs. 3.10 A and B). All the fault blocks were relatively narrow and long (Figs. 3.10 A and B).

The flower structure that formed in the model with the 45° bend comprised five fault blocks after a displacement of 24.7 cm (Fig. 3.16 A). The southern fault block had an angle of c. 20° relative to the main fault trend (N-S), and the blocks further north were angled c. 40-50° relative to the main fault. These blocks were wider compared to the ones that formed in the 30° experiment.

Three fault blocks constituted the positive flower structure in the model with the highest angled bend (60°) after a displacement of 24 cm (Fig. 3.23 A). The angles between the fault blocks and the main fault were approximately 45-50°. The fault blocks were wide and much shorter compared to the ones that formed in the other two experiments.

The first fault block within the flower structure in the model with the lowest-angled bend (30°) had formed c. 21 % into the movement, which was equivalent to 4.4 cm of displacement. In the model with a 45° bend the first fault block within the flower structure had developed c. 25 % into the movement, equal to 6.2 cm of displacement. In the experiment with the highest-angled bend (60°) the first block within the flower had formed approximately 37 % into the displacement, equivalent to 8.9 cm of displacement. The fault blocks thus formed at a later stage in the models with the higher-angled bends, and the blocks that formed at a later stage in the deformation also followed this trend.

From these above observations it appears that the flower structures comprise more fault blocks in experiments where the basement geometry contains lower-angled restraining bends. The blocks also form at an earlier stage for the models with lower-angled bends. The flower structures that develop at high-angled restraining bends comprise fault blocks with large angles to the main fault trend, based on the results from this study. According to Cunningham and Mann (2007) large positive flower structures will form in areas where $\sigma_1$ (sh max) is at a high angle to the transpressional zone (Fig. 4.1). The flower structures from the experiments discussed thus far were quite similar in size, and the flower in the 60° experiment was slightly shorter in length and height (by 1 cm) from the other two flowers discussed. The models in this study thus behaved differently from what

Cunningham and Mann (2007) stated. Figure 4.1 shows the direction of $\sigma_1$ to 30°, 45° and 60° restraining bends, where the largest bend is close to normal to the orientation of the maximum stress.

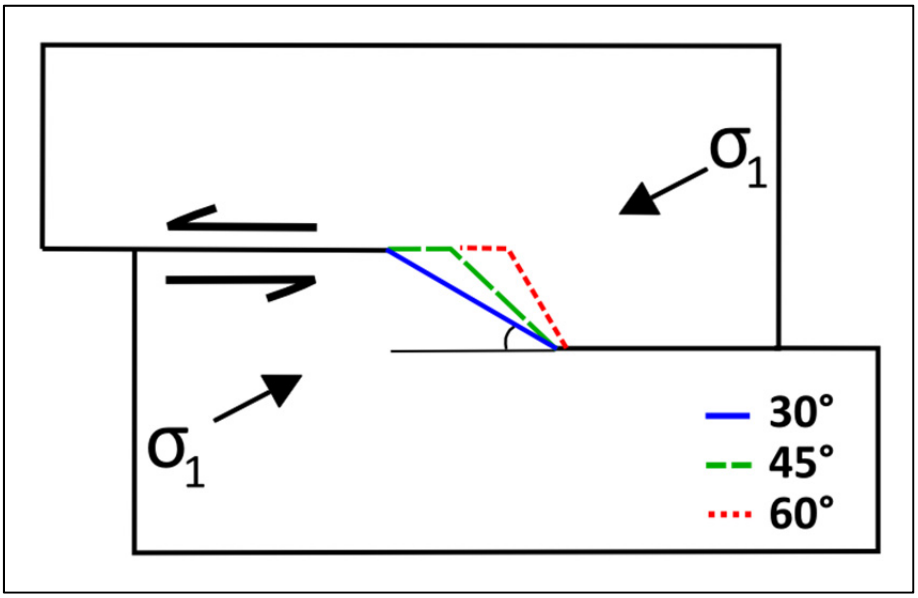


**Figure 4.1:** The orientation of $\sigma_1$ relative to restraining bends and the strike-slip fault.

The major flower structure in the model with two basement irregularities (19-14) developed in a very different manner from the flower structures discussed above. It was the result of transpression along a restraining bend with a 65° angle (Fig. 3.50 A). It comprised two fault blocks, although the reverse fault that separated these two blocks did not fully cut through the entire flower. The reverse fault was oriented N-S, thus with the same orientation as the main fault, this is illustrated in Figure 3.50 A.

The shape of the flower structure was also very different from the other mentioned pop-up structures; it was more round whereas the flowers in the 30° and 45° experiments were more oval (Figs. 3.50 A, 3.9 A and 3.16 A). The flower structure in the 60° experiment had a rhomboidal shape (Fig. 3.23 A). In the analogue modeling study performed by McClay and Bonora (2001) the geometry of the positive structures mostly depended on the angle and width of the stepovers and the thickness of the material layer (they used sand as the modeling material). The model observations made in this thesis suggest that higher-angled bends result in more rhomboidal or round shapes, whereas smaller angles lead to more oval structures. The fault blocks constituting the flowers also differ according to bend angles, as discussed earlier. The width of the bend has been 7 cm in all the experiments performed in this study. If a narrower bend would have been used the resulting flower structure would have been narrower and the flower would have more complex internal deformation, based on the study by McClay and Bonora (2001).

The displacement of the experiment (19-14) with two irregularities was 6 cm, thus much less than for the other experiments discussed (Fig. 3.53 A). Because a second fault block started developing c. 47 % into the movement in the 60° bend model (after c. 11 cm of displacement; Fig. 3.22 A), one can assume that more fault blocks would develop if this model (with two irregularities) would have been further displaced. Irregularity Y south of the pop-up structure might have stopped it from developing as freely as the other flower structures. The small flower structure south of irregularity Y also comprised two fault blocks, oriented N-S (Fig. 3.52 A). This flower structure had an oval-shaped and formed from a restraining bend with an angle of c. 20-30°.

The first fault blocks that formed in the flower structures were more affected by fracturing than the ones that formed later on in the development. Because of the amount of uplift that these fault blocks underwent relative to the younger fault blocks tensile fractures were more abundant on these blocks (3.9 A, 3.16 A, 3,23 A, 3.50 A and 3.52 A).

**Riedel shear fractures**

Riedel shear fractures formed in the three transpressive experiments when brittle deformation commenced (Fig. 3.3 A). These structures had an angle between 10-20° relative to the main fault orientation. In the model with two irregularities in the basement geometry (19-14), riedel shear fractures formed after c. 30 % of the movement was reached with angles between 20-30° from the main fault trend (Fig. 3.52 A). For the model with the 30° bend these fractures formed after a movement of c. 1.5 cm, they formed after c. 2 cm movement in the 45° bend model and for the experiment with the 60° bend riedel shears formed after a movement of c. 2.2 cm. The model with two irregularities formed riedel shears after 1.8 cm displacement. The riedel fractures thus formed after a similar amount of movement in all these experiments. (Measurements of the angles for these fractures were made after displacement).

**Summary**

General similarities between the experiments were:

- The first fault blocks that formed in the flower structures were more affected by fracturing compared to the younger fault blocks due to the amount of uplift.
- Riedel-shear fractures formed after similar amounts of displacement in the transpressive experiments.

When increasing the angle of the restraining bend, the following observations were made:

- The flower structures comprised less fault blocks after similar amounts of displacement. (The two models with higher angled bends were displaced further than the model with the 30° bend and still comprised less fault blocks).
- The fault blocks constituting the flower structures formed at a later stage in the deformation process in the models with higher-angled restraining bends.
- The fault block angles relative to the main fault trend were higher for the experiments with higher angled bends.
- The fault blocks constituting the flower structures were shorter and wider in the models with higher angled bends.
- The shape of the flower structures varied for the different angled bends. The flowers that formed by smaller-angled bends were more oval-shaped and the ones formed by higher-angled bends were rhomboidal or rounder.

**Comparisons with natural examples and other experimental work**

Many positive structures in nature have been formed by restraining bend uplift, such as several of the mountains comprising the Gobi-Altai orogen in southern Mongolia (including Ih Bogd, Baga Bogd, Bayan Tsagaan Uul and Chandiman Uul; Cunningham, 2010; Cunningham et al., 1996). Eemeltik Uul, which is one of the mountains in this range, was interpreted as an asymmetric flower structure with more thrust faults propagating towards the south compared to the north (Cunningham et al., 1996). The flower structures that formed in the three experiments with simple restraining bends share similarities with this structure, as they are asymmetric flowers with the majority of the faults propagating towards the foreland.

Another example of a flower structure is one bordering the Dent Fault in NW-England. The faults comprising the middle part of the flower structure cut through a monocline, showing that ductile and brittle deformation occurred as a result of transpression; folding most likely occurred before the faults cut through to the surface (Woodcock & Rickards, 2003). The flower structures from the experiments were affected by both ductile and brittle deformation as well. The fault blocks constituting the flowers (particularly the 30° and 45° models) displayed various amounts of folding when new blocks were generated and they moved up from the flat plaster layer. This can be seen particularly well in the figures showing the evolution of the 30° experiment (Figs. 3.5-3.9).

McClay and Bonora (2001) did a sand modeling study where they focused on the geometry and evolution of pop-up structures. They varied the width and the angle of the stepovers and they studied the effect of synkinematic sedimentation in some experiments. The pop-up structure that

formed in their experiment with a 30° stepover share similarities with the 30° restraining bend model made for this thesis (Figs. 4.2 A, B and C). Their model was displaced 10 cm, thus c. half of the movement compared to the experiment discussed earlier in this chapter. It comprised five fault blocks and it had a slightly rhomboidal shaped. The model made for this study had an eye-shape, and comprised three fault blocks after having been displaced the same amount as their model. The flower structure in the model made for this study comprised Riedel shears formed 20 % into the displacement in their model (after 2 cm displacement), compared to 1.5 cm (equivalent to 7 % of the displacement) in the model in this thesis.

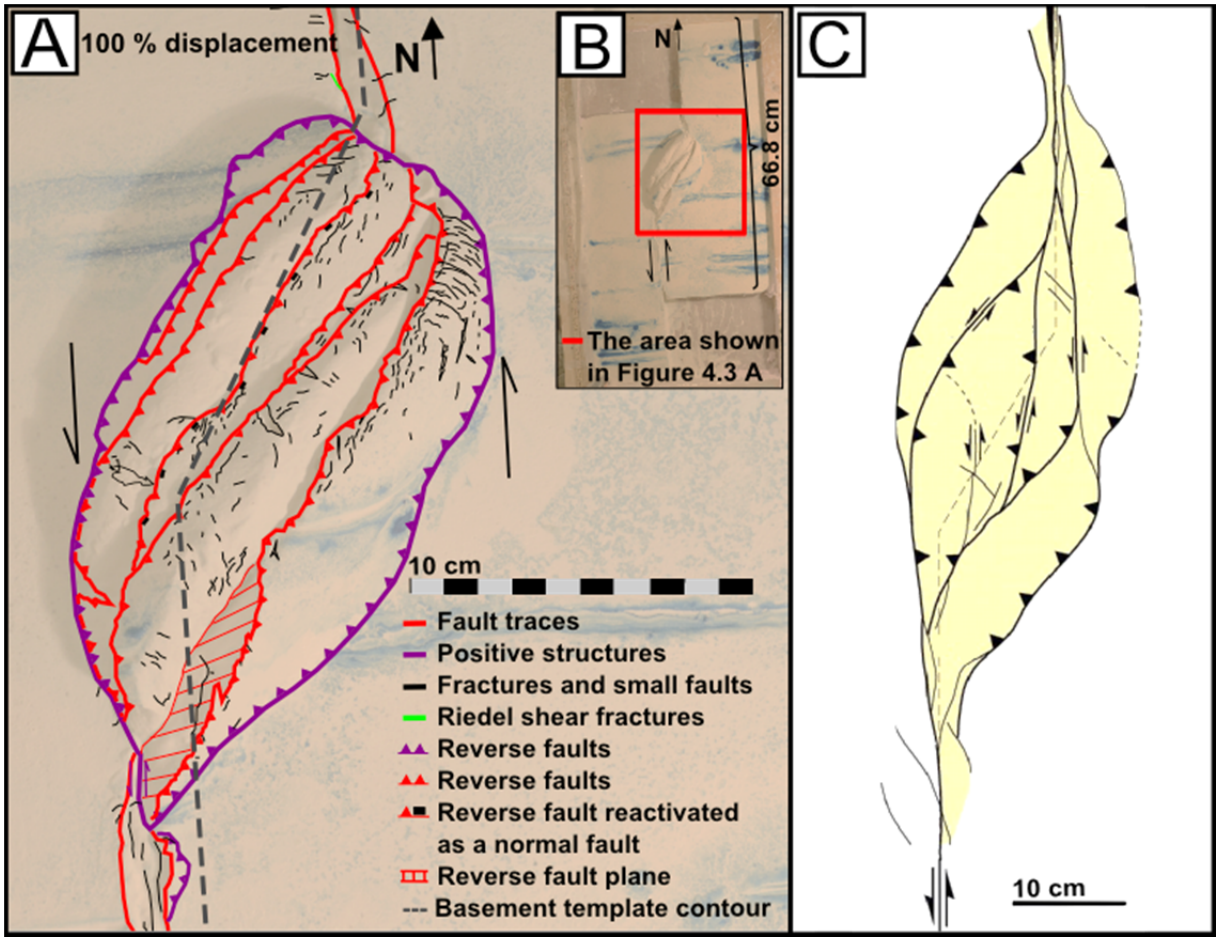


**Figure 4.2 A:** The positive flower structure that formed in the 30° experiment. **B:** The area lined in red represents the area shown in Figure 4.2 A. **C:** The pop-up structure that formed by a 30° stepover in the study done by (McClay & Bonora, 2001).

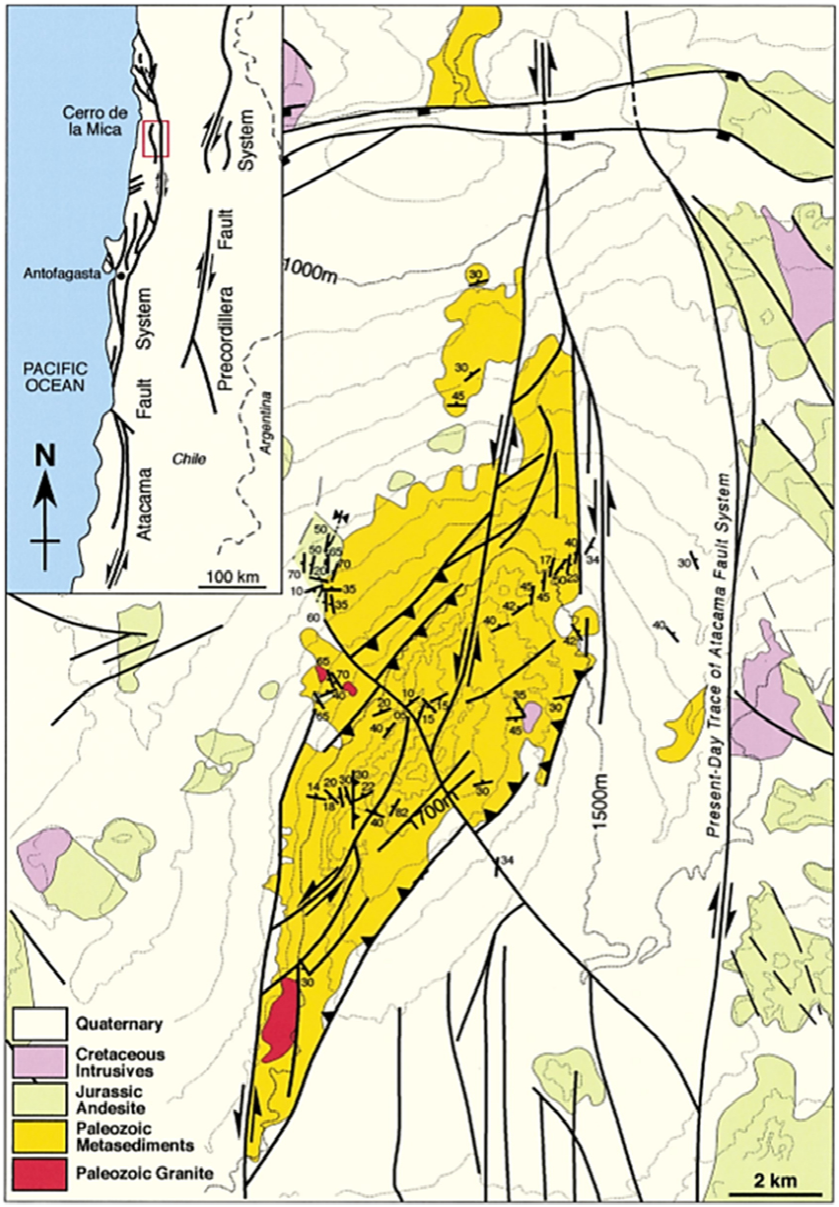


**Figure 4.3:** The Cerro de la Mica pop-up structure
in the Atacama fault zone, Chile (McClay & Bonora, 2001).

The analogue models shown in Figures 4.2 A (and B) and C closely resemble the pop-up structure called Cerro de la Mica, located in Chile (Fig. 4.3). It formed at a stepover between two faults in the Atacama fault zone in Chile. Steep reverse faults define the outer edges of this structure (McClay & Bonora, 2001). The shape of this structure particularly resembles the sand model made by McClay and Bonora (2001), and the orientation of its fault blocks is quite similar to the blocks within the two analogue models (Figs. 4.2 A and C).

Not many flower structures studied in the field have been described in detail. One does not always get a detailed overview of structures in the field, both due to their large scale, lack of exposures and

due to erosion after their formation. Based on the comparisons between the analogue models and the natural examples, several similarities are observed, such as the shape and the asymmetric geometry of the structures. This study offers an insight to the flowers' structural development, which cannot be studied in the field. Structures can be studied as a whole in analogue models, whereas in the field one often has limited access to the full structures. The models can provide a better understanding of the full fault architecture, which is often difficult in nature as the structures have been subjected to erosion. Small-scale structures that form on top of the flower structures (and in the other parts of the model) can be studied in the plaster models, whereas sand models, such as the one shown in Figure 4.2 C, can be used to study the large-scale deformation.

## 4.3 Transtensive experiments

A comparison between the four transtensive experiments (40-14, 39-14, 37-14 and 08-13) described in chapter 3 has been done. The experiment with the large releasing bend and small irregularity in the basement geometry (08-13) had very different experimental conditions from the other experiments, and was therefore compared to the other models at the end of the section "Pull-apart basins".

**Pull-apart basins**

The width of the bends in the three models with simple releasing bends was 7 cm (measured normal to the main fault orientation). The plaster mixtures used in these experiments were of the same consistencies when deformation commenced and the plaster mixture condition can therefore largely be disregarded when comparing the experiments. The three experiments with simple releasing bends were moved far, shown by the wide faults through the entire models (Figs. 3.31, 3.37 and 3.43). Brittle deformation commenced c. 18 % into the movement in the experiment with the 30° releasing bend and c. 25 % and 26 % into the displacement for the 45° bend model and the 60° bend model, respectively.

Elongated pull-apart basins formed in the models with 30°, 45° and 60° releasing bends (Figs. 3.31, 3.37 and 3.43). The main basins that formed in the area of the releasing bend connected to basins that had formed further south after 75-80 % of the displacement, therefore making the basins in the finished models quite large. Experiment 37-14 was an exception in this regard, as the small southern basin opened up towards the southern model edge, although it did connect to the main pull-apart via the down-faulted plaster that constituted the lower part of a relay ramp.

A relay ramp formed in the same area in all three models, dipping northwestwards into the pull-apart basins from the eastern fault blocks (Figs. 3.29, 3.35, 3.41). The faults that formed in the northern and the southern part of the models were connected by an oblique transfer fault. The transfer fault connected the two main fault segments c. 49 % into the displacement in the experiment with a 30° bend, which was equivalent to 6.4 cm of movement (Fig. 3.29). In the model with a 45° bend the transfer fault linked the two fault segments together c. 58 % into the movement, equivalent to 6 cm of displacement (Fig. 3.35) and the fault segments in the model with the highest angled bend (60°) were connected when c. 82 % of the displacement was reached, after 7.4 cm of the movement (Fig. 3.42). The transfer fault in each experiment thus formed after 6-7.4 cm of the displacement.

The basin that formed in the model with the smallest angle in the basement template was 28 cm long and had a maximum width of 4 cm after a total displacement of 13 cm (Fig. 3.31). The aspect ratio of this basin was 1:7 (the ratio of the basin's width to its length). The majority of the basin was narrower than the widest area just north of the big relay ramp. The basin had an overall small angle relative to the main fault orientation; a rough estimate would be between 13-20° (the curvature of the basins in all experiments made measurements of angles difficult).

The experiment with a 45° releasing bend resulted in a 23.5 cm long basin with a maximum width of 4 cm, after a total displacement of 10.4 cm (Fig. 3.37). The aspect ratio was 1:5.9, thus slightly higher than for the basin that formed by the 30° bend. This basin was also the widest north of the relay ramp, elsewhere it was quite narrow. The overall angle of this basin was less than 20° relative to the main fault trend, but a part of the wall on both the northeastern side as well as the southwestern side had an angle between 40-50°.

The basin that developed in the experiment with a 60° bend was 5 cm at its widest and had an approximate length of c. 18.5 cm, after a total movement of 9 cm (Fig. 3.43). The aspect ratio of this basin was 1:3.7 based on these measurements, and it therefore had the highest ratio out of the three experiments discussed. Figure 4.4 is a conceptual diagram showing the relationship between the aspect ratio of the basins and the releasing bend angles. The angle of the basin that formed at a 60° bend was very hard to estimate due to its high curvature, but a part of the northeastern side of the basin was c. 45-50° relative to the main fault. The angle of the basin overall was much smaller. Basins that form as a result of transtension are often wider and deeper where $\sigma_1$ is at a high angle to the releasing bend, thus where the bends are at a high angle to the overall fault trend (Cunningham & Mann, 2007). The basins that formed in the three experiments discussed thus far did not follow this general trend, but the aspect ratio did increase with an increase in releasing bend angle.

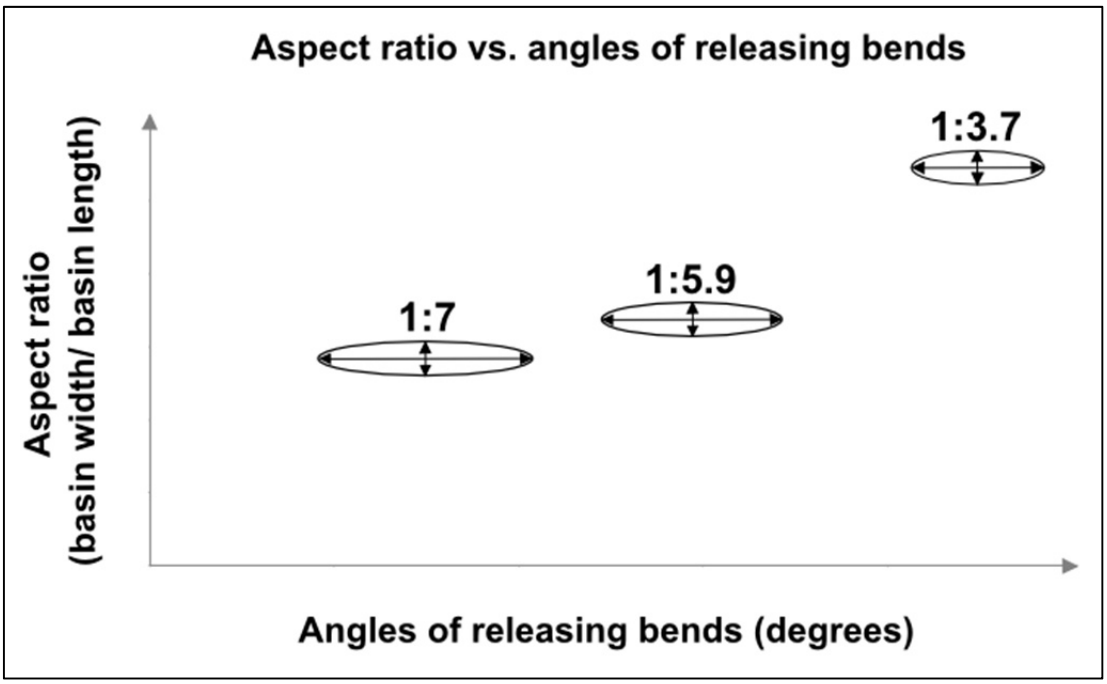


**Figure 4.4:** A conceptual diagram showing the relationship between the aspect ratio and the releasing bend angle. The numbers are the aspect ratio values for the three pull-apart basins in the models with 30°, 45° and 60° bend angles.

Brittle deformation commenced c. 11 % into the deformation in the experiment with the large releasing bend, thus earlier compared to the other transtensive experiments. The pull-apart basin that formed in this model had different characteristics compared to other basins discussed. It had a length of c. 28 cm and the maximum width of the basin was 3.6 cm (when including the down-faulted area northwest of the large pull-apart basin; Fig. 3.59). The aspect ratio was 1:8, thus smaller compared to the other basins' ratios. The main part of the basin (the part that was located over the highest-angled part of the releasing bend relative to the main fault orientation) was oriented WNW-ESE, thus similarly to the underlying releasing bend (Fig. 3.59). Several relay ramps dipped into the basin from both the southwestern and the northeastern fault block.

The total amount of displacement was 3.8 cm for the large releasing bend experiment, thus much less compared to the other models' displacements, but it was not less affected by brittle deformation (Figs. 3.59 and 3.60). The basement geometry north and south of the releasing bend area was more angled compared to the basement templates for the other experiments. Several structures formed along the fault traces over these basement areas, such as three basins along the fault trace south of the bend and basins as well as a positive structure northwest of it (Figs. 59 and 60). If this model would have been displaced further, the fault would probably have become wider through the model, due to the angle of the faults relative to the movement direction (movement towards north). The small basins would most likely have linked up or opened with the fault, based on observations from

the other experiments. The fault trace in the north might also have extended. For all the models, the fault traces have become more continuous with increased displacement and a lot of the smaller structures have evened out or opened up towards the edges. According to Christie-Blick and Biddle (1985) strike-slip faults with small lateral displacement tend to contain discontinuous faults and folds, and faults with large displacement tend to comprise continuous fault traces. The faults in the models made for this study thus had large displacements, as the fault traces were continuous through the finished models.

The basin that formed in the experiment with two irregularities (19-14) evolved from a tensile fracture already present at the start of deformation (Fig. 3.46). This may have had an effect on the development of the basin in this area, as already present structures strongly influence the nucleation and growth of structures along strike-slip faults, according to Christie-Blick and Biddle (1985). Although an extensional structure was expected here due to irregularity X forming a releasing bend of c. 20-30° relative to the main fault, the fracture may have affected the shape or the timing of its development.

**Fractures**

The areas east and west of the pull-apart basins in the experiments with 30°, 45° and 60° bends were characterized by a lot of fracturing and some normal faulting, as shown in Figures 3.31, 3.37 and 3.43. For the two models with the higher angled bends these structures covered a larger area on the western fault block compared to the eastern side (east of the relay ramp) (Figs. 3.37 and 3.43). The area just north of the basin that formed in the model with the large releasing bend (08-13) was more affected by fractures and normal faults than the area south of it (Figs. 3.59 and 3.60); the plaster overlying the basement template was thus less affected. This was the case for the other three transtensive experiments as well.

Riedel shear fractures and riedel marked fractures formed in the three experiments with the simple bends (30°, 45° and 60°) when brittle deformation commenced. These types of fractures developed in the model with the large releasing bend after the formation of tensile fractures in the area of this bend. The angles of the riedel fractures were between c. 10-20° relative to the main fault trend in all four transtensive experiments. Riedel shears formed in the model with the 30° bend after c. 18 % of the movement, which was equivalent to 2.3 cm of the displacement (Fig. 3.27). In the model with the 45° bend these fractures formed after a movement of about 2.8 cm, equivalent to c. 25 % of the movement. They developed after 26 % of the displacement in the experiment with a 60° bend, which was equivalent to 2.3 cm of movement. Riedel shears became evident in the southern area of the

model with the large releasing bend after c. 34 % of the movement, equivalent to 1.3 cm of movement.

Riedel marked fractures formed at approximately the same time as the riedel shears in all four experiments. In the three experiments with simple releasing bends these fractures were angled between c. 74-83° relative to the main fault trend. In experiment 08-13 the angles between these structures and the main fault were between c. 60-70°. As the riedel marked structures had a curvature these angles are estimates.

**Summary**

General similarities between the experiments were:

- Transfer faults connected the two main fault segments together after 6-7 cm of displacement in the models with 30°, 45° and 60° bends.
- A relay ramp formed with a dip-direction northwestwards into the pull-apart basin, from the eastern fault block in the 30°, 45° and 60° bend models.
- The main pull-apart basins connected to basins located further south after 75-80 % of the displacement for the experiments with simple releasing bends in the models with simple bends in the basement templates.
- The fault blocks that were not underlain by the basement templates were more affected by brittle deformation in the releasing bend area for the transtensive experiments, except for the 30° bend model.
- Riedel shear fractures and riedel marked shear fractures formed in all the transtensive models.

When increasing the angle of the releasing bend the following happened:

- The aspect ratio increases when using a higher-angled bend.

**Comparisons with natural examples and other experimental work**

The Baikal Rift System, located in Siberia, Russia, share similarities with the pull-apart/ rift basin that formed in the experiment with the large releasing bend and the small irregularity in the basement template (08-13) (Jolivet et al., 2013). The deformation mechanism for this rift system is largely debated, but one of the main theories, which is further studied by Jolivet et al. (2013), is that this was the result of movement along large sinistral strike-slip systems. The shape of these two basins is remarkably similar and the area to the east of Lake Baikal and north of the basin in the plaster model (Figs. 4.5 and 4.6 A and B).

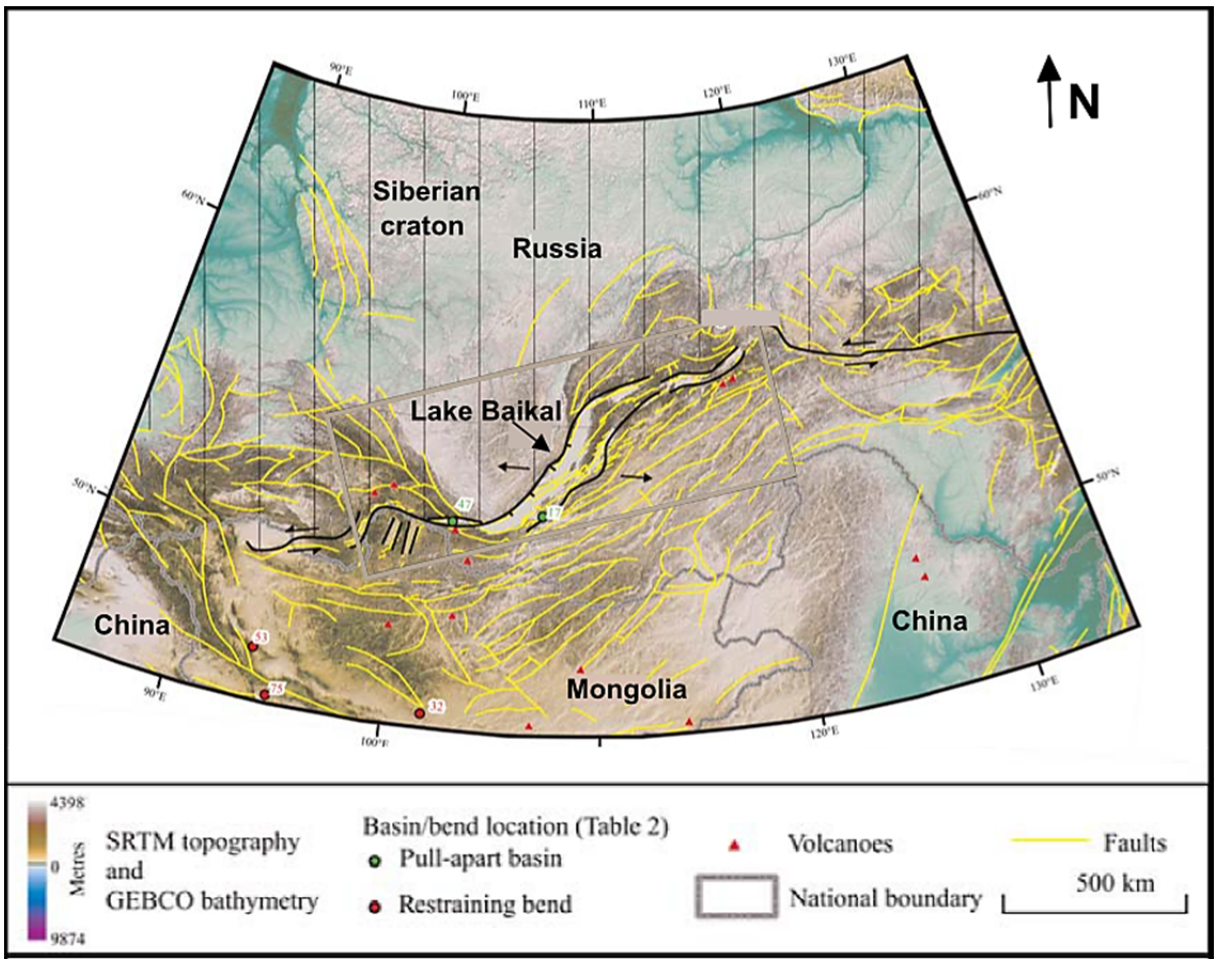


**Figure 4.5:** Lake Baikal along with structures in the area of this feature is presented in the figure by Mann (2007).

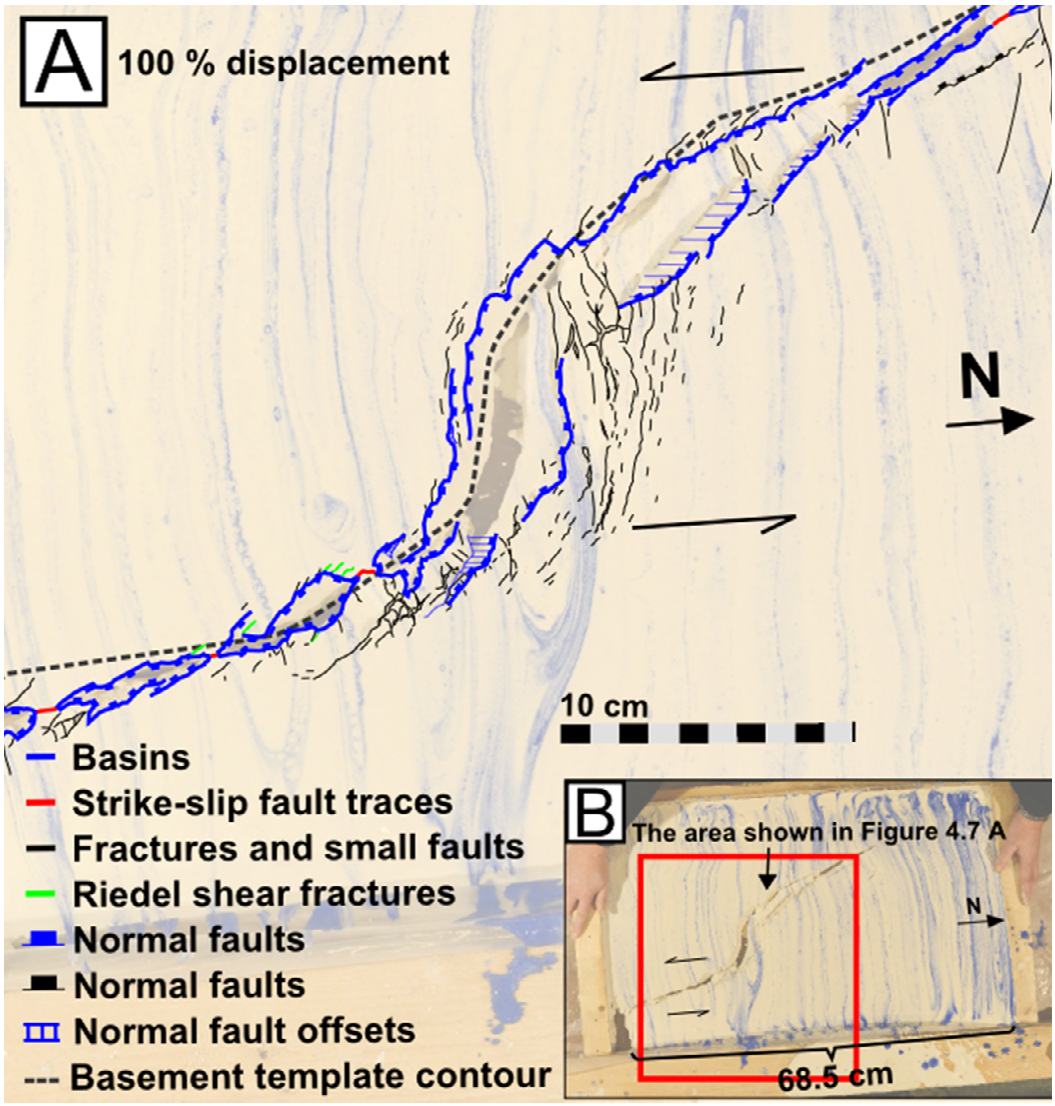


**Figure 4.6 A:** The pull-apart basin that formed in the experiment with the large releasing bend (08-13). **B:** The red square outlines the area shown in Figure 4.7 A.

The pull-apart basins that formed in the experiments with 30°, 45° and 60° releasing bends share similarities with the basins formed in the sand experiments performed by Smit et al. (2008). In their experiments, they studied the geometry and development of basins that had formed on varying widths of stepovers as well as varying rheology. The overall shape of the two basins shown in figures 4.6 A (and B) and C is quite similar and the basement geometry for the two structures contain a 30° bend with different widths. The width of the bend in the plaster model is 7 cm, whereas the width of the stepover is 10 cm in the sand model (Smit et al., 2008).

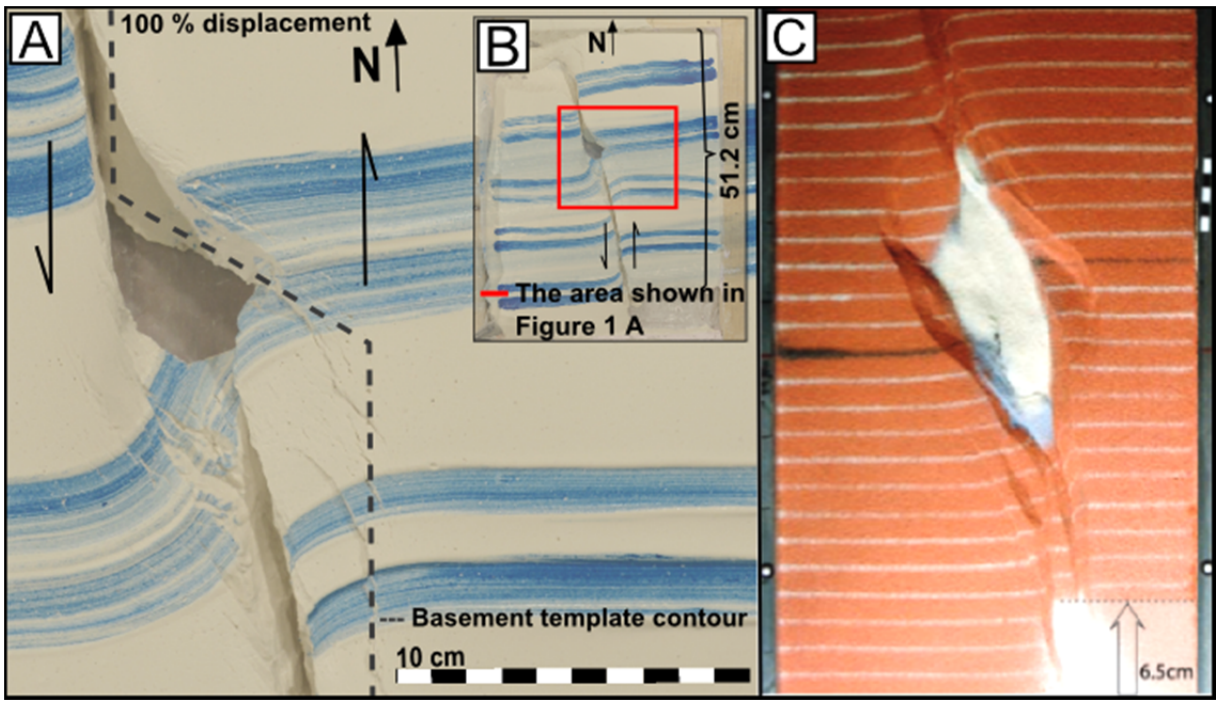


**Figure 4.6 A:** The pull-apart basin from experiment 37-14 after displacement.
**B:** The red square portrays the area shown in Figure 4.6 A.
**C:** A sand model made by Smit et al. (2008).

**Source of errors**

Although the experiments used in this study can be useful analogues to natural structures associated with transtensional and transpressional deformation, there are several factors that must be taken into consideration when comparing models to natural fault systems.

- The plaster mixture is relatively homogeneous whereas the crust is heterogeneous. The material properties will influence the deformation during displacement. The material utilized for these experiments is quite homogeneous compared to the heterogeneous rock constituting the natural sedimentary cover, and this may have an effect on the material's behaviour during deformation (Schlische et al., 2002).
- No material is added during the deformation process in the experiments whereas in nature, where the deformation generally occurs over long periods of time sediments are deposited over the active structures.
- The structures in nature often have a complex deformation history with phases of transpression and phases of transtension. The models are only subjected to one direction of movement and each part of the model is therefore subjected to one type of deformation.

- Due to the fact that the plaster models are moved by hand, the strain rate changes throughout the experiments. According to (Fossen & Gabrielsen, 1996), this may be accurate to how seismogenic faults behave in nature.

# 5 Conclusions and further work

Through this study the aim was to gain a better understanding of deformation along strike-slip faults, with a particular focus on differently angled restraining and releasing bends. To accomplish this, analogue plaster models with varying basement configurations have been made. It has been shown that the angle of the bend/ stepover is an important factor along with the amount of displacement along the fault. The condition of the material used also affects the results, and the models in this study have therefore been made with similar material conditions (e.g. consistency and water to plaster ratio). From the experimental work presented herein, the findings are listed in the following section.

**Transpressive experiments**

Observations made of the experiments with simple restraining bends (30°, 45° and 60° bends) in the basement templates suggest that the geometry of the positive flower structures was affected by the angles of the bends. The model with two irregularities in the basement template differed from the other transpressive models, and the general findings listed below were drawn from the three models with simple bends, unless otherwise stated.

The main findings for these models were:

- The angles of the restraining bends influenced the amounts of fault blocks that constituted the positive flower structures.
- The fault blocks constituting the flower structures formed at a later stage in the deformation process in the experiments with higher-angled bends.
- The angles between the fault blocks and the main fault were higher for higher-angled restraining bends.
- The first fault blocks that developed as parts of the final flower structures in each experiment were more affected by brittle deformation in the form of fractures.

**Transtensive experiments**

The pull-apart basins that formed in the transtensive experiments appeared to be less affected by the angles of the bends in the basement templates. Similarities between the three models with simple releasing bends (30°, 45° and 60° bends) were found. The experiment that had a very different basement geometry resulted in a model that was not easily comparable to the other

experiments, and the general findings listed below were drawn from the three experiments with simple bends, unless otherwise stated.

The main findings for the transtensive experiments were:

- A relay ramp formed, dipping northwestwards into the pull-apart basins from the eastern fault block in the simple bend models.
- A transfer fault oriented obliquely to the main fault trend formed and connected the two fault segments after 6-7 cm of displacement in the simple bend experiments, making them hard-linked.
- When increasing the angle of the releasing bend the aspect ratio of the pull-apart basins increased.
- The fault blocks that were not underlain by basement templates were subjected to more brittle deformation compared to the opposite blocks, apart from in the 30° bend model.

**Significance and wider implications**

This study provides a valuable insight to the geometry and the development of positive and negative structures associated with transpressive and transtensive deformation. As the structures that form in plaster experiments share similarities with structures in nature, these types of experiments can be used to improve the understanding of the nucleation and growth of natural structures in 3D.

**Suggestions for further work**

- A study of models made with a wider variety of angled restraining and releasing bends could give more information about the development of positive and negative structures, and the general trends could be validated or not.
- The effect of varying the bend widths on the structures formed in the plaster could be studied.
- The aspect ratios of the pull-apart basins could be studied further and compared to the aspect ratios for natural basins or other analogue model studies.
- The small-scale structures could be studied more intricately.

# References


Braun, J., Batt, G. E., Scott, D. L., McQueen, H., & Beasley, A. R. (1994). A simple kinematic model for crustal deformation along two-and three-dimensional listric normal faults derived from scaled laboratory experiments. *Journal of Structural Geology, 16*(10), 1477-1490.

Brun, J.-P., & Fort, X. (2011). Salt tectonics at passive margins: geology versus models. *Marine and Petroleum Geology, 28*(6), 1123-1145.

Brun, J.-P., Sokoutis, D., & Van Den Driessche, J. (1994). Analogue modeling of detachment fault systems and core complexes. *Geology, 22*(4), 319-322.

Cadell, H. M. (1889). VII.—Experimental Researches in Mountain Building. *Transactions of the Royal Society of Edinburgh, 35*(01), 337-357.

Christie-Blick, N., & Biddle, K. T. (1985). Deformation and basin formation along strike-slip faults.

Clifton, A. E., Schlische, R. W., Withjack, M. O., & Ackermann, R. V. (2000). Influence of rift obliquity on fault-population systematics: results of experimental clay models. *Journal of Structural Geology, 22*(10), 1491-1509.

Cloos, E. (1955). Experimental analysis of fracture patterns. *Geological Society of America Bulletin, 66*(3), 241-256.

Cloos, H. (1930). Zur experimentellen Tektonik. *Naturwissenschaften, 18*(34), 741-747.

Crowell, J. C., Sylvester, A. G., Galehouse, J. S., Hay, E., Hall, N., Cotton, W., . . . Sims, J. D. (1989). Sedimentation and tectonics along the San Andreas transform belt. *The San Andreas Transform Belt: Long Beach to San Francisco, California July 20-29, 1989*, 32-35.

Cunningham, D. (2010). Tectonic setting and structural evolution of the Late Cenozoic Gobi Altai orogen. *Geological Society, London, Special Publications, 338*(1), 361-387.

Cunningham, W., & Mann, P. (2007). Tectonics of strike-slip restraining and releasing bends. *Geological Society, London, Special Publications, 290*(1), 1-12.

Cunningham, W. D., Windley, B. F., Dorjnamjaa, D., Badamgarov, J., & Saandar, M. (1996). Late Cenozoic transpression in southwestern Mongolia and the Gobi Altai-Tien Shan connection. *Earth and Planetary Science Letters, 140*(1), 67-81.

Dauteuil, O., & Mart, Y. (1998). Analogue modeling of faulting pattern, ductile deformation, and vertical motion in strike-slip fault zones. *Tectonics, 17*(2), 303-310.

Dooley, T., McClay, K., Hempton, M., & Smit, D. (2005). *Salt tectonics above complex basement extensional fault systems: results from analogue modelling.* Paper presented at the Geological Society, London, Petroleum Geology Conference series.

Dooley, T. P., Jackson, M., & Hudec, M. R. (2007). Initiation and growth of salt-based thrust belts on passive margins: results from physical models. *Basin Research, 19*(1), 165-177.

Dooley, T. P., Jackson, M. P., & Hudec, M. R. (2009). Inflation and deflation of deeply buried salt stocks during lateral shortening. *Journal of Structural Geology, 31*(6), 582-600.

Eisenstadt, G., & Withjack, M. O. (1995). Estimating inversion: results from clay models. *Geological Society, London, Special Publications, 88*(1), 119-136.

Emmons, R. (1969). Strike-slip rupture patterns in sand models. *Tectonophysics, 7*(1), 71-87.

Fort, X., Brun, J.-P., & Chauvel, F. (2004). Salt tectonics on the Angolan margin, synsedimentary deformation processes. *AAPG Bulletin, 88*(11), 1523-1544.

Fossen, H. (2010). *Structural Geology*. Cambridge: Cambridge University Press.

Fossen, H., & Gabrielsen, R. H. (1996). Experimental modeling of extensional fault systems by use of plaster. *Journal of Structural Geology, 18*(5), 673-687.

Gabrielsen, R. H., & Clausen, J. A. (2001). Horses and duplexes in extensional regimes: A scale-modeling contribution. *MEMOIRS-GEOLOGICAL SOCIETY OF AMERICA*, 207-220.

Henza, A. A., Withjack, M. O., & Schlische, R. W. (2010). Normal-fault development during two phases of non-coaxial extension: An experimental study. *Journal of Structural Geology, 32*(11), 1656-1667.
Henza, A. A., Withjack, M. O., & Schlische, R. W. (2011). How do the properties of a pre-existing normal-fault population influence fault development during a subsequent phase of extension? *Journal of Structural Geology, 33*(9), 1312-1324.
Hubbert, M. K. (1937). Theory of scale models as applied to the study of geologic structures. *Geological Society of America Bulletin, 48*(10), 1459-1520.
Jolivet, M., Arzhannikov, S., Chauvet, A., Arzhannikova, A., Vassallo, R., Kulagina, N., & Akulova, V. (2013). Accommodating large-scale intracontinental extension and compression in a single stress-field: A key example from the Baikal Rift System. *Gondwana research, 24*(3), 918-935.
Knipe, R. J., Jones, G., & Fisher, Q. (1998). Faulting, fault sealing and fluid flow in hydrocarbon reservoirs: an introduction. *Geological Society, London, Special Publications, 147*(1), vii-xxi.
Koenigsberger, J., & Morath, O. (1913). Theoretische Grundlagen der experimentellen Tektonik. *Zeitschrift der Deutschen Geologischen Gesellschaft*, 65-86.
Langhaar, H. L. (1951). *Dimensional analysis and theory of models* (Vol. 2): Wiley New York.
Lindanger, R., Øygaren, M., Gabrielsen, R., Mjelde, R., Randen, T., & Tjøstheim, B. (2004). Analogue (plaster) modelling and synthetic seismic representation of hangingwall fault. *first break, 22*(1).
Mann, P. (2007). Global catalogue, classification and tectonic origins of restraining-and releasing bends on active and ancient strike-slip fault systems. *Geological Society, London, Special Publications, 290*(1), 13-142.
Mansfield, C., & Cartwright, J. (2001). Fault growth by linkage: observations and implications from analogue models. *Journal of Structural Geology, 23*(5), 745-763.
Mart, Y., & Dauteuil, O. (2000). Analogue experiments of propagation of oblique rifts. *Tectonophysics, 316*(1), 121-132.
McClay, K. (1990). Extensional fault systems in sedimentary basins: a review of analogue model studies. *Marine and Petroleum Geology, 7*(3), 206-233.
McClay, K., & Bonora, M. (2001). Analog models of restraining stepovers in strike-slip fault systems. *AAPG Bulletin, 85*(2), 233-260.
Molda 3 Normal. (n.d.). Saint Gobain Formula. Retrieved May 1, 2015, from <http://www.saintgobainformula.com/Products/Plaster/Molda-3-Normal>
Morley, C. (1988). Out-of-sequence thrusts. *Tectonics, 7*(3), 539-561.
Naylor, M., Mandl, G. t., & Supesteijn, C. (1986). Fault geometries in basement-induced wrench faulting under different initial stress states. *Journal of Structural Geology, 8*(7), 737-752.
Odinsen, T. (1992). *Modellering av normalforkastninger; analoge ekstensjons-gipsmodeller og balansering*. Bergen: [T. Odinsen].
Ottesen, S. (1991). *Den strukturelle utviklingen av Swaengraben, og dens implikasjoner for struktureringen av Lopphøgda med omgivelser*. Bergen: [S. Ottesen].
Pringle, J., Westerman, A., Clark, J., Drinkwater, N., & Gardiner, A. (2004). 3D high-resolution digital models of outcrop analogue study sites to constrain reservoir model uncertainty: an example from Alport Castles, Derbyshire, UK. *Petroleum Geoscience, 10*(4), 343-352.
Ramberg, H. (1981). *Gravity, deformation, and the earth's crust: In theory, experiments, and geological application*: Academic press.
Sales, J. K. (1987). TECTONIC MODELS, Tectonic models *Structural Geology and Tectonics* (pp. 785-794): Springer.
Sanderson, D. J., & Marchini, W. (1984). Transpression. *Journal of Structural Geology, 6*(5), 449-458.
Schlische, R. W., & Withjack, M. O. (2009). Origin of fault domains and fault-domain boundaries (transfer zones and accommodation zones) in extensional provinces: Result of random nucleation and self-organized fault growth. *Journal of Structural Geology, 31*(9), 910-925.

Schlische, R. W., Withjack, M. O., & Eisenstadt, G. (2002). An experimental study of the secondary deformation produced by oblique-slip normal faulting. *AAPG Bulletin, 86*(5), 885-906.

Smit, J., Brun, J. P., Cloetingh, S., & Ben-Avraham, Z. (2008). Pull-apart basin formation and development in narrow transform zones with application to the Dead Sea Basin. *Tectonics, 27*(6).

Steen, Ø., Sverdrup, E., & Hanssen, T. (1998). Predicting the distribution of small faults in a hydrocarbon reservoir by combining outcrop, seismic and well data. *Geological Society, London, Special Publications, 147*(1), 27-50.

Sylvester, A. G. (1988). Strike-slip faults. *Geological Society of America Bulletin, 100*(11), 1666-1703.

Vendeville, B., Cobbold, P., Davy, P., Brun, J., & Choukroune, P. (1987). Physical models of extensional tectonics at various scales. *Extensional Tectonics, 28*, 95-107.

Vendeville, B. C. (2005). Salt tectonics driven by sediment progradation: Part I—Mechanics and kinematics. *AAPG Bulletin, 89*(8), 1071-1079.

Wilcox, R. E., Harding, T. t., & Seely, D. (1973). Basic wrench tectonics. *AAPG Bulletin, 57*(1), 74-96.

Woodcock, N. H., & Daly, M. (1986). The Role of Strike-Slip Fault Systems at Plate Boundaries [and Discussion]. *Philosophical Transactions of the Royal Society of London. Series A, Mathematical and Physical Sciences, 317*(1539), 13-29.

Woodcock, N. H., & Rickards, B. (2003). Transpressive duplex and flower structure: Dent fault system, NW England. *Journal of Structural Geology, 25*(12), 1981-1992.

# Appendix A

An overview of the videos showing the experiments is found in Table A.1.

**Table A.1**

| Video Number | 1 | 2 | 3 | 4 | 5 | 6 | 7 | 8 |
|---|---|---|---|---|---|---|---|---|
| Experiment Number | 32-14 | 34-14 | 36-14 | 40-14 | 39-14 | 37-14 | 19-14 | 08-13 |

**Figure A.1:** An overview of the videos showing the experiments is given in this table.